Design and Assessment of the Superconducting Magnetic Energy Storage and the Battery Hybrid Energy Storage System

Li, Jianwei

Award date:
2017

Awarding institution:
University of Bath

Design and Assessment of the Superconducting Magnetic Energy Storage and the Battery Hybrid Energy Storage System

Jianwei Li

A thesis submitted for the degree of Doctor of Philosophy (PhD)

Department of Electrical and Electronic Engineering

University of Bath

2017

Signature_____ Date_____

Abstract

The major challenges in power systems are driven by the energy shortage and environmental concerns, namely facilitating the penetration of renewable energy and improving the efficiency of the renewable sources. Due to the variable nature of renewables, the generated power profile may not be able to match the load requirement. Accordingly, much attention has been focused on the development of energy storage technologies to guarantee renewable power penetration. Recently, advances in the superconducting energy storage system (SMES) have made SMES/battery hybrid energy storage systems (HESS) technically attractive. Compared with other energy storage technologies, the principle advantages of SMES are: the high power density, unlimited cycle-life and high peak current handling capacities. However, SMES has low energy density. The battery is characterised by large energy density, but low power capacity. In renewable energy systems, high-frequency power fluctuations will cause a significant degree of battery power cycling. This, in turn, has been shown to lead to a significant reduction in battery service life. Therefore, the concept of the SMES/battery hybrid energy storage is proposed by combining two kinds of complementary energy storages, achieving an optimised system which has the advantages of both primary energy storage systems (ESS) meanwhile complementing the disadvantages of each ESS.

However, the fields of the implementation and optimisation of the proposed hybrid system are relatively new and with challenges remaining in the power management design, the optimal sizing study and the control of the HESS. The main contributions of this project that the thesis introduces are the detailed development and assessment of the SMES/battery HESS with the related power management, system sizing, synergetic control and quantitative evaluation.

To achieve the active combination of two kinds of ESSs, an overall power management integrating the different characteristics of SMES and battery is absolutely essential.

Three kinds of power management methods, therefore, are developed to be used in different power applications and analysed in respect of their strengths and weaknesses.

A novel hybrid energy storage sizing method is developed, which is able to return an optimal matching of the SMES and the battery. The different energy and power demands for the battery and the SMES are considered in the sizing method. Moreover, the proposed sizing method is proved to be able to address the SMES oversize problem.

The synergistic control of the battery and the SMES is the key factor to achieve the expected power management in the power systems. A new kind of droop control is, therefore, developed in this study, which effectively co-ordinates the operation of the different storage technologies such that they complement each other. In addition, the droop coefficients for both the SMES and the battery are more carefully determined using the system operating constraints and the energy storage capacities, which makes the control method more efficient.

The proposed SMES and battery hybrid energy storage scheme, together with its control method, is tested by both simulation and experiment. The real-time computing capability of the Real-Time Digital Simulator (RTDS) makes it possible for the HESS system to be interfaced with the outside hardware. To verify the proposed HESS scheme with the new control method experimentally, a hardware-in-the-loop (HIL) test platform is developed coupling with the RTDS. The experimental results show that the presented control method is able to exploit the different characteristics of the ESSs and optimise the power-sharing between the SMES and the battery. Additionally, the battery in the experiment is protected from the continual short-term charge/discharge cycles and abrupt power changes and, as a result, the battery lifetime is improved.

In order to evaluate the improvement of the battery lifespan in the proposed hybrid scheme, a novel battery lifetime model is developed. The new battery lifetime model advances previous ones by taking the battery discharge rate into account, returning a more accurate evaluation. Quantitative analysis of the battery lifetime extension is carried out in this thesis to investigate the long-term performance of the battery in the simulation environment. In the case study, the battery lifetime is extended from 6.2

years in the battery only system to 8.7 years in the SMES/battery HESS, which further highlights the benefits of hybridisation.

Graphical Abstract

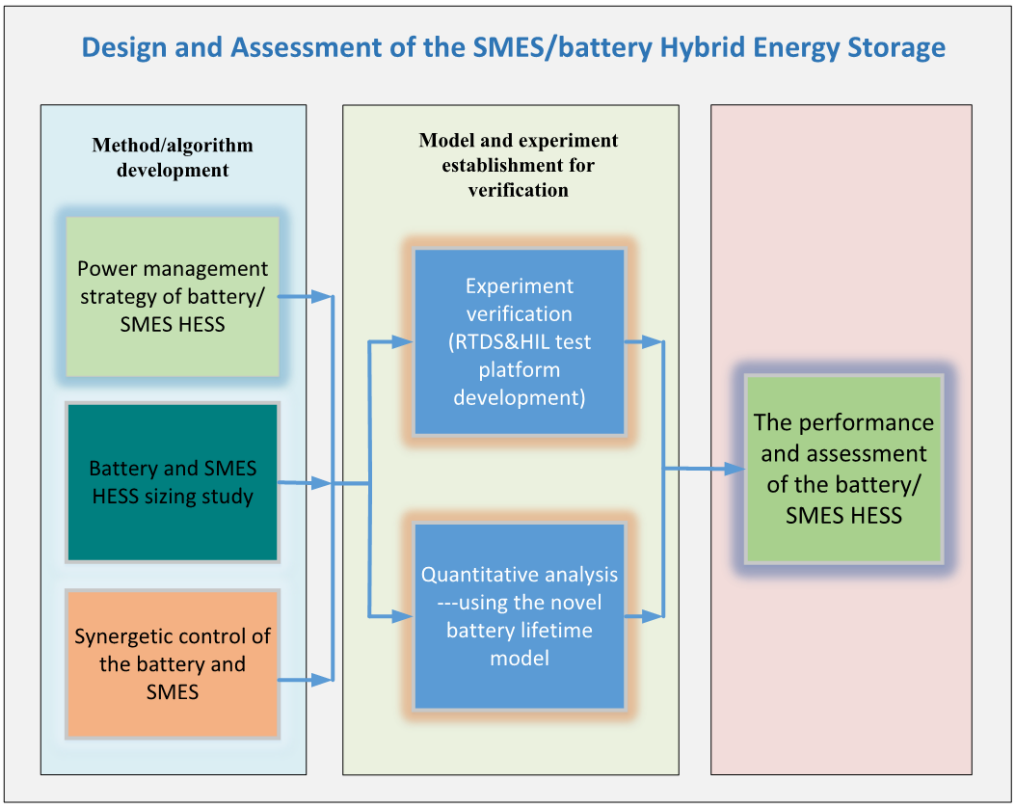

The graphical abstract shown above highlights the primary contributions of this thesis. Firstly, three kinds of algorithms and methods are developed as the foundation of this thesis in respect of the system power management, the energy storage sizing study and the HESS control. Then, the methods are verified at system level by both experiment and simulation. An RTDS&HIL platform is developed to give the experimental performance of the proposed hybrid design. A novel battery lifetime model is also presented to analyse the battery performance in the HESS quantitatively. Finally, the proposed five parts of the works tell the whole story about the design and assessment of the SMES and the battery hybrid energy storage system.

Acknowledgement

Firstly, I would like to express my sincere and deepest gratitude to my supervisor, Dr. Weijia Yuan, for his encouragement, guidance and support throughout the duration of my research. He taught me the skills required for independent research. With his support, I have achieved a number of accomplishments in the last four years and published a number of papers in some excellent journals. Also, I would like to thank Dr. Min Zhang and Dr. Xiaoze Pei for their generous advice and support.

I am grateful to all the staff in the electrical power system group at the University of Bath for creating an atmosphere of friendship and cooperation.

At the Tsinghua University, I would like to thank Prof. Xiaohua Jiang for her insight and warm-hearted supervision during my stay in her group. The research experience at the Tsinghua University broadens my horizon about the industrial applications of the power electronics. Many thanks to Dr Simon Le Blond, Pengfei Yao and Xudong Wang for their help and collaboration within this work stream.

I would also to thank my colleagues, in no particular order, Dr. Xiaojian Li, Dr Yawei Wang, Dr. Jie Sheng, Dr. Zhenyu Zhang, Dr. Huiming Zhang, Fei Liang, Mariam Elshiekh, Sriharsha Venuturumilli, Qixing Sun, Jay Patel, Dong Xing, Hamoud Alafnan, Zixuan Zhu and Muhammad Zulfiqar Ali.

Last but not the least, I am grateful to my parents who always love me unconditionally and give me enormous encouragements though all my study and life. Thank my wife, Qingqing Yang for being by my side all the time and sharing both the pain and the happiness. Without their love, I would not have achieved all that I have thus far.

List of Publications as the First Author

[1]. **Jianwei Li,** Gee AM, Zhang M, Yuan W. *"Analysis of battery lifetime extension in a SMES-battery hybrid energy storage system using a novel battery lifetime model* [J]*."* **Energy.** 2015;86:175-85.

[2]. **Jianwei Li,** Zhang M, Yuan W. et al. *SMES/Battery Hybrid Energy Storage System for Electric Buses* [J]. **IEEE Transactions on Applied Superconductivity**, 2016, 26(4): 1-5.

[3]. **Jianwei Li,** Robinson F, et al. *Design and test of a new droop control algorithm for a SMES/battery hybrid energy storage system* [J]. **Energy**. 2017;118:1110-22.

[4]. **Jianwei Li,** Wang X, Zhang Z, et al. *"Analysis of a new design of the hybrid energy storage system used in the residential m-CHP systems"* [J]. **Applied Energy**, 2017, 187:169-179.

[5]. **Jianwei Li,** Xiong, R., Yang, Q., Liang, F., Zhang, M., & Yuan, W. *"Design/test of a hybrid energy storage system for primary frequency control using a dynamic droop method in an isolated microgrid power system"* [J]. **Applied Energy**, 2016, http://dx.doi.org/10.1016/j.apenergy.2016.10.066.

[6]. **Jianwei Li,** Yuan W et al. *"A Novel use of the Hybrid Energy Storage System for Primary Frequency Control in a Microgrid"* [J]. **Energy Procedia**, 2016, 103: 82-87.

[7]. **Jianwei Li,** Qingqing Yang, Zhenyu Zhang, and Weijia Yuan*, *"Analysis of Superconducting Magnetic Energy Storage Used in a Submarine HVAC Cable Based Offshore Wind System"*, **Energy Procedia** 75, 691-696, 2015.

Contents

Nomenclature

C	DC bus capacitor
d_1	*duty ratio of M1 while M2 is constantly on*
d_2	*duty ratio of M2 while M1 is constantly off*
E_{max}	*largest energy deficiency*
E_{SMES}	*SMES energy*
Ibat	*battery current*
I_c	*critical current*
I_{bat_conv}	*output current of the battery DC/DC converter*
I_{S_conv}	*output current from SMES DC/DC converter*
Imaxc(x)	*maximum charge current of the ESS x*
I_{max_bat}	*maximal battery current*
I_{max_SMES}	*maximal SMES current*
I_{ref}	*reference current in sliding mode control*
I_{SMES}	*SMES current*
Ix	*charge or discharge current of the ESS x*
k_{bat}	*battery droop coefficient*
k_{SMES}	*SMES droop coefficient*
$P_{bat}(t)$	*battery power*
$P_d(t)$	*power deficiency*
P_{HF}	*high frequency power*
P_i	*provisional SMES power defined in SMES sizing study*
$P_L(t)$	*instantaneous load demand*
P_{LF}	*low frequency component*

$P_m(t)$	*power in the largest net power fluctuation cycle*
P_{mean}	*average value of SMES power*
$P_{net}(t)$	*instantaneous net power*
P_{net_max}	*peak value of the net power*
P_{n_SMES}	*power dealt by the SMES in sizing study*
$P_{SMES}(t)$	*power dealt by the SMES*
P_{SMES_max}	*maximal power dealt by the SMES*
$P_w(t)$	*instantaneous wind power output*
V_{bat}	*battery voltage*
$Vbus$	*DC bus voltage*
$Vlow\_end$	*lower DC bus voltage boundary*
$Vmax(x)$	*upper voltage limit of the ESS x*
V_{max_bat}	*upper voltage limit of the battery*
V_{max_SMES}	*upper voltage limit of the SMES*
$Vmin(x)$	*lower voltage limit of the ESS x*
Vr	*DC bus reference voltage*
V_{SMES}	*SMES voltage*
Vup_end	*upper DC bus voltage boundary*
ΔP	*power increment for SMES sizing study*
η	*degradation factor*

List of Abbreviations

BOS	*battery only system*
CTF	*cycles to failure*
CHP	*combined heat and power*
DDLWEC	*direct drive linear wave energy converter*
DOD	*depth of discharge*
DSP	*digital signal processor*
EES	*energy storage system*
EV	*electric vehicles*
FESS	*flywheel energy storage system*
FD	*frequency-dominate*
HESS	*hybrid energy storage system*
HIL	*hardware-in-the-loop*
HTS	*high temperature superconductor*
LPSP	*loss of power supply probability*
MG	*microgrid*
PD	*power-dominate*
PMS	*power management strategy*
PHS	*pumped hydro energy storage*
RTDS	*Real-Time Digital Simulator*
SC	*super-capacitor*
SMES	*superconducting magnetic energy storage*

List of Figures

List of Tables

Chapter 1 Introduction

1.1 Thesis background

The major challenges in power systems are driven by environmental concerns, such as the carbon emissions and the energy crisis [1]. A general realisation has been reached that significant efforts need to be made to boost renewable energy. However, variability and intermittency are key inherent characteristics of renewable resources, which means the renewable sources may not be able to provide a high-quality power supply and immediate response to the demand [2]. Therefore, the increasing growth of renewable applications means more severe stability problems in power grids [3]. Energy storage systems, ESSs, have the potential to play a significant role in expanding the penetration and permitting fuller utilisation of renewable power generation [4-8].

Energy storage technology refers to the process of converting the energy (mainly electrical energy) to a form that can be stored for converting back to electrical energy when needed [1, 2]. Previous work has shown the different functions of ESSs, including power balancing [3, 4], frequency control [5], voltage control [6], oscillation damping [7], etc. Various kinds of ESSs have been designed and widely demonstrated in renewable power applications [8-12]. Battery energy storage systems have high efficiency, large energy density and elevated levels of robustness and are, therefore, a desirable component used in renewable power generation.

However, a battery has a limited number of charge/discharge cycles, which limits its service life [2, 13]. The operating stress is particularly onerous when batteries are used with renewable sources since they are subjected to many short-term charge/discharge cycles and high transient current levels [14, 15]. To address these problems, the pairing of complementary storage technologies to form a hybridised energy storage system has, therefore, become the focus of recent research. For example battery storage hybridised with supercapacitors has been widely investigated in many power applications, with the benefits shown to be improved system response speed and the extension of battery lifetimes. Compared with supercapacitors, superconducting magnetic energy storage has higher power density, lower self-discharge rate and higher peak current handling capabilities [7, 16-18]. Despite these advantages, few studies focus on the SMES/battery HESS because of the lack of SMES technology. However, with the continuous development of superconductive material, some recent studies have shown positive cost-benefit analysis of SMES [19-21] and SMES/battery HESS [14, 22]. An active combination of the SMES and the battery could produce an optimal HESS that yields various advantages over each single ESS, including higher power capacity, higher energy density, peak current handling capacity, an extension of service lifetime, etc. [23-26].

However, less work has been done to investigate the SMES/battery hybrid energy storage scheme and its matched power-sharing strategy, sizing algorithm and the control method. Hence, to ensure the optimal utilisation of the SMES and the battery HESS, this thesis describes the detailed development and assessment of the SMES/battery HESS.

1.2 Research motivation

The research motivations mainly come from the mismatch between the increasingly growing opportunities for the SMES/battery HESS and the lack of related technologies for design and operation of the SMES/battery HESS. Furthermore, the extension of the battery lifetime is one of the key merits of the proposed SMES/battery hybrid design. The quantitative analysis of the improvement of the battery lifespan in the HESS is, therefore, very necessary in this study. Consequently, it leads to the other motivation of this study, which is to create a battery lifetime prediction method.

1.2.1 The growing opportunities for the HESS

A. Renewable energy and the HESS

Significant changes in the structure of the world energy market have been observed in recent years. Although fossil fuels are still the main resource to generate electricity on a global scale, the past few decades have witnessed a remarkable development of renewable energies. A great many targets and policies are set by worldwide governments to encourage the blossoming of renewable energy. According to the Electricity Ten Year Statement published by the National Grid in Great Britain, the renewable energy will make up 15% of energy consumed across the UK by 2020, and the target for the European Union is 20% [27]. However, characterised as intermittent and variable power sources, the renewable generation presents a significant challenge in the operation of today's power systems, because renewable power generations are unlikely to match the load requirement [1]. Hence, the increasing penetration of the renewable energy is challenging stabilities and reliabilities of the current power systems. Endeavours have been made in searching for effective solutions, and the energy storage

technologies are believed to be the most promising approaches [1, 2, 10, 17]. Many different kinds of energy storage devices are currently available for renewable power generations. There are distinct advantages and disadvantages with each kind of ESS, and, normally, a single type of energy storage can hardly meet all the requirements in the renewable generations. Hence, the combination of different kinds of ESSs is a creative idea that may make an optimal hybrid energy storage system that has better performance in renewable generations than either ESS.

B. Electrical vehicles and the HESS

In many metropolises, the particulates which generate toxic haze and adversely affect human health are mainly caused by burning of fossil fuels in vehicles [28]. The use of Electric Vehicles (EV) is believed to be a possible solution for fossil fuels; insufficiency and environmental issues [29]. Also, the increasing development of EV technology will significantly reduce CO_2 emissions. Many countries have established targets for EV development and encourage residents to use electrical cars. Rechargeable batteries are widely used as energy sources for EVs [25, 29, 30]. However, batteries are challenged with limited life-cycles, sensitivity to high discharge current and low power density, which has provided the impetus to develop additional solutions [16, 25, 31, 32]. Also, since operation conditions (start, accelerate, brake, etc.) change fast and irregularly, batteries used in EVs are always required to meet an instantaneous power demand and, under such conditions, the battery will undergo many irregular charge/discharge cycles, which will decrease battery service time [33]. Hybrid energy storage schemes such as the SMES/battery HESS provide an ideal solution to address such problems. A SMES system working as a power buffer is able to deliver a huge amount of power in a short time, which is ideal for the motor start, accelerate and brake

processes, hence, improving the battery lifetime. Meanwhile, the battery also performs as an energy buffer to the SMES for long-term operation requirement.

1.2.2 Lack of the methodological approaches to the SMES/battery HESS

The SMES and battery hybrid energy storage scheme is a relatively new concept, and little work has been done to investigate the design, control and operation of the HESS at the system level. The deficiencies in the methodological approaches to the SMES/battery HESS mainly lie in three areas:

- The power management strategy (PMS).

  To fulfil the active combination of two kinds of ESSs, an overall power management strategy designed based on the different characteristics of SMES and battery is needed.

- The sizing method of the SMES/battery HESS.

  The main function of the HESS is to compensate the unbalanced power between the generation and the load demand. To fulfil this basic function, as well as to obtain an optimal capacity of energy storage devices, a sizing study is essential. The sizing study of the SMES/battery hybrid energy storage is very complicated.

- The synergetic control method for the SMES/battery HESS.

  Power balancing is the major challenge for the efficient use of the HESS. The control of the HESS is the key factor to achieve the expected power managements and distributions. In the hybrid energy storage scheme, the synergetic control method is needed to effectively co-ordinate operation of two storage technologies so that they complement each other.

1.2.3 Lack of battery lifetime prediction model

Batteries are regarded one of the propular energy storage. However, it is generally agreed that batteries are the most important, but weakest, parts in the long-term operation of an energy storage project [34]. Batteries have a significant impact on the budget when taking the whole life cost, replacement and maintenance into account [34]. Battery lifetime prediction is necessary for this study since the extension of battery lifetime is one of the main advantages of the HESS.

A quantitative analysis of the battery lifetime improvement is an essential process to evaluate the effectiveness of the SMES/battery HESS. Various kinds of battery-life models are available. However, the capacity fading mechanism is so complicated that it is hard to create a practical model which considers the extreme non-linearity of many underlying ageing processes [35]. Experiments have been done by Bindner [34] aiming to compare several battery life models, and the results showed that the cycle counting algorithm generates a relatively more accurate prediction. The method of cycles counting has already been employed in battery lifetime estimation applications [34, 36, 37]. However, the previous works simply counted the number of cycles in each level of depth of discharge (DOD, refers to the extent to which batteries are discharged). This means that the conventional battery life model only regarded the range of DOD of each cycle as the factor related to battery lifetime, but neglected other factors, such as discharge rate, which has a significant influence on battery degradation. Therefore, a new battery lifetime model which quantifies the effect of both the battery charge/discharge cycles and discharge rate is needed.

1.3 The challenges and contributions of the thesis

1.3.1 Power management strategy for the HESS

Power management strategy is not a new concept in the power systems. In the traditional power system, the PMS refers to the method by which the power is dispatched and the power flow is controlled [38]. Power management strategy is essential for the HESS to enhance its primary advantage, whereby different ESSs come into action in respect of various power requirements. Furthermore, when the HESS is applied in complex conditions and works together with many other power devices, the PMS is the determinant factor to ensure the sound operation of the HESS. Song et al. in [39] and Zhang et al. in [40] introduced the PMS of the battery and SC HESS to be used in the electrical vehicles with the benefit of improving the EV's mile-range. The PMS for the HESS is also studied in terms of its application in the microgrid, as described in [41-43]. However, to the author's best knowledge, there is no published work which gives a guidance of the PMS for the SMES and battery hybrid scheme. Therefore, this highlights one of the main contributions of this thesis in that PMSs are developed for the first time to be used for the SMES and battery HESS. The PMSs are summarised in three categories: frequency-dominant PMS, SMES fully active PMS and the power-dominant PMS. The typical applications of these PMSs are also discussed with respect to their advantages and disadvantages.

1.3.2 The sizing study

The main function of the proposed hybrid energy storage system is to compensate the unbalanced power between the generation and the load demand. Therefore, in aiming to obtain an optimal capacity of energy storage devices, the sizing study is very necessary. The sizing study of the SMES/battery hybrid energy storage is very complicated. Both the essential functions and functional complementation between ESSs need to be considered in the sizing method. Fewer published works can be found to describe the sizing problem for a hybrid energy storage system. The hybrid energy storage is introduced in many works on renewable generations [11, 44], microgrid [45, 46] and transportation [16, 40], but there is not a critical sizing method for the HESS. The battery and the supercapacitor hybrid scheme is investigated in electrical vehicle applications [40, 47, 48]. In these works, the capacities for the ESSs in the HESS are given, but a sizing study is not introduced.

Anther contribution of this study lies in the development of a new kind of sizing method for the SMES and battery HESS. In the new method, the battery and the SMES work together as an overall module to satisfy both the energy and power constraints, whereas neither the SMES nor the battery needs to meet all the system constraints. As a consequence, the novelty of this sizing method is reflected in two aspects. Firstly, the battery and the SMES can be sized according to their own merits rather than restricted by system constraints. Secondly, the energy/power requirements for the signal ESS are more flexible, which means the capacity requirement of the ESS may be reduced.

1.3.3 The control method for the HESS.

The control of the battery and the SMES is the key factor to achieve the expected power management and distribution in power applications. For the single energy storage technology used in the power system, the charge/discharge demands for the single ESS are very straightforward. However, in the hybrid energy storage scheme, the control task is much more complicated, because the control needs to effectively combine the harmonious operation of two storage technologies such that they complement each other.

Droop control, which is able to take advantage of various kinds of power sources to match different load demands, is very appropriate to control the power sharing between the SMES and the battery. In this study, a new control method is developed by a novel use of the droop control method. The advantages of the proposed control are reflected in the following aspects:

- The SMES and the battery work together to meet both the energy and power demand.
- Able to arrange the charge and discharge priority of the SMES and the battery in different situations. For example, the SMES in the HESS is expected to act preferentially to satisify the short-term high power requirement.
- Able to protect the battery from the frequent charge/discharge processes

This control method is, therefore, anther important contribution of this thesis.

1.3.4 Quantitative analysis of the battery lifetime extension

By integrating the battery with the SMES, the battery lifespan can be greatly improved, which is one of the key merits of the HESS. Qualitative analysis is not difficult as it can be observed from either experiment or simulation that the battery is protected by the SMES from the high-rate of discharge. In fact, many works [16, 44, 46, 47, 49] have already studied battery life extension in the HESS scheme. However, in these works, it cannot be found as to what degree the battery lifetime is extended. In other words, the battery lifetime improvements in these studies are not quantified. However, in aiming to evaluate the HESS performance, quantitative analysis of the battery lifetime extension is very necessary. Therefore, to fill this gap, the contributions of this thesis are reflected in the following two areas:

- A novel battery lifetime model is developed and introduced in this thesis. This model is particularly designed for the HESS and able to link both the charge/discharge cycles and the battery currents with the battery degradation process.

- By using the novel battery lifetime model, the improvement of the battery lifespan in the HESS is evaluated in this thesis. In the case study shown in Chapter 8, the battery service time is improved from 6.2 years to 8.7 years, which is very meaningful in the energy storage project.

1.3.5 The RTDS and HIL experimental platform

A synergetic control method is developed to achieve the complementary performance of the SMES and the battery. A real-time experiment is important to verify the proposed

HESS and its control method. In the final case study, the proposed SMES/battery HESS was designed to be used in the domestic power system, but it is very difficult to build a real domestic power system in the laboratory environment at the University of Bath. The Real Time Digital Simulator, which has real-time computing capability, is regarded as a very effective tool for the experimental verification of power systems. Also, the signals and measurements in the RTDS are real-time data, which make it possible to interface with the external hardware/devices. By adopting these advantages of the RTDS, a new experimental platform in established in this study. The real-time power system is built in the RTDS, and all the control methods are implemented in the outside hardware (DSP 28335 in this study). The real-time data generated from the RTDS are sent to the outside DSP, and the DSP will generate the physical signals (PWM signals) back to the system in the RTDS. In this way, the RTDS, together with the DSP control board, forms a hardware in the loop (HIL) test circuit which is used to test the control algorithm.

1.4 Thesis outline

The rest of the thesis is organised as follows:

Chapter 2 reviews different types of ESSs and their strengths and weaknesses in power applications. The literature review provides a means of better understanding the differences between ESSs. Various applications of the ESSs are provided. By analysing the different characterises the ESSs, it is concluded that the hybridisation of different energy storages may create an optimal energy storage system, namely the hybrid energy storage system. An overview of the battery-based HESS is also given in this chapter. The challenges and opportunities for the SMES/battery HESS are discussed.

Chapter 3 is dedicated to the development of a novel battery lifetime model, which is highly important for the evaluation of the battery lifetime extension in the HESS. The improvement of the battery lifespan is one of the key merits of the HESS and, by using the proposed model, the battery lifetime extension can be quantitatively analysed.

Chapter 4 is one of the key chapters which presents the methodologies developed in this study for the SMES/battery HESS. This chapter is composed of three parts:

- Power management strategies used for the power sharing between the SMES and the battery are introduced. Three kinds of methods are summarised. The advantages and disadvantages of each method are discussed. In respect of the different features of the PMSs, their application occasions are investigated. Additionally, a case study is introduced to describe the detailed implementation of the power-dominate PMS in an electrical vehicle system.
- A sizing method for the battery and the SMES in a hybrid scheme is presented. The different energy and power demands for the battery and the SMES are considered in the sizing method so that the complementary function of the HESS is achieved.
- A novel use of a droop control method for controlling the power sharing between the SMES and battery is proposed. By selecting the optimal droop coefficients for the different ESSs, the charge and discharge priority of the SMES and the battery are differentiated according to the power situations. The implementation of the droop control in the DC/DC converters is introduced for both the SMES and the battery. The droop coefficient study which successfully couples with the system constraints is also presented.

Chapter 5 describes the experimental verification of the SMES/battery HESS by using the RTDS and HIL test platform. The original idea and the implementation of the experiment are introduced. A domestic CHP system is used as case study in the RTDS and HIL platform. The performances of the HESS and its control method are verified in the experiment.

Chapter 6 presents the quantitative analysis of the battery lifetime extension in the HESS. A method based on simulation works is introduced to enable the long-term operation of the proposed HESS and, hence, to provide rich samples for the battery lifetime analysis. By taking advantage of the battery lifetime study, the cost analysis of the SMES/battery HESS is also provided in this chapter.

Chapter 7 gives the conclusion to this thesis with a summary of the contributions and suggestions regarding future investigations.

Chapter 2 Literature Review

2.1 Introduction

The literature review provides a means of better understanding the differences among energy storage systems. In respect to the characteristics of the different kinds of ESSs, the various applications are introduced in Section 2.3. By analysing the various characterises and applications of the ESSs, it comes to the fact that the hybridization of different energy storages will create an optimal energy storage system, namely, hybrid energy storage system. An overview of the battery based HESS is given in Section 2.4. The challenges and opportunities for the SMES/battery HESS are also discussed.

2.2 Energy storage systems

Electrical Energy Storage is a process of transferring electrical energy to chemical energy, potential energy or some other form of the energy that can be stored and retrieved back to electrical when necessary [15, 17]. The history of ESS is very long. During the time of the early 20th century, lead-acid accumulators were firstly used to offer direct current. A pumped hydroelectric storage system was established in the year of 1929 as the importance of ESS has been realised. Subsequently, demand for stable electricity and application of renewable generations signify that ESS begins to obtain its reputation in the new century. Although pumped hydro systems are the primary energy storage systems in the conventional power system, a wide range of technologies

is currently available [2]. Fig. 2.1 is made based on [1, 2, 17] and lays out the different types of energy storage form in electrical power applications.

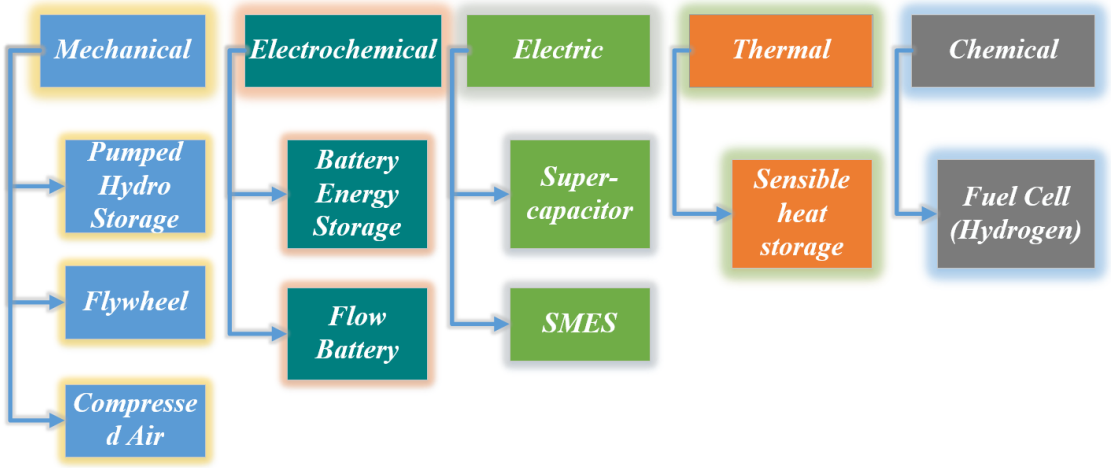

Fig. 2.1 Energy storage technologies used in the electrical power applications

The following sub-sections reviews some of the most popular types of energy storage that the short-term energy storage systems (flywheel, supercapacitor and SMES) and long-term energy storage systems (battery and pumped hydro energy storage) [50]. The main characteristics are evaluated, and the advantages and disadvantages of each ESS are listed followed by analysis.

2.2.1 The battery energy storage system

Battery energy storage systems are one of the most popular technologies used in the power systems [17]. The basic unit of battery is the cell. Each cell consists of an electrolyte having a positive and a negative electrode placed together in a sealed container and connected to the outside source or load. During the charging or discharging conditions, the electrolyte enables the exchange of ions between the two electrodes resulting in the converting of a different form of energy.

A. Lead-acid batteries

The concept of the lead-acid battery is first proposed in 1859 and since then the lead acid battery was one of the most popular and most used energy storage devices. Table 2.1 lists the main features of lead-acid batteries.

Table 2.1 Main features of lead-acid batteries

Characteristics	**References**
The lowest cost among battery storage systems	($300-600/kWh [2]; $50-100/kWh [51]; €210-270 /kWh [52]; €185/kW h [53]
High reliability	[2]
Relatively high efficiency	75–80% [52]; 70–80% [54]; 65–80% [2]
Low self-discharge	<0.1% /day [51]
Life cycle	500–1000 cycles [2]; 200–300 cycles [55]; 500 cycles [56]; 1200–1800 cycles [51]
Power density (weight-based)	180W/kg [51]
Energy density (weight-based)	30 Wh/kg [51]; 35–50Wh/kg [2]

B. Lithium-ion batteries

Compared with other batteries lithium-ion battery is a relatively new kind of technology which was firstly proposed in the 1960s and commercialised by Sony in 1991 and since then, lithium-ion battery has become one of the most commonly used batteries. This type battery is normally used in small applications, taking over 50% of small portable devices market. Also, lithium-ion batteries are positioned as the leading technology platform for the electric vehicles (EV) [30]. The recent years have witnessed a booming

development of EVs, which results in a dramatical requirement for Li-ion batteries. The main features of this type of battery are listed in Table 2.2.

Table 2.2 Main features of lithium-ion batteries

Characteristics	References
Energy density (weight-based)	80–150 Wh/kg [51]; 100–150 Wh/kg [57]; 120–200 Wh/kg [58]; 75-200 Wh/kg [2]
Power density (weight-based)	500-2000 W/kg [51]
Low self-discharge	1% /day [59]; 5% /day [51]
Life cycles	>1500 cycles [51]; 1000-10000 cycles [2]
efficiency	88% [60]; almost 100% [2]; 90-100% [51]
Cost	>$600/kWh [2]; $900-1300/kWh [51]

The lead-acid battery and the lithium-ion battery have very high energy density. Hence are widely used in the energy projects.

2.2.2 Pumped hydro energy storage (PHS)

PHS is the world widely implemented large energy storage system [61]. It takes advantage of the gravitational potential energy difference between two different levels of reservoirs. PHS station stores potential energy by pumping the water from the lower reservoir to the upper one during the off-peak hours, then releases the water to get electrical energy during the peak times. According to [15], the PHS systems represent approximately 3% of the world's total installed power capacity, and 97% of the total storage capacity. PHS gets its popularity for the high efficiency, large storage capacity, a long life and relatively low cycle cost.

Fig. 2.2 shows a typical PHS consisting of two reservoirs located at different elevations, a unit to pump water to the high elevation during the off-peak hours and a generator converting the potential energy to electricity during peak hours.

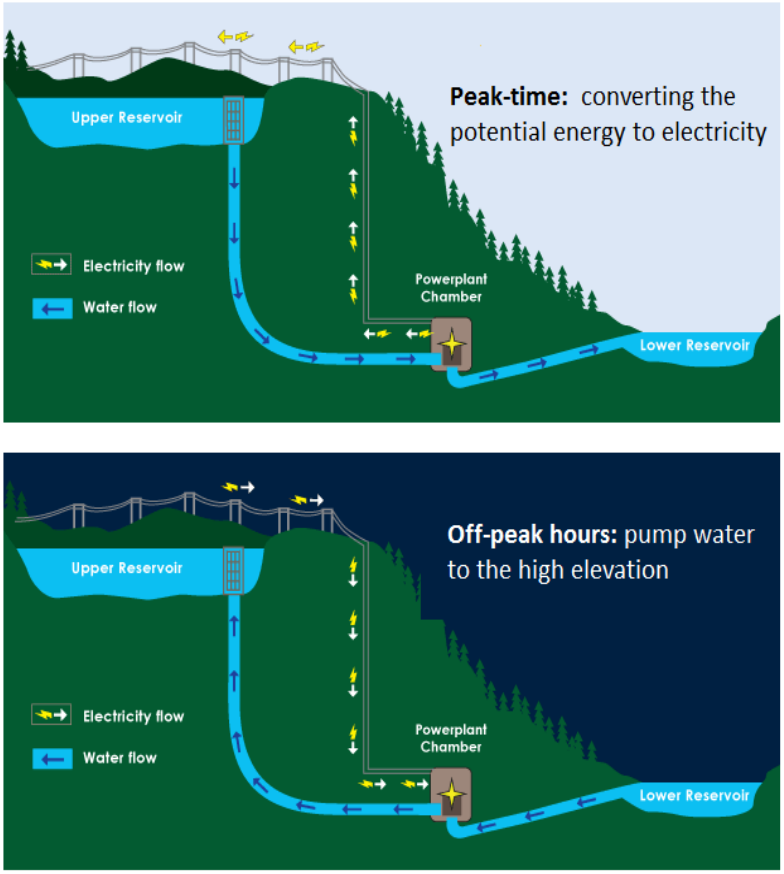

Fig. 2.2 A typical PHS system [2]

However, because of the high capital investment, environmental damages and long project lead time, PHS systems are limited in high power applications [61]. The main characteristics of the PHS are summarised in Table 2.3.

Table 2.3 Main features of PHSs

Characteristics	References
Energy rating	100–8000 MWh [2]
Power rating	10–1000 MW [15] 100–5000 MW [2], 1–4000 MW [17],
Power capacity cost	$/kW 5–100 [2], $/kW 10–12 [15], $/kW 50–100 [61]
Response time	Minutes- hours [2]

2.2.3 The flywheel energy storage system (FESS)

FESS may be the oldest ESS that can be dated back to thousands of years ago. It is a spinning mass and stores or releases energy according to its change in rotational velocity. When discharging, FESS works as a generator that generates electrical power sourcing from the rotational energy of the mass and is spun up by a motor during the charging period. FESS has high efficiency of 90–95%, long lifetime, high power density but high capital cost and high self-discharge rate (over 60%, even 100% per day) [1, 2, 15, 62]

The total power of a FESS depends on the size of the motor and the amount of stored energy depends on the size and speed of the rotor. As a result, the power rating of the FESS can be designed to be relatively high, and the stored energy is relatively low compared with the long-term storage system [33, 62].

The main features of the FESS are summarised in Table 2.4.

Table 2.4 Main features of FESSs

Characteristics	References
Energy rating	2.2–570 kWh [2]
Power rating	0.1–20 MW [2], 1.65 MW [67],
Discharge time	2.7 × 10− 7–0.25hours [2], 0.000–0.01hours [15], < 1 cycle [17]
Cost	$/kW 1000–5000 [2], $/kW 300–25,0001[11], $/kW 400–800 [17], $/kW 100–800 [8]
Efficiency	90–95% [2]
Self-discharge rate	over 60% /day [1, 15], even 100% /day [2]

2.2.4 The supercapacitor (SC) energy storage system

Unlike the conventional capacitors, the electrodes of supercapacitors are made with the porous microstructure such as carbon resulting in larger surface area hence higher capacitance to be achieved. The principle of SCs is more like the batteries that are based on electrochemical cells relying on conductor electrodes, electrolytes and a porous membrane [2, 62].

The electrons at the cathode can attract positive ions and vacancies of electrons at the anode attract negative ions. The electrically insulating separator is placed between the two electrodes allowing ions to pass. No redox-reaction occurs in the SC, and the charges are stored on the interface between the conductor electrodes. Therefore, it is also named double-layer capacitor.

The energy stored in the capacitors is proportional to their capacity, and the square of the terminal voltage see Eq. 2.1 and the capacity C see equation Eq. 2.2:

$$E = \frac{1}{2}CV^2 \quad 2.1$$

$$C = \frac{A\varepsilon_0}{d} \quad 2.2$$

Where A is the electrode-surface area; d is the distance between the electrodes; ε_0 is the vacuum permittivity. Therefore, again it highlights the main difference between capacitors and super-capacitors is the application of porous electrodes with high surface-areas which can offer higher energy densities to the system [63]. The main features of the SC are summarised in Table 2.5.

Table 2.5 Main features of SCs

Characteristics	References
Energy rating	2.2–570 kWh [2]
Power rating	5-1000kW [10] 2500kW [17]
Discharge time	< 1/4 cycle [2] Seconds–hours [67], < 1 cycle [15]
Self-discharge rate	15-20% /day [2]
Cost	$20,000 kWh [15], €6800 /kWh [69]
Efficiency	75-90% [1,10,71]

2.3.5 Superconducting magnetic energy storage

SMES is getting the popularity in recent years. SMES is a device that stores energy in the magnetic field which is created by the DC current flowing through the superconducting coils [64-67]. Fig. 2.3 shows the SMES unit (3.2 kJ) rative project between the University of Bath and China Electric Power Research Institute.

Fig. 2.3 SMES unit above the cryostat

Similar to the normal inductance coil, the energy stored in the SMES, as shown in Eq. 2.3 is the product of the self-inductance of the coil and the square of the flowing current:

$$E = \frac{1}{2} LI^2 \qquad 2.3$$

Pickard [59] states that "Flux density around 10 T at 4.2 K is able to provide energy densities of 40 MJ/m^3". SMES is well known for the high power density. The recently second-generation high-temperature superconductors (2G HTS) have been

significantly enhanced in terms of increased operational magnetic field and current density which enables SMES systems to achieve a substantially higher energy and power capacity [21]. The main features of the SMES are summarised in Table 2.6.

Table 2.6 Main features of SMESs

Characteristics	References
Energy rating	0.2-3000 kWh [2],
Power rating	100 kW–10 MW [15]
Discharge time	Milliseconds–8 s [2], seconds [86], 200kJ in 20ms [87]
Power capacity cost	$700–10,000 kWh [2], $200–300 kW [15]
Self-discharge rate	<7% /day [67]
Efficiency	>90% [21], 95-98% [84]

2.3 The applications of the ESSs

The outlook for EESs with various characteristics have been widely reported in recent years, and Table 2.7 summarises the some of the currently used EESs in power applications.

Table 2.7 Overview of current electrical energy storage applications

Applications	**Application characteristics and specifications**	**Experienced ESS technology options**

Power quality(voltage/frequency compensations) **[1, 2, 3]**	kW and up to MW, response time (milliseconds, <1/4 cycle), discharge duration (milliseconds to seconds)	Flywheels, SMES, capacitors, supercapacitors. Batteries (but have short lifetime)
Emergency back-up power **[4, 5,6, 7]**	Up to 1 MW, response time (milliseconds to minutes), discharge duration (up to 24 h)	Batteries, flywheels, flow batteries
Integration renewable smoothing intermittent **[7, 8, 9 10]**	Several kW to MW, up to 20 MW response time (milliseconds to hours), discharge duration (seconds to hours)	Flywheels, supercapacitors, and SMES. Batteries (but have short lifetime)
Bridging power [7, 11, 12]	kW–10 MW, response time (up to 1 s), discharge duration (seconds to hours)	Batteries, flow batteries supercapacitors
Peak shaving and Load levelling **[1, 7,13, 14,15]**	MW level response time (minutes), discharge duration (up to hours and even more)	PHS, and batteries;
Transmission and distribution deferral **[1, 7,16,17,18,19]**	kW to 100 MW, response time (milliseconds - minutes), discharge duration (milliseconds to minutes)	PHS and batteries, SMES and fuel cells flywheels
Energy management **[8, 20, 21]**	Large (>100 MW), medium/small (~1–100 MW), response time (minutes), discharge duration (hours–days)	Large: (PHS); Small: (batteries, flow batteries)

As shown in Table 2.7 the response speed of the energy storage technology is directly linked to its applications in the power system. In respect of the discharge durations and the storage characteristics, the ESSs can be classified into two groups as shown in Fig. 2.4.

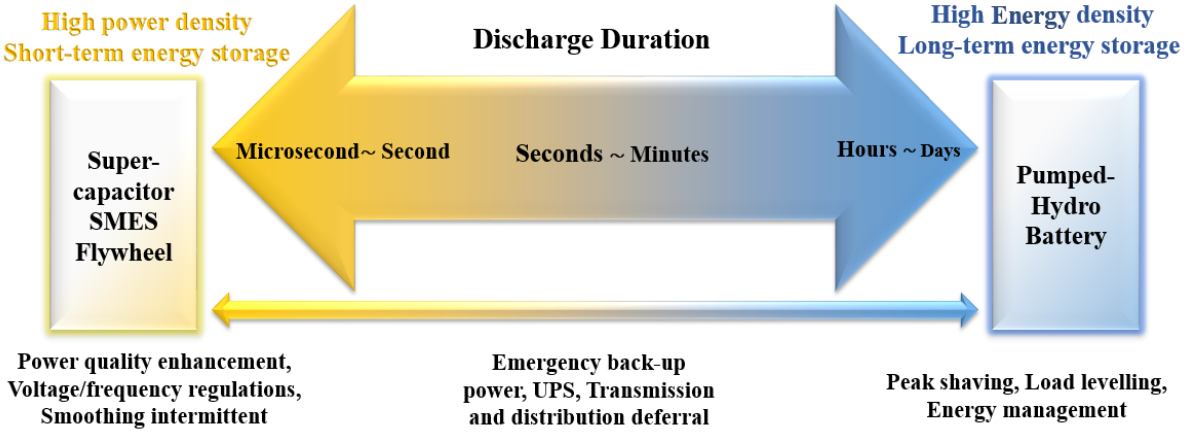

Fig. 2.4 ESS classification according to discharge speed

In Fig. 2.4 ESS technologies are categorised into those are intended for high power ratings with a relatively small energy capacity (short-term energy storage system) making them suitable for power quality or uninterruptible power supply applications, and those have a large energy density (long-term energy storage system) and designed for long-term usage. It should be figured out that, although the battery is regarded as the long-term energy storage system and has high energy density, it can be designed to have high power capacity and controlled to achieve fast discharge. However, in these cases, a great many of battery cells is need to provide the high power capacity. Moreover, the short-term high power demands seriously accelerate the battery degradation process. Hence, the battery is not suggested to be used as the short-term energy storage system.

By analysing the various characterises and applications of the different energy storage systems, it comes to the fact that the combination of the short-term energy storage and the long-term energy storage will create an optimal energy storage system, namely, hybrid energy storage system.

2.4 The hybrid energy storage system

2.4.1 Overview of the HESS

The idea of the HESS lies on the fact that some ESSs may have complementary characteristics in terms of power and energy density, life-cycle, response speed, and so on [14, 68]. Therefore, it comes to the concept of the HESS that combine two kinds of complementary energy storage technologies achieving an optimised system which has the advantages of both primary energy storage systems meanwhile complementing the disadvantages of each ESS.

The battery, characterised by high efficiency and large energy density, is regarded as the most flexible ESS and increasingly being used in many power applications [17]. The disadvantages of the battery such as the low power density and the limited cycle life can be exactly addressed by the short-term energy storage systems. Therefore, in this study, it is reasonable to select the battery as the long-term energy storage in the HESS design. In fact, the battery-based hybrid energy storage system is the most used scheme in the literature. Table. 2.8 summarises the update hybrid design in different applications.

Table 2.8 The summary of the battery based HESS in different applications

HESS scheme	Applications	References
Battery and supercapacitor	Photovoltaic systems; Wind energy systems; Hybrid	[23, 25, 26, 32, 40-42, 46, 47, 49, 63, 69-75]

	wind-solar systems; EV; Microgrids; UPS	
Battery and Flywheel	UPS, EV, wind applications, domestic usage	[24, 76, 77]
Battery and SMES	Photovoltaic systems; Wind energy systems; EV; Microgrids; CHP system	[14, 16, 22, 44, 78-82]

The flywheels have high efficiency of 90–95%, long lifetime and high power density [1, 2, 15, 62]. However, the most severe drawback of flywheels is the high power losses because of the high self-discharge rate (over 60%, even 100% per day) [76, 83]. This disadvantage makes the flywheel and the battery hybrid design less attractive than the SMES/battery and the SC/battery.

The battery and supercapacitor HESS is regarded as the most mature hybridization among the literature. Indeed, a large number of works can be found to describe the battery and SC HESS, and they are ranging from the HESS modelling, control method design, power management, sizing study, topology optimisation and so on. Then, it comes to the question that why to study the SMES/battery hybrid system in this thesis.

2.4.2 Why choose SMES as the short-term ESS in the HESS.

A. Advantages of SMES

A typical SMES is mainly composed of three components: superconducting coils, cooling system and control systems. The cooling system is necessary to keep the coil

in the superconducting state. Even taking into account the energy consumed by the cooling system and other kinds of energy losses such as the control system losses, SMES still performs in very high energy efficiencies [21]. This configuration resulting in over 90% efficiency of energy converting [21] and 95%–98% efficient in storing electricity [2, 84].

The SMES is able to make the rapid and independent power response possible in all the four quadrants [85]. Hence, SMES has broad applications associated with power systems. Since there is almost no fatigue cumulative damage in SMES, it has the longest lifetime compared with all the other ESS technologies. Report [86] states SMES has "unlimited number of charge and discharge cycles".

SMES is able to respond to the requirement in milliseconds level because the conversion of energy stored in SMES is an electrical process. The rated capacity of SMES ranges from 100 kW to 10 MW, and tests have shown that SMES can inject the rated power in a few seconds before being discharged [86]. Report [87] tested a 1 MW SMES unit and it could be charged to 200 kJ in only 20 ms. Also, SMES seems more environmentally friendly since they do not have any toxic chemical materials [21].

B. Challenges and opportunities of the SMES/battery HESS

The high cost is the biggest challenge for the wide application of such advanced technology: the capital power cost ranges between $1000 and $10,000/kWh [62]. While, in the hybrid energy storage scheme, with the integration of the battery the size requirement for both the SMES and battery can be dramatically reduced. Also, compared with the battery only system, the hybrid design has the advantage of extending battery lifetime. One of the reasons that this study proposes a battery and

SMES hybrid energy storage system is to reduce the rated energy requirement of SMES and hence to reduce the investment on SMES system.

Buckles said in [88] that we should not stop to do research on superconductor just because it is expensive. With the fast development of superconductor manufacturing technology, there are more and more commercial companies around the world being able to produce the cheap superconducting tape, such as SuNam and Shanghai Superconductor [89, 90]. The price of the superconductor is reduced from $60 per meter in 2012 to $22 per meter in 2016, which is a significant cost reduction in the last five years. Some published works also make the estimation that in the future, it is achievable to decrease the price of superconductor less than $10 [91, 92]. Therefore, with the continuous development of superconductive material, it could be known for sure that the cost of SMES could be further reduced. With the continuous developing of superconductive materials science many published researches [19, 20, 93, 94] have shown positive cost-effective analysis of SMES. Also, as already been discussed in Chapter 1, the technologies for the SMES/battery hybrid energy storage system is not mature enough to make this HESS available to the customers. Hence, it is meaningful to investigate the technologies of the SMES/battery HESS.

Chapter 3 The Battery Lifetime

3.1 Overview

The extension of battery lifetime is one of the key metrics for assessing the benefits of the hybrid energy storage system [16, 23, 43, 70, 73, 95, 96]. A novel battery lifetime is, therefore, developed by advancing the previous rain-flow cycle-counting method. The improvement of the new battery lifetime model is proved by comparison with the previous method. Also, case studies are described in this chapter to verify the new battery lifetime evaluation method.

3.2 The battery lifetime model.

As the improvement of battery lifespan is one of the key advantages of the proposed hybrid energy storage system, it is necessary to incorporate a battery life prediction model in this research. The life of the rechargeable battery is defined as the period that the battery remains serviceable before the predefined minimum capacity (normally 80%) is reached [97]. Various kinds of battery lifetime models are available. However, the capacity fading mechanism is so complicated that it is currently difficult to create a practical model which considers the extreme non-linearity of many underlying ageing processes [35].

The method of cycle counting has already been successfully employed in battery lifetime estimation application. In addition, the battery life prediction method has been successfully applied in a commercial program known as HYBIRD2 [98]. However, the

previous works simply counted the number of cycles for each level of depth of discharge. This means that the conventional battery life model only regarded the range of DOD of each cycle as the factor related to battery lifetime, but neglected other factors such as the discharge rate. James F. Manwell proposed an improved model in [98] by adding the effect of the mean value of each charge/discharge cycle, but this improved model did not consider the discharge rate, which has a great impact on the battery life.

The discharge rate is referred to as the discharge current and is often expressed as a C-rate by normalised means. The C-rate is normally defined as the rate at which a battery is discharged [99]. Many research works have shown that higher discharge rates would decrease the battery lifetime dramatically. For example, experiments were carried out in [100] to study the capacity fade of Sony 18650 batteries under different C-rates. The results showed that a battery lost 9.5% of its capacity after the full 300 cycles at 1 C-rate, but 16.9% at 3 C-rate. Therefore, the impact of C-rate on battery life is so great that it should not be ignored.

This study proposes a novel battery life model which has quantified both the effect of battery discharge rate and depth of discharge and gives a more precise prediction for battery lifetime. Error analysis has been done by means of case study.

3.3 The rain-flow cycle-counting algorithm

3.3.1 The principle of the rain-flow cycle-counting algorithm

The rain-flow cycle-counting algorithm is usually used for analysing the fatigue data and was firstly used in metal fatigue estimation. In this research, this method is used to

extract the irregular charging and discharging cycles that the battery experienced during the simulation period.

Basically, the cycle counting can be achieved by the following three steps, as shown in Fig. 3.1.

- Firstly, the data (for the battery, the data is the DOD that presents the battery charge/discharge cycles) are pre-processed by searching for adjacent data points with reverse polarity so that the local maxima and minima can be found and stored in a matrix.
- Secondly, compose full cycles by analysing the turning points and combine these sub-cycles to obtain full-cycles together with the summing up of the amplitudes.
- Thirdly, extract and count the number of cycles in varying amplitude and store them for later use.

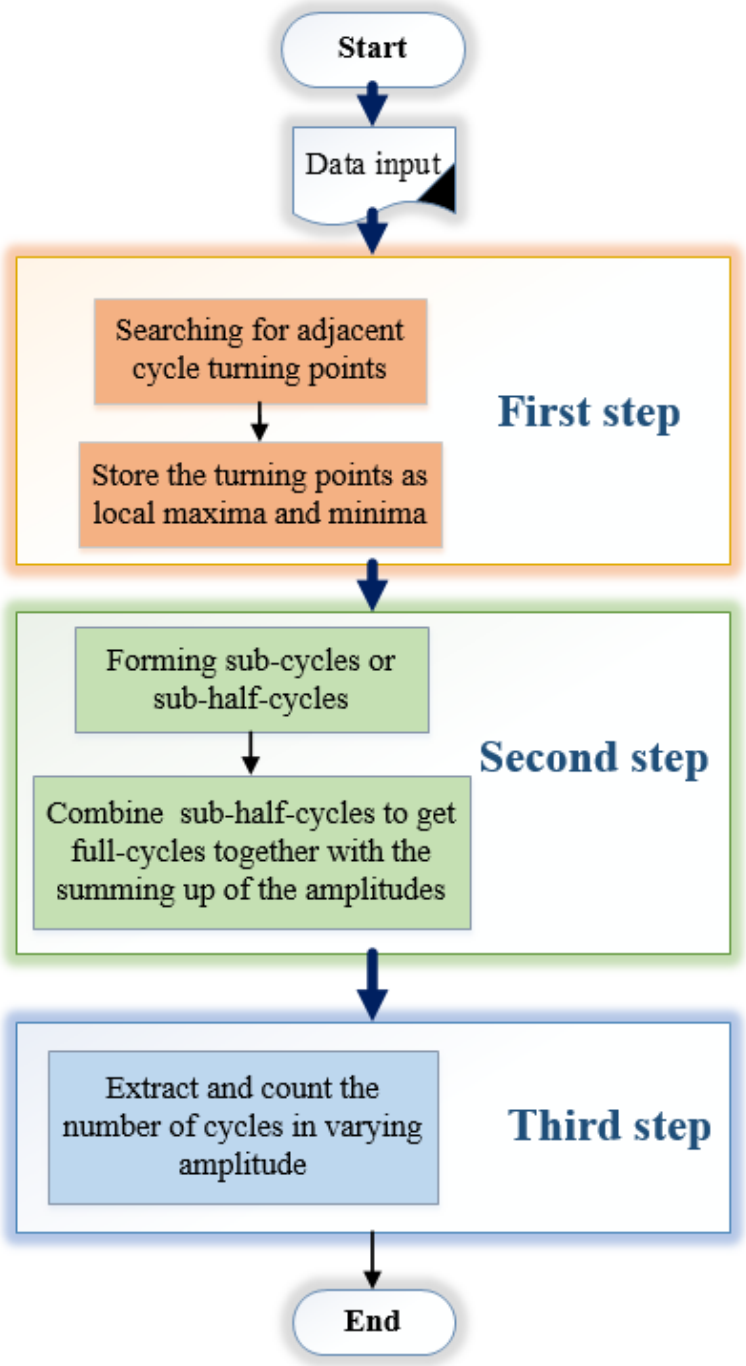

Fig. 3.1 The principle of the previous rain-flow cycle-counting algorithm

As a result, the complex data can be resolved into a set of equivalent sub-half-cycles and rearranged to compose the full cycles in different amplitude. To give a better

introduction to the rain-flow cycle-counting method, a data processing example is given, as shown in Fig. 3.2 and Fig. 3.3.

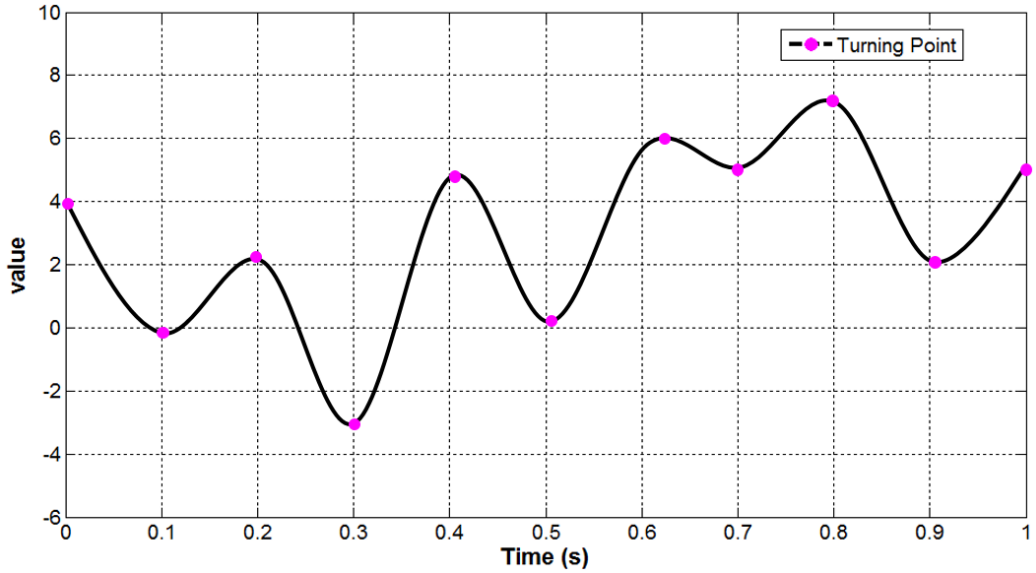

Fig. 3.2 Example data for rain-flow cycle-counting

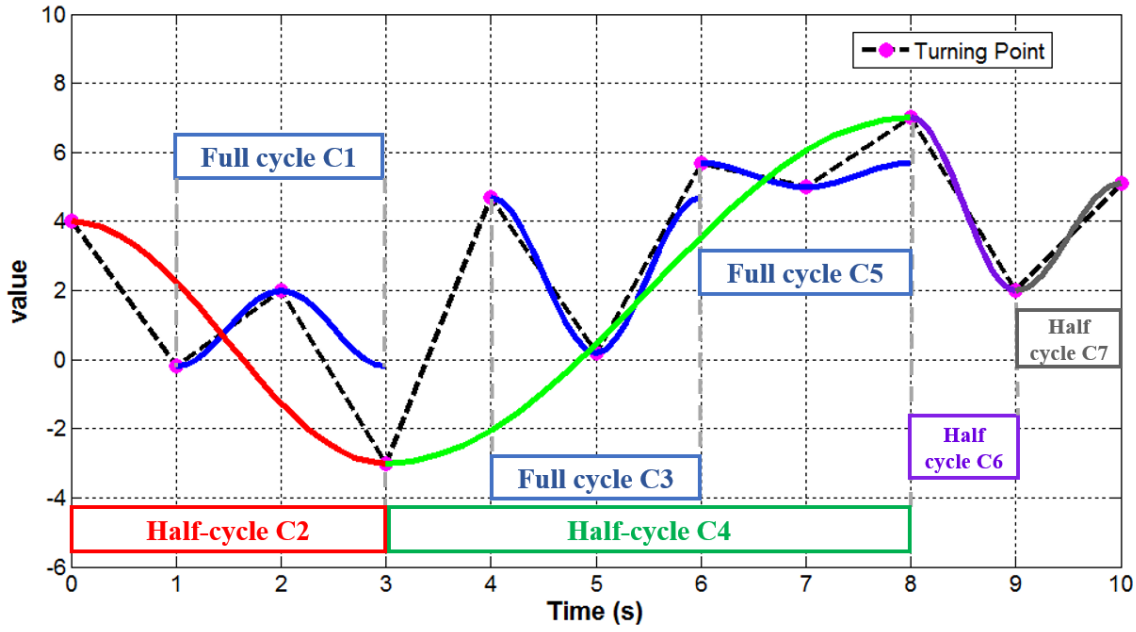

Fig. 3.3 Results from the rain-flow cycle-counting

As can be seen from Fig. 3.2 and Fig. 3.3, the exemplary signal is resolved and recombined by several cycles and half-cycles. Together with the cycle numbers, the amplitudes of these cycles are also stored in the algorithm. Table. 3.1 and Fig. 3.4 illustrate the counting results.

Table 3.1 Counting results from the rain-flow cycle-counting

Labels (Cx)	**C1**	**C2**	**C3**	**C4**	**C5**	**C6**	**C7**
Amplitude	2.2	7.0	4.5	10	0.7	5.0	3.1
Number of cycles	1	0.5	1	0.5	1	0.5	0.5

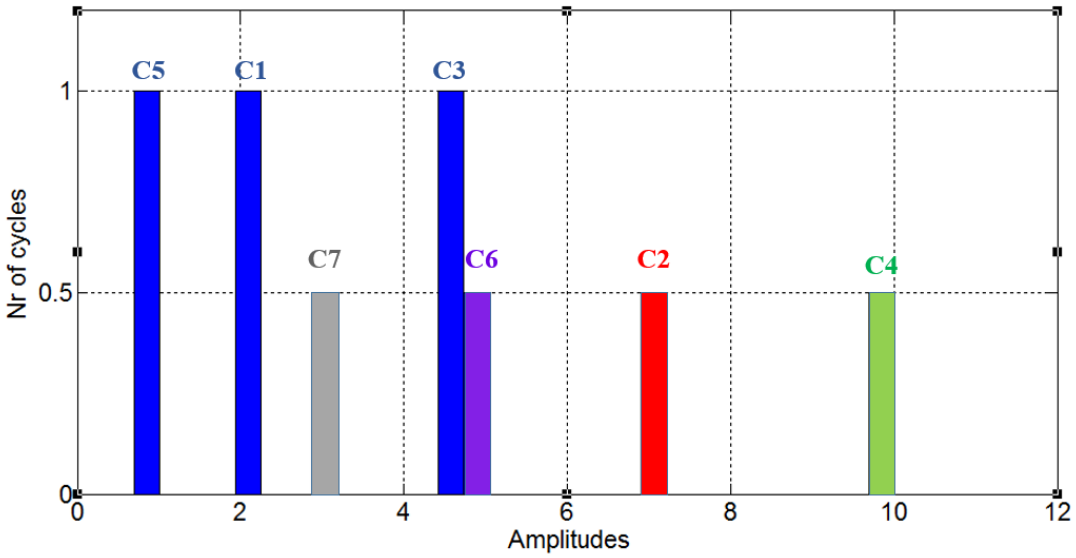

Fig. 3.4 Counting results from the rain-flow cycle-counting

The battery charges and discharges to meet the power requirements, which will return the data sheet of battery state of charge (or depth of discharge) with time series. Therefore, by using the rain-flow cycle counting algorithm, the battery depth of discharge can be resolved into a range of sub-cycles with amplitudes. If the lifetime degradation of each sub-cycle can be calculated, the total battery lifetime reduction can be obtained. However, it should be noted that the battery lifetime model based on the previous rain-flow cycle-counting method is only able to evaluate the impact of the DOD of each cycle, but ignores the very significant C-rate factor, as mentioned earlier. Therefore, it forms the main contribution of this chapter in that a new battery lifetime model is developed by adding the evaluations of C-rate into the previous method.

3.3.2 The modified the rain-flow cycle-counting algorithm

The discharge rate is in accordance with the discharge current and is often expressed as a C-rate by normalised means. The C-rate can be calculated based on Eq. 3.1. Therefore, the modified rain-flow cycle-counting algorithm is required, not only to give the amplitude but also the C-rate of each sub-cycle as well. The modified rain-flow cycle-counting algorithm is illustrated in Fig. 3.5. For example, a battery discharges 20% of its capacity in 1800s, then the C-rate can be obtained as 0.8 ($3600\times0.2/1800=0.8$).

$$C\text{-}rate=3600\ A/T \tag{3.1}$$

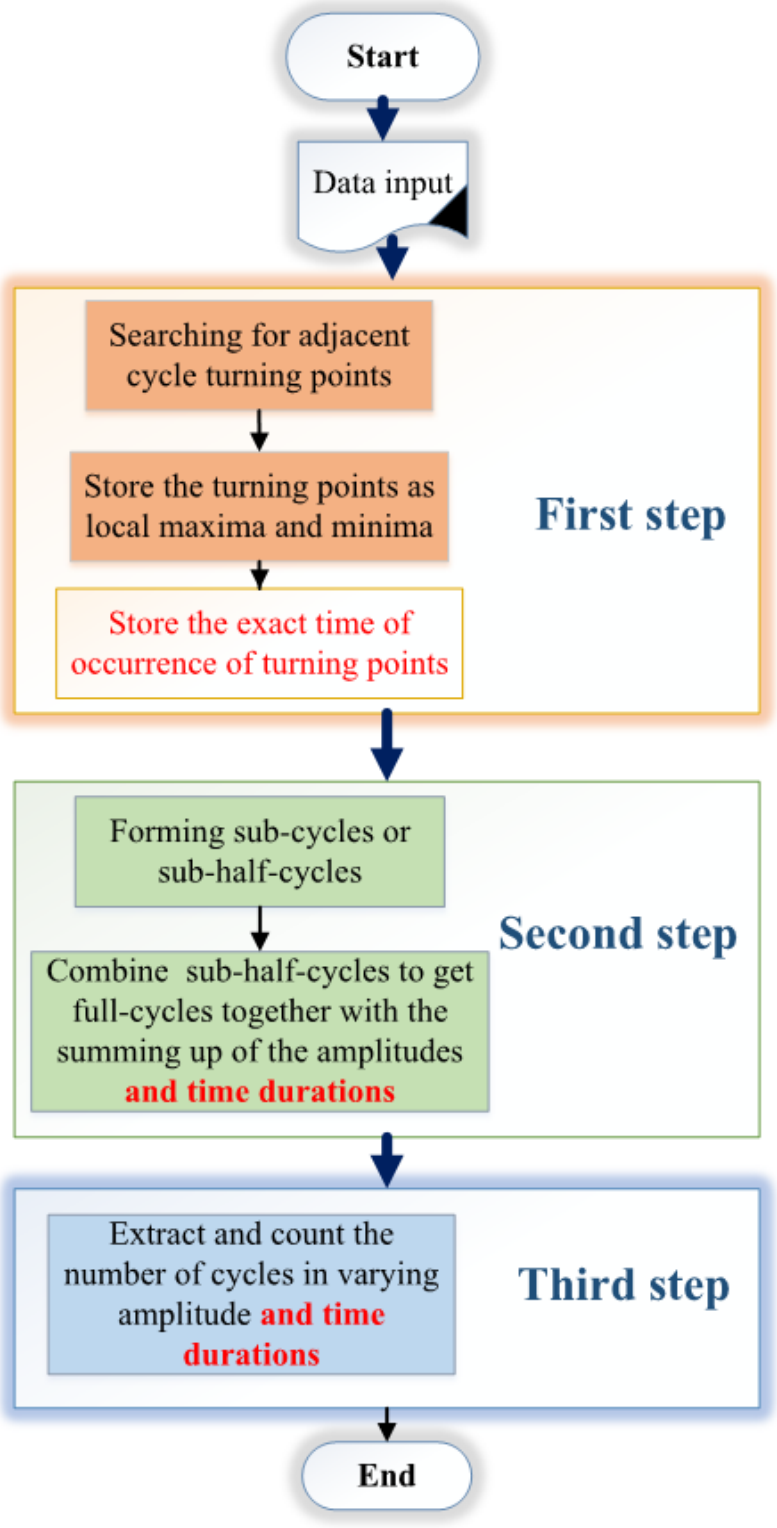

Fig. 3.5 The principle of the modified rain-flow cycle-counting algorithm

Firstly, similar to the previous method, the data of the battery are pre-processed by searching for adjacent data points with reverse polarities so that the local maxima and minima can be found and stored in a matrix. In the new method, the exact time of occurrence of turning points is also stored in the same matrix. Secondly, full cycles are obtained by analysing the turning points and combining these sub-cycles to obtain full-cycles together with the summing up of the amplitudes and time durations. Thirdly, the number of cycles in varying amplitude and time duration are extracted and stored for later use. For the same signal, as shown in Fig. 3.2, the modified algorithm gives more information including the C-rate of each cycle shown in Table. 3.2.

Table 3.2 Counting results from the new rain-flow cycle-counting

Labels (Cx)	**C1**	**C2**	**C3**	**C4**	**C5**	**C6**	**C7**
Amplitude	2.2	7.0	4.5	10	0.7	5.0	3.1
Number of cycles or half-cycles	1	0.5	1	0.5	1	0.5	0.5
Begin time of extracted sub-cycle	1	0	4	3	6	8	9
Period of a cycle	2	6	2	10	2	2	2
C-rate	2.2	2.3	4.5	2	0.7	5	3.1

3.4 The novel battery lifetime modelling

For a rechargeable battery, the active substance transformed with each cycle is proportional to the range of discharge [101]. Therefore, the deeper the battery is discharged, the more lifetime will be consumed. Battery manufacturers usually provide an experiment datasheet to describe the relationship between battery cycle life and DOD. Fig. 3.6 gives a typical cycles-to-failure (CTF) vs. DOD curve obtained by curve fitting using experiment data.

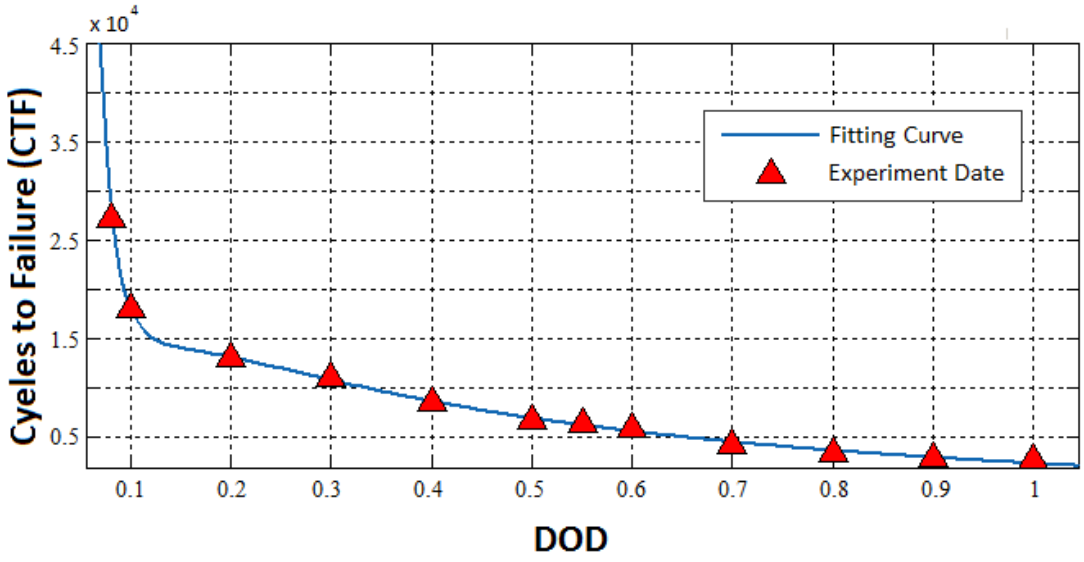

Fig. 3.6 Cycles to Failure vs. DOD curve [14]

Battery CTF is defined as the number of cycles that the battery can be charged and discharged before the end of life condition is reached [73]. For example, as can be observed in Fig. 3.6, the battery would undergo over 5000 cycles at 60% DOD before it reached the end of life. A logarithmic polynomial function F_{CD} is used to describe the relationship between the CTF and the DOD, $F_{CD} = f(CTF, DOD)$:

$$\text{CTF}=f_{CD}(DOD) = a_0+a_1 DOD^{-1} + a_2 DOD^{-2} + a_3 DOD^{-3} \ (0<\text{DOD}<1) \quad 3.2$$

Where $a_0 - a_3$ are the curve fitting coefficients, and the values are -4790, 7427, -1077, 55.4, respectively.

Previous work [100, 102, 103] has shown the functional relationship of the capacity retention and discharging current. Based on the experiments in [103], this study defines the function F_{CC} to show that the capacity retention of a Li-ion battery will decrease with the increase of the discharging current, $F_{CC} = f(C-rate, Capacity)$:

$$Capacity = f_{CC}(C-rate) = b_0 + b_1 e^{-[(C-rate-b_2)/b_3]^2} \quad 3.3$$

Where $b_0 - b_3$ are the curve fitting coefficients and the values are 0.8800, 0.0929, -0.0639, -1.3770, respectively.

In general, the capacity retention of a Li-ion battery is proportional to the battery life cycles [104]. Function $F_{CTFC}$is defined in this study to describe how the CTF changes with the capacity of Li-ion battery, $F_{CTFC} = f(CTF, Capacity)$:

$$Capacity = f_{CTFC}(CTF) = c_0 + c_1 \cdot CTF \quad 3.4$$

Where c_0, c_1 are the curve fitting coefficients and they are -0.00177 and 0.96, respectively.

As a result, for a charge/discharge cycle with the given range of DOD and C-rate, the objective function can be obtained by combining the Eq. 3.2-3.4, $F_{CDC} = f(CTF_C, DOD, C-rate)$:

$$CTF_C = f_{CD}(DOD) \cdot f^{-1}{}_{CTFC}(f_{CC}(C-rate)) \quad 3.5$$

CTF_C is the corrected CTF number and the degradation factor is defined as η, which is used to describe the battery degradation in a cycle at certain range of DOD and C-rate, then:

$$\eta = 1/CTF_C \quad 3.6$$

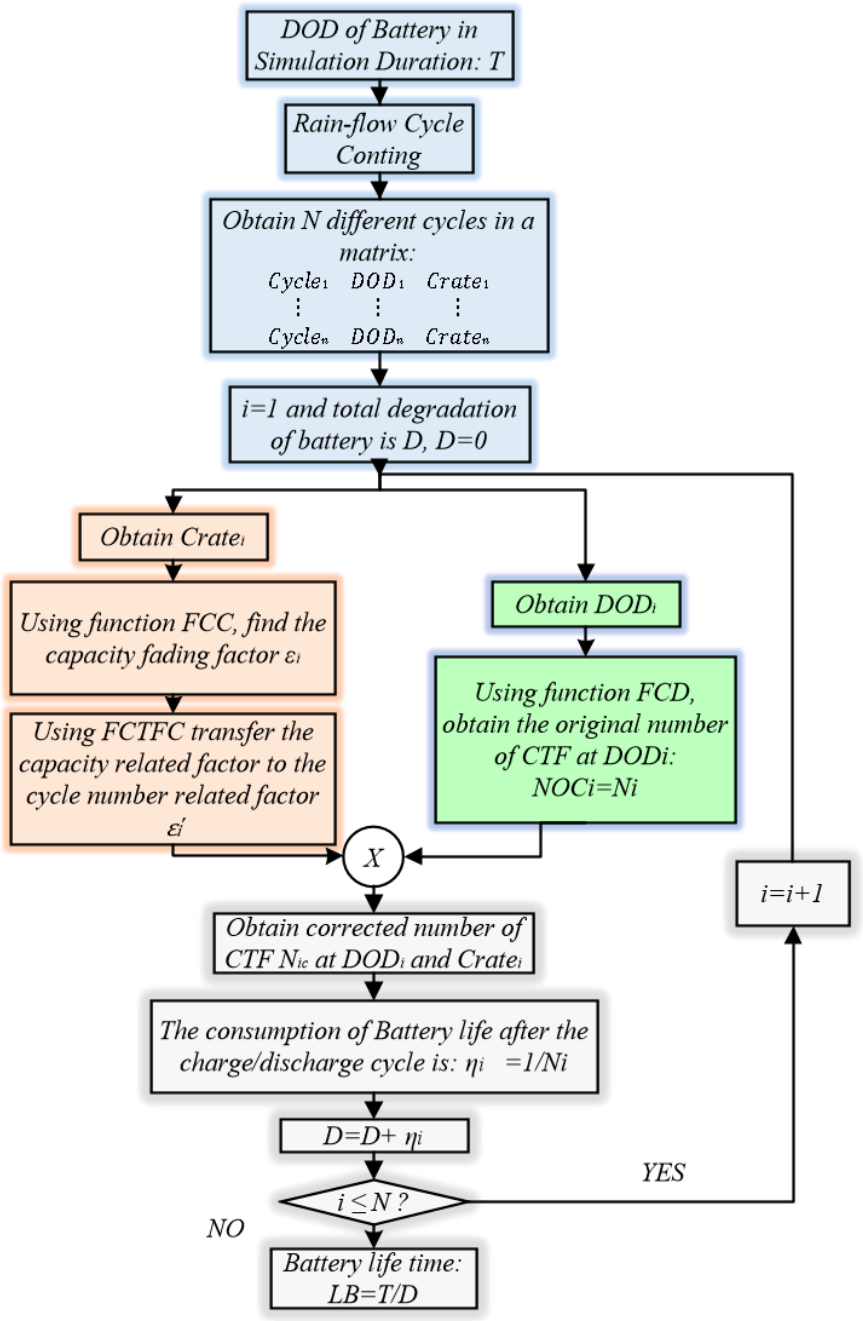

Fig. 3.7 Algorithm of the novel battery lifetime model

The algorithm of the novel battery lifetime model is shown in Fig. 3.7. As shown in this figure, the rain-flow cycle-counting algorithm processed the data of battery DOD thereby obtaining the different cycles varying in different ranges of DODs and C-rates in a matrix. Take *ith* cycle as an example:

Substitute DOD_i into F_{CD} obtaining the original number of cycles N_i. Similarly, F_{CC} generates the capacity fading factor ε_i ($\varepsilon_i = f_{CC}(C - rate_i)$) at the given $C - rate_i$. This factor is a capacity related factor, hence F_{CTFC} is needed to transfer it into a cycle number related factor ε_i'($\varepsilon_i' = f^{-1}{}_{CTFC}(f_{CC}(C - rate))$). The original number N_i multiplied by factor ε_i' resulting in the corrected number of cycles N_{ic} at $C - rate_i$ and DOD_i .Therefore, the consumed fraction of battery life after the charging/discharging cycle i is $\eta_i = 1/N_{ic}$. The total number of different cycles is n, hence, the total degradation D is:

$$D = \sum_{i=1}^{i=n} \eta_i \quad 3.7$$

Assuming the simulation duration is T, the battery lifetime can be estimated as:

$$L_B = T/D \quad 3.8$$

It should be noted that the battery lifetime is predicted based on the room temperature in this study.

3.5 Case study

The novel battery lifetime model is valued for taking the discharging rate into account. A case study is carried out to prove the validity of the new model. Li-ion battery accelerated ageing tests in [105] showed results that described the normalised capacity retention declined as a function of C-rates at a fixed DOD of 0.3. The capacity retention limit is defined as 80%, which means the end of battery life.

Based on [105], the experimental battery lifetime at different C-rate can be obtained as shown in Table 3.3.

Table 3.3 Experimental battery lifetime at different C-rate[105]

C-rate	**0.6**	**1.2**	**1.5**	**1.8**
Lifetime(h)	8800	4300	3300	2800

The battery DOD data can be generated based on the same situation with the experiment. For example, if the DOD is set as 0.3 and C-rate as 1.5, the SOC curve as shown in Fig. 3.8 can be obtained.

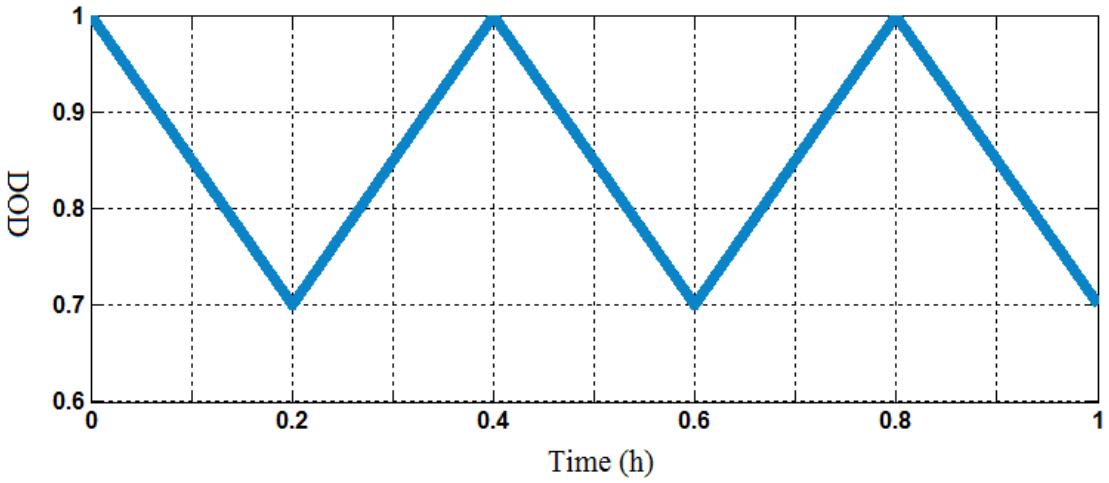

Fig. 3.8 Example of the DOD data at C-rate 1.5

Using the Eq. 3.4, C-rate=1.5 means that battery is discharged of 30% of its capacity in 0.2 hours hence the whole cycle time is 0.4 hour. Based on the algorithm illustrated in Fig. 3.7, if the DOD is set as 0.3 and C-rate as 1.5 the following data can be obtained in Table 3.4:

Table 3.4 Computed result based on the novel model at a given C-rate 1

Original cycle number	Capacity fading factor	Cycle related factor	Corrected cycle number	Degradation factor η	Cycle time(h)	Battery life (h)
10052	0.906	0.86	8600	1.162e-4	0.4	3440

The error between the calculation and experiment is 4.2%, which is acceptable. However, if the impact of discharge rate is not considered, the lifetime is 4021 h (cycle time 0.4 h multiplied by original cycle number 10052) and the error is 21.8%. Applying the same process to the other three situations, Table 3.5 and Fig. 3.9 can be constructed as follows:

Table 3.5 Comparison of experimental results with the results from novel battery lifetime model and results from the previous model

Crate	Experimental battery lifetime(h)	Novel model based battery lifetime(h) and error	Cycle time T(h)	Previous model based battery lifetime(h) and error
0.6	8800	9185, 4.38%	1.00	10052, 14.2%
1.2	4300	4430, 3.02%	0.50	5026, 16.8%
1.5	3300	3440, 4.2%	0.40	4021, 21.8%
1.8	2800	2930, 4.6%	0.34	3418, 22.1%

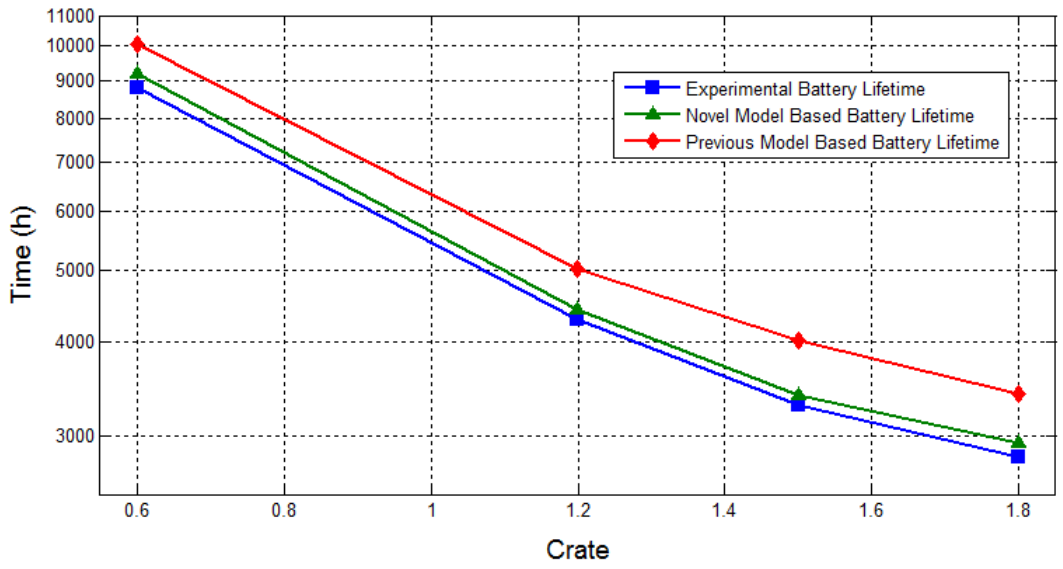

Fig. 3.9 Comparison of battery lifetimes from experiments (blue), the novel model (green) and the previous model (red)

Obviously, this new algorithm, which has taken the discharge rate into account, generates fewer errors and gives a more precise prediction of battery lifetime.

3.6 Conclusions

The improvement of battery lifetime is one of the key advantages of the proposed SMES/battery HESS. The prediction of the battery lifetime is, therefore, very necessary in this study to evaluate the HESS design. A novel battery lifetime model based on a modified rain-flow cycle-counting algorithm is presented in this chapter. The new method advances the previous ones by adding the C-rate into the consideration of the battery degradation process and, hence, returns a more accurate prediction of battery lifetime. As can be seen from the battery lifetime model, the cycles-to-failure curve is a very important reference for lifetime prediction. Hence, it should be noted that insufficient cycles-to-failure data may result in the errors in the prediction.

Chapter 4 Methodologies

In this chapter, the development of the power management strategy, the sizing study and the hybrid control method are introduced in details.

4.1 Power management strategy

To achieve the active combination of two kinds of ESSs, an overall power management method, which is designed based on the different characteristics of SMES and battery, is essential. The hybrid control for the SMES and battery is also developed based on the power management method. In this study, the power management strategy should be designed to meet the following constraints:

- The HESS should meet the system power requirement;
- The strategy is able to arrange power contributions according to the characteristics of different energy storage devices;
- The battery is protected from high-frequency charge/discharge and high currents;
- The SMES is prevented from long-duration discharge;

To fulfil the functions shown above, three kinds of power management strategies are developed and compared in this study: the frequency-dominant strategy, SMES fully active strategy and power-dominant strategy. These three methods are introduced in detail in this chapter and the advantages and disadvantages of each method are described. These power management strategies have different performance in different

power applications. A case study based on the electrical bus system is introduced to give a detailed implementation of the power-dominant strategy.

4.1.1 Frequency-dominant strategy

To ensure the security of supply by preventing the load from being unsupported, the battery is typically integrated into the system to store power at times when there is a surplus and to release it during a deficit of available power [15]. However, the variation of renewable power means the battery may undergo high-frequency charge/discharge cycles. In the SMES/battery hybrid design, the high-frequency power fluctuations dealt by the SMES and battery are protected from frequent cycling processes. Hence, it returns to the principle of the frequency-based power management strategy in that the short-term ESS, such as SMES, compensates the high-frequency power and the long-term ESS, such as batteries, offers long-term energy support. Power filtration method, which takes advantage of the lowpass filtering characteristics of the SMES, is usually used to implement the frequency-based power management strategy. In this study, this kind of power management method is designed and used in an isolated wind power system, as shown in Fig. 4.1

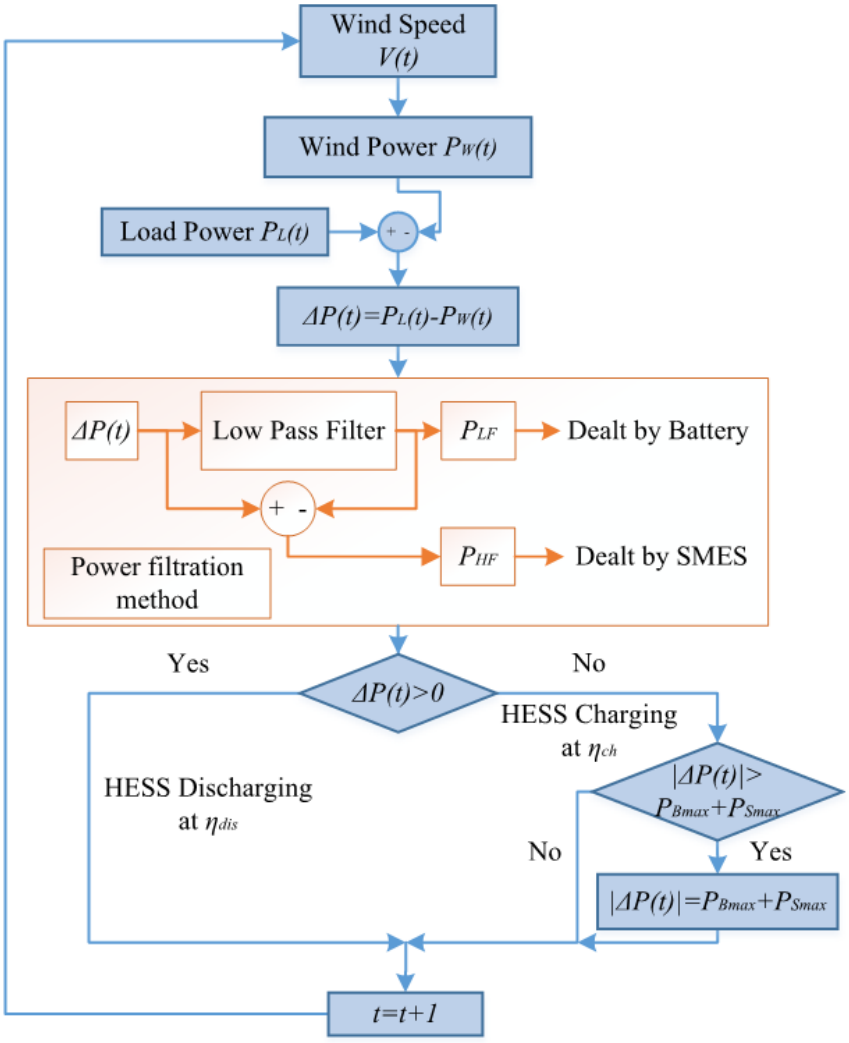

Fig. 4.1 Frequency-dominant power management strategy in an off-grid wind application

- During the windy period, when the generated power from the wind turbine $P_w(t)$ is greater than the load demand $P_L(t)$ ($\Delta P(t) = P_L(t) - P_w(t), \Delta P(t) < 0$), the HESS will be charged by the excess power ($\Delta P(t)$). The high frequency component (P_{HF}) of the excess power will charge the SMES, while the battery will be charged by the low frequency component (P_{LF}) of $\Delta P(t)$. If the excess power is greater than the rated power of the SMES (P_{Smax}) and battery (P_{Bmax}), the over-charging protection will come into effect and make $|\Delta P(t)| = P_{Smax} + P_{Bmax}$.

- During the generation deficiency condition, where the wind power cannot meet the load demand ($\Delta P(t) = P_L(t) - P_w(t), \Delta P(t) > 0$), the HESS is designed to be discharged and support the required power deficit $\Delta P(t)$. The battery will deal with the long-term component and SMES will supply the short-term component.

As shown in Fig. 4.1, this strategy is simple and achieves the objectives: meeting the load demand and balancing the power; successfully combining long-term and short-term storage systems. Also, the battery lifetime will be improved by reducing the charge/discharge frequency. However, compared with the other two methods, the service efficiency of SMES in this strategy is not very high.

4.1.2 SMES fully active strategy

In the frequency-dominant power management method, the battery and the SMES are in parallel positions and the power disturbances are seen by the SMES and the battery at the same time. The advantage of this design is that the battery can be protected from the short-term power fluctuation. However, in this method, the SMES is controlled only to deal with the high-frequency components, which cannot fully take advantage of the benefit of SMES. The SMES has unlimited charge/discharge cycles and high current handling capability and can be used to respond to any requirements without capacity degradation. Therefore, the SMES fully active strategy proposes a new dispatch of the overall power, as shown in Fig. 4.2: the SMES responds to the power surplus/deficiency directly and the battery works as an energy buffer to the SMES.

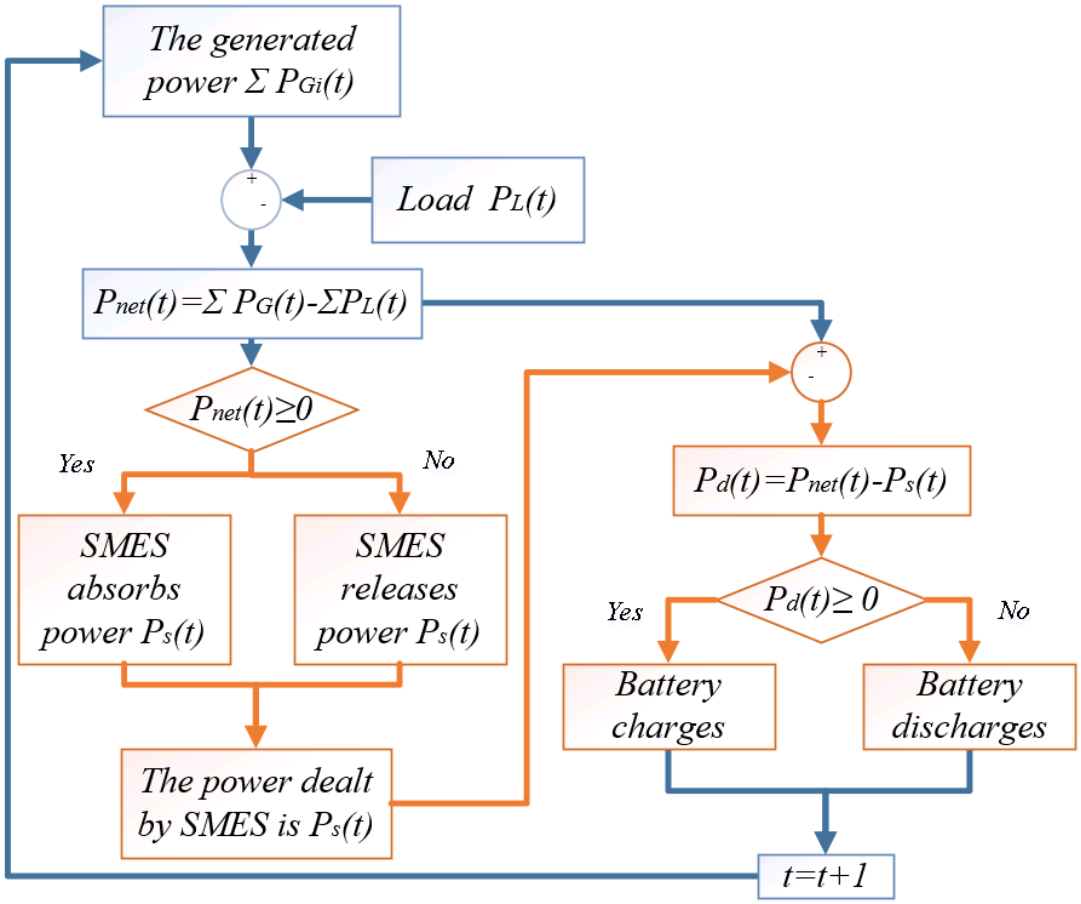

Fig. 4.2 SMES fully active power management strategy

As shown in Fig. 4.2, given the varying load power requirements, instantaneous net power can be obtained: $P_{net}(t) = \sum P_G(t) - \sum P_L(t)$. The SMES will come into action depending on the value of the net power: if $P_{net}(t) > 0$, it means the generated power is greater than load demand and the SMES will be charged, otherwise the SMES will discharge. Assuming the power dealt by SMES is $P_s(t)$, then it obtains the power deficiency $P_d(t) = P_{net}(t) - P_s(t)$ and the battery is expected to handle this amount of power. In this way, the SMES is fully active to the power disturbance and the energy of the SMES is buffered by the battery.

The proposed scheme is able to fulfil all the power management requirements of the hybrid energy storage system. Meanwhile, the SMES is fully used. However, the

disadvantages are also obvious. As can be seen from the design, the SMES is active all the time during the operation, which means exacting requirements on both safety and stability of the SMES operation. As can be seen, the SMES fully active PMS is very suitable for small-scale power applications.

4.1.3 Power-dominant strategy

The frequency based and the SMES fully active power management strategy are very straightforward that they mainly distribute the power demand into two different parts according to the different characteristics of the ESSs. However, in some power applications such as an electrical vehicle system, the power situation is so complicated that simple management strategies can hardly achieve an optimal dispatch, hence the power-dominate strategy. The power-dominate method makes decisions not only based on the different features of the ESSs but also on the instantaneous power demand. In the method, the varying power is classified by several sub-levels and the SMES and the battery are controlled to perform different charge and discharge strategies in the sub-levels. An example of the power-dominate management strategy for the SMES/battery used in an electrical bus system is illustrated in the Fig. 4.3 and Fig. 4.4.

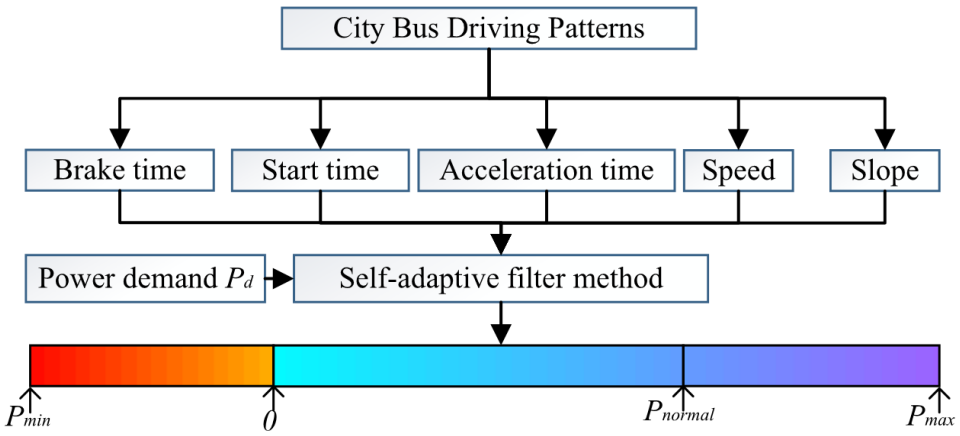

Fig. 4.3 Power grading.

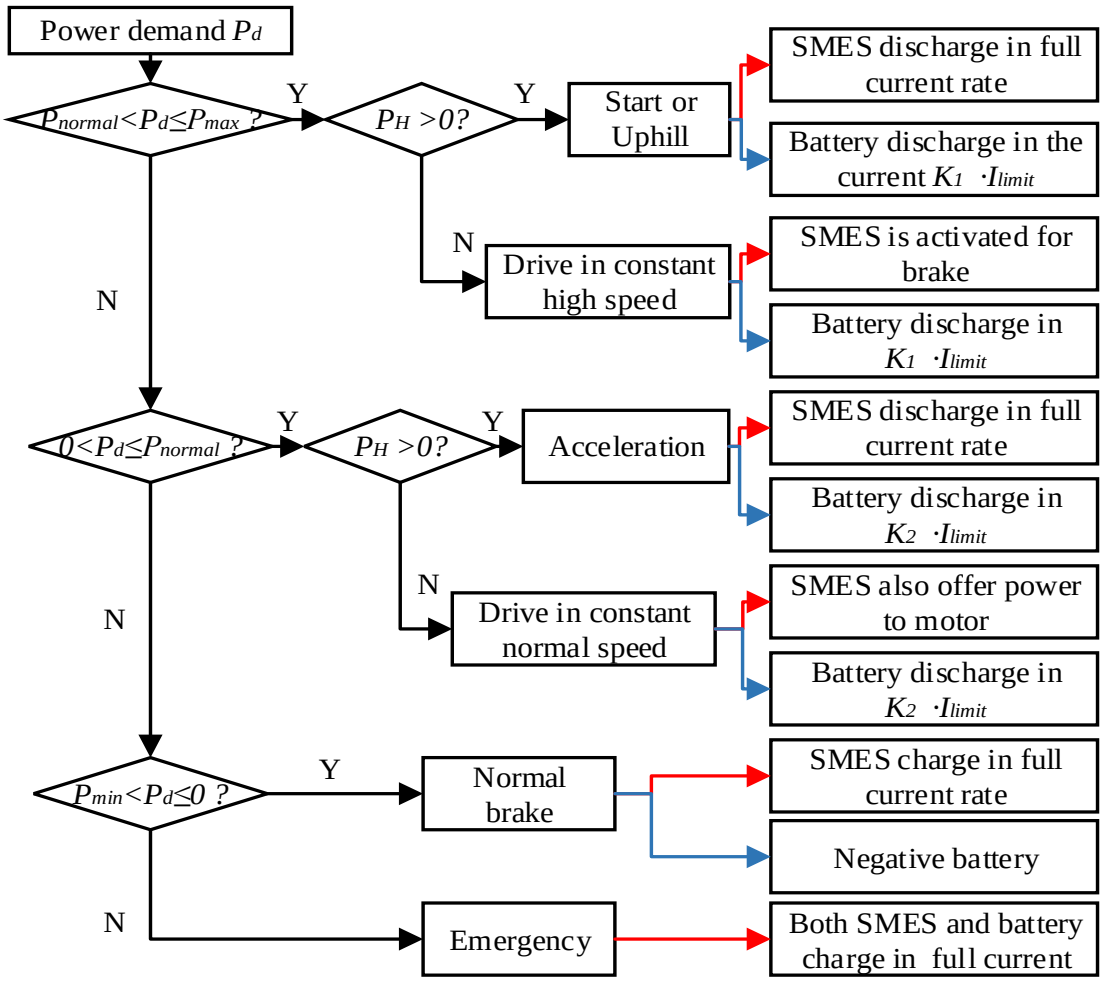

Fig. 4.4 SMES and battery working strategies

As shown in Fig. 4.3, the driving pattern model gives the different actions of EV with time labels. A self-adaptive filter method [106] is used to compare the power demand in different events along time series, which gives four optimal values: P_{min}, 0, P_{normal} *and* P_{max}. Hence, in the first step of the power grading, all the events are classified by those four values. Fig. 4.4 shows the strategies of SMES and battery in different conditions.

In high power demand conditions ($P_{normal}<P_d \leq P_{max}$), as shown in Fig. 4.4, the battery supply the power demand by the discharge current $K_1 \cdot I_{limit}$, where I_{limit} is the maximum allowable discharge current provided by the battery manufacturer and K_1 is defined as an optimal discharge ratio determined by real-time power demand $P_d(t)$ and P_{max}. In high power case, K_1 is ranged from 0.5 to 0.8, based on the trade-off between the battery usage efficiency and battery peak current limitation. The actions of the SMES is determined by high-frequency component P_{HF}. If $P_{HF} > 0$, it means the engine is starting, or the EB is going uphill, and the SMES will discharge as fast as possible; If not, it means the power demand is high but gentle, so regenerative braking power charges the SMES.

$$K_1 = \frac{P_d(t)}{P_{max}} \; K_1 \in [0.5, 0.8] \tag{4.1}$$

In normal driving conditions ($0<P_d \leq P_{normal}$), the battery supplies the power demand by the discharge current $K_2 \cdot I_{limit}$. In this case, K_2 is ranged from 0.2 to 0.6 as shown in Eq. 4.2. The SMES is controlled either discharge in fully or partly based on the demand power fluctuation. In normal constant speed, the SMES is expected to discharge partly of its energy when the stored energy is high enough, which is different with the high-speed conditions where the energy demand is too high for SMES to handle. It should be figured out that sizing study of the HESS should be done in order to make sure that the battery can be kept discharging in $K_1 I_{limit}$ and $K_2 I_{limit}$.

$$K_2 = \frac{P_d(t)}{P_{max}} , \; K_1 \in [0.2, 0.6] \tag{4.2}$$

In normal braking conditions, the SMES will absorb the regenerative power, whereas the battery will be disconnected from the motor with the benefits of system efficiency improvement and battery charging cycles reduction. However, in the emergency case ($P_{min}<P_d\leq 0$), the SMES and the battery will work together to absorb the braking power to achieve a faster brake hence more secure.

For sure, the power-dominate method performs a better power management in the complicated power situations. However, the design and implement of the power-dominate method are very difficult. Also, this method needs to be particularly designed for certain system and any changes to the target system may make this strategy less efficient. The flexibility of the power-dominate strategy is not as good as the other two schemes.

4.1.4 Case study

A case study based on the electrical bus system is introduced as an example of implementing the power management strategies.

A. System description

Several sub-systems including driving pattern model, EB model, SMES/battery HESS, battery lifetime model and the novel control algorithm, are built in Matlab/Simulink to demonstrate the performance of the HESS with the novel control method. The overall system configuration is shown in Fig. 4.5. As shown in Fig. 4.5, the driving pattern model is able to transfer four series of data to the EB, and these data are used to calculate the total power demand to perform such driving behaviour. The HESS power is managed by the power-dominant PMS. Then, the HESS gives the battery performance

to the battery lifetime model which could quantify the battery degradation. As it can be seen from Fig. 4.5, the realistic driving patterns also have an influence on the PMS.

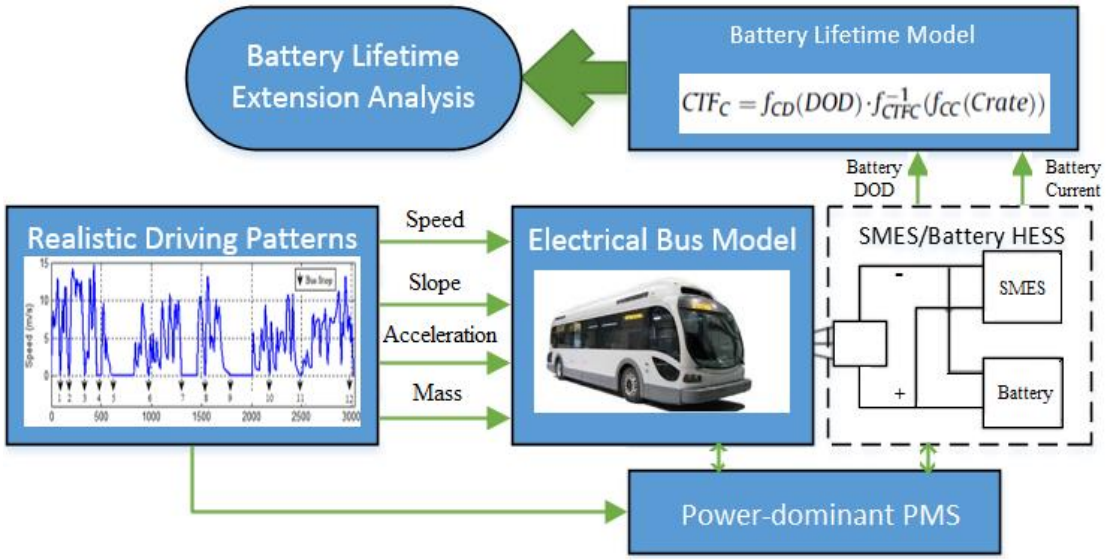

Fig. 4.5 The overall system configuration

This work has advanced the driving pattern model by introducing four factors including speeds, landform slopes, accelerations and the mass variations. Vehicle speed and landform slopes of the hill are measured by a smartphone placing on the city bus with the software named Viewranger, around the full route. The acceleration a can be obtained calculating the derivation of the velocity. The total weight of the EB is varying with the people getting on or getting off the bus and Eq. 4.3 is used to describe the mass variations m. Where M_{bus} is bus self-weight, m_{ave} is the average weight of human and n is the counting people which may vary with different bus stops.

$$m = M_{bus} + n \cdot m_{ave} \tag{4.3}$$

As shown in Fig. 4.5, the EB model is implemented to calculate the power demand of the motor to perform the given driving patterns and this amount of power will be supplied by the SMES and batteries. Fig. 4.6 shows the speed, slope and acceleration variation based on the driving pattern model in a full driving cycle. As shown in Fig. 4.6, the total power demand around each bus stop varies largely and instantaneously. The highest power demand can be observed between bus stop 11 and 12, where the bus goes uphill at a high speed.

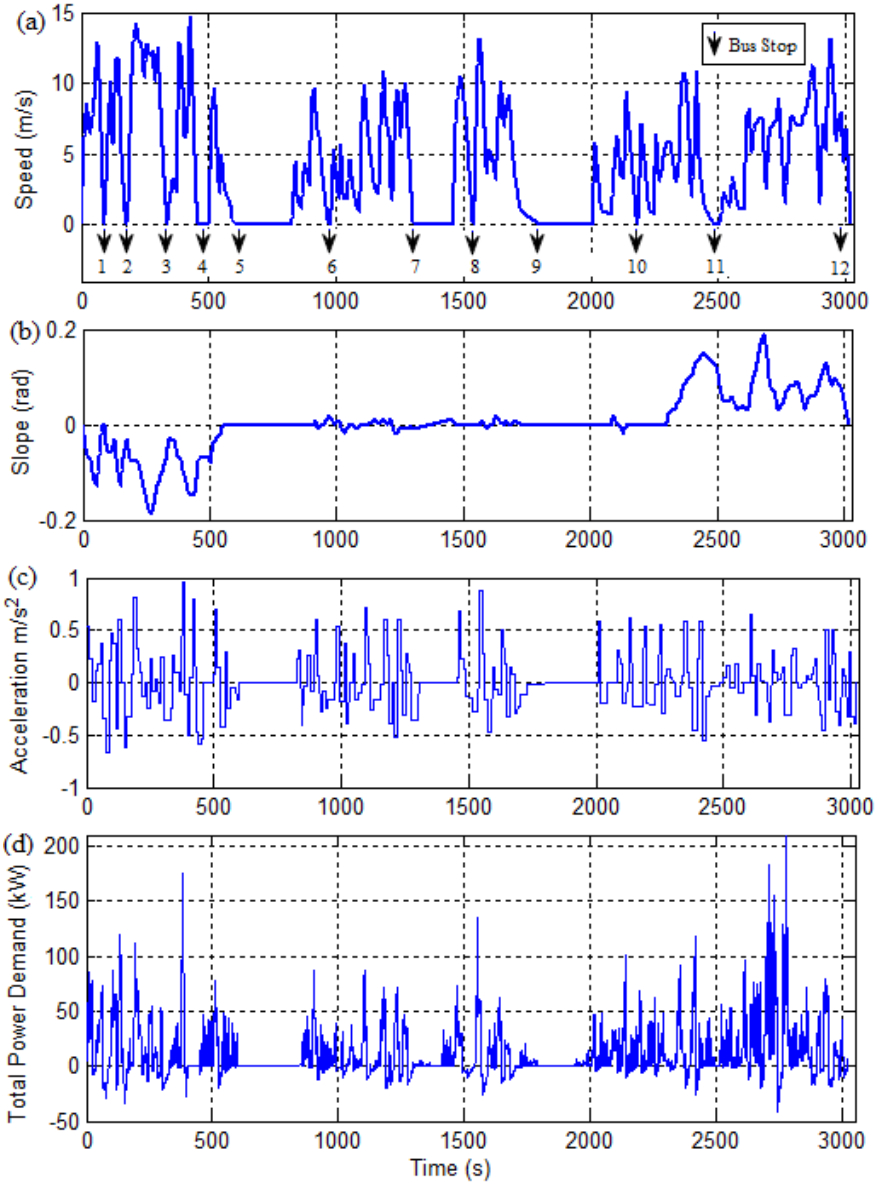

Fig. 4.6 EB speed, route slope, EB acceleration and power demand in a full driving cycle with 12 bus stops

B. The power management strategy

In the case study, the power-dominant management strategy as introduced in Section 4.1.3 is implemented.

C. Simulation result and discussion

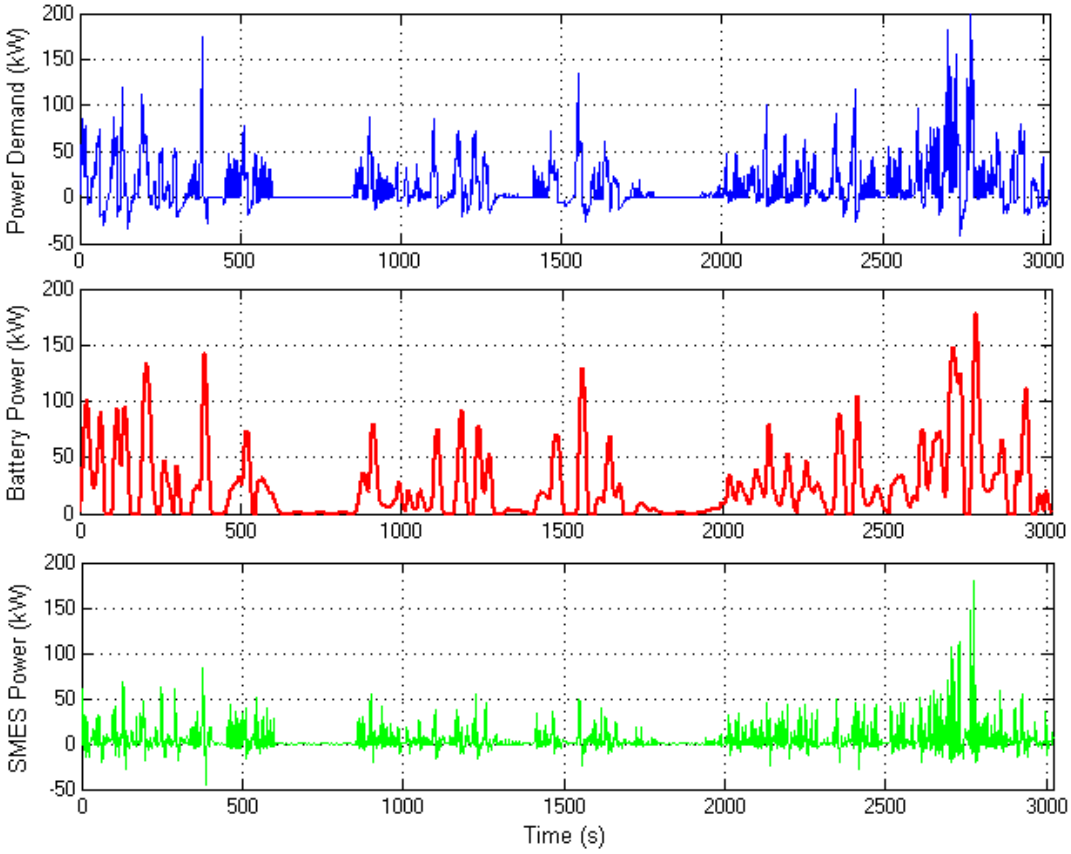

Fig. 4.7 Variations of total power demand, battery power and SMES power in a full route cycle

As shown in Fig. 4.7, the battery (red curve) and the SMES (green curve) work together to supply the total engine power demand (blue curve). The performance of the HESS is

same as it has been designed that the battery mainly deals with the low-frequency power whereas, the SMES takes care of the high-frequency fluctuations. Also, compared with the SMES, the battery have no negative power, which means that in normal brake conditions, only the SMES is charged by the regenerative power in order to reduced battery charge frequency.

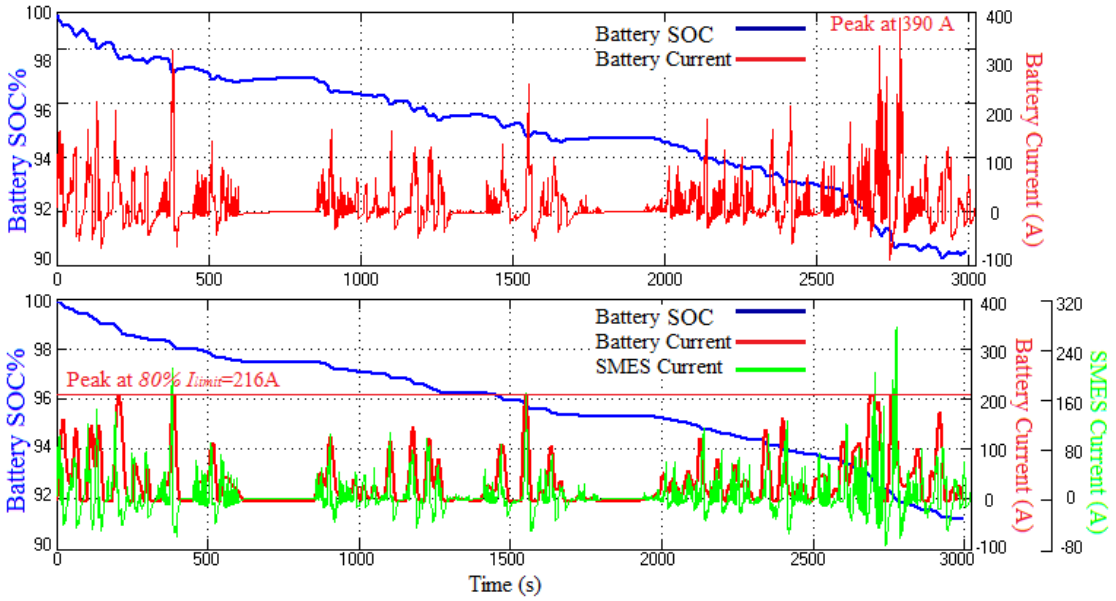

Fig. 4.8 The performance of the battery in (a) battery only system and (b) HESS

The battery current and state of charge are the two factors that usually used to evaluate battery performance. Fig. 4.8 compares the performance of the battery in a battery only system and HESS. In terms of SOC, battery in HESS has a more gentle curve than that in the BOS. Moreover, after a full route cycle, the battery in the BOS discharges to a deeper value (90.5%) compared with 91.2% in HESS. In terms of the battery current, we can see that the battery in BOS undergoes not only more charge/discharge cycles, but higher peak current as well. In the design of the novel control strategy, the peak currents in HESS are limited below 216 A (80% I_{limit}), while the peak value in the BOS is 390 A. The current of SMES (green curve) charges and discharges very fast with

higher values. Hence, in the HESS, the SMES works as a power buffer that helps the battery to supply the instantaneous high power demand. The performance of battery current and SOC both show a tendency of extension of battery lifetime in HESS.

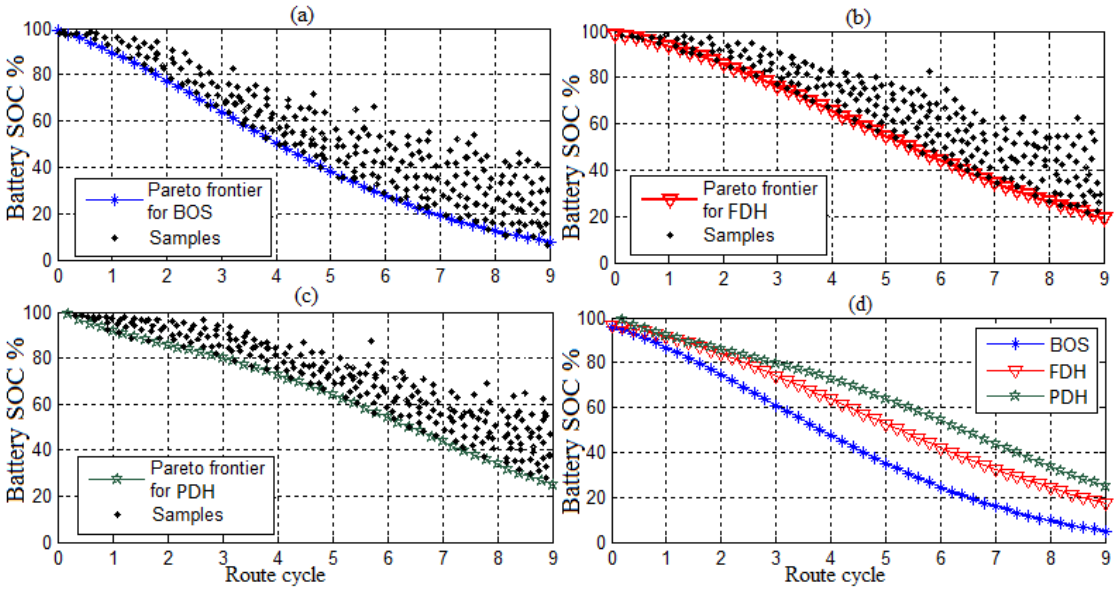

Fig. 4.9 Pareto analysis of battery SOC against route cycles: (a) battery only system; (b) frequency-dominant-based HESS (FDH); (c) power-dominant-based HESS (PDH); (d) comparison of the Pareto frontiers in the three scenarios

The EB is designed to accomplish nine route cycles for a single charge. The data, used to carry the Pareto analysis, are gathered randomly 10 times in each route cycle at three times fully charged/discharged. Hence, there are 270 ($10 \times 9 \times 3$) samples representing the SOC conditions of battery in each scenario, which is enough to generate the Pareto frontiers to represent the general performance of the battery in each case. A higher SOC value at the end of the ninth cycle means a more efficient battery discharge strategy and, hence, a longer battery lifetime. As shown in Fig. 4.9 (d), the SOC curves are higher in both HESSs compared with BOS. The SOC curve in PDH

has the best performance. The PDH is, therefore, more efficient than the FDH in the EB application.

4.1.5 Discussion

Table 4.1 Summary of the three methods

Type of PMS	Advantages	Disadvantages	Ideal applications
Frequency-dominant strategy	Principle is simple; Very good high-frequency response	The SMES utilisation efficiency is low	Systems have high-frequency power fluctuation such as wind applications
SMES fully active strategy	The SMES utilisation efficiency is very high; The battery life in the HESS is further extended.	Exacting requirements on both the safety and stability of the SMES operation	Renewable power system in small scale
Power-dominant strategy	Both the SMES and the battery in the HESS have very high efficiency	The design of the strategy is very complicated.	Ideally, for the systems have complex power conditions elements such as EVs and microgrids.

The analysis of the proposed three kinds of the power management strategies in respect of their advantages and disadvantages are shown in Table 4.1. The appropriate applications of the different methods are also given in Table 4.1. For the frequency-dominant strategy, a wind power system is an ideal application because of its good high-frequency power handling capability. The SMES fully active method is suitable for the renewable power system in small scale. Both the SMES and the battery in the power-dominant method have high efficiency, but the design of the strategy is very complicated. Hence, for power systems that have complex power situations, power-dominant is the ideal choice.

4.2 Energy storage sizing algorithm

The main function of the proposed hybrid energy storage system is to compensate the unbalanced power between the generation and the load demand. Therefore, in order to obtain an optimal capacity of energy storage devices, a sizing study is essential. The optimisation study for single energy storage is not very challenging and many published works have introduced various kinds of sizing methods. However, the sizing study of the SMES/battery hybrid energy storage is very complicated. To the best knowledge of the author, there is very little published work that gives a cooperative sizing design to effectively combine the battery and the SMES based their different characteristics. Therefore, the sizing strategy for both the battery and the SMES in the HESS is studied in this chapter. The basic principles of the new sizing method are introduced, and a case study is carried out to give an implementation of the sizing method. It should be noted that the sizing method presented in this section mainly references my published work shown in Appendix.

4.2.1 The principles of the sizing strategy

Basically, in an electrical energy storage project, the energy storage devices need to achieve the following two objectives:

- Meet system power requirement
- Meet system energy requirement

Known as the long-term storage system [107], the battery has large energy density and is very suitable for energy management functions. On the other hand, the SMES is used as short-term energy storage system and, while it cannot store much energy, it can handle the high-frequency power fluctuations [21].

Therefore, it is reasonable to divide the sizing study into two steps:

1. Regarding energy dispatching requirement, size battery to make sure that the load energy demand is always met. The energy density of the battery is much higher than that of the SMES and the supercapacitor. Hence, the battery is normally used to provide energy support in the electrical power system. The power capacity of the battery bank can reach as high as the SMES or the supercapacitors, but the battery needs to be designed in a very large size. Also, the high charge/discharge power requirements normally mean abrupt high charge/discharge currents, which are believed to be the main reasons that cause battery lifetime degradation.

2. In view of the short-term power fluctuation mitigation function, determine the size of SMES. The SMES is able to discharge all the stored energy in microseconds, hence, the rated power of the SMES can be designed very high.

For example, if total energy stored in the SMES is 1kJ and the SMES is able to fully discharge in 1ms, then the power level of the SMES in this process can reach as high as 1MW. Therefore, the SMES is very good at dealing with short-term high power fluctuations. The energy stored in a SMES coils can be given as shown in Eq. 4.4. As can be seen, the energy is proportional to the I^2 and the inductance L. However, because of the high cost of the superconducting material, the SMES devices is very expensive and the larger inductance means higher superconducting material cost. Therefore, in the hybrid scheme, the SMES is regarded as a kind of "power" storage device. Compared with the battery, the energy stored in the SMES is too small and can be neglected.

$$E_{SMES} = \frac{1}{2} L I^2 \qquad 4.4$$

One of the advantages of the HESS over the single energy storage system can be identified from the two-step sizing strategy in that the energy/power requirements for the signal ESS are more flexible. The SMES and the battery can be designed according to their own merits rather than restricted by the system constraints. The HESS should be designed to satisfy all constraints, whereas neither the SMES nor the battery needs to meet both the power/energy requirements.

4.2.2 Case study

The two-step sizing strategy is used to determine the sizes for the SMES and the battery in different power applications in this study. In this section, a case study based on an off-grid power system is used to describe the detailed implementation of the sizing method. The objective of the HESS is to work together with the wind generator to meet

the critical load demand on an island. The annual wind speed and load demand are given.

A. Battery sizing based on the energy

The essential function of the proposed off-grid power system is to meet the load request in the island. Hence, the battery and the wind generator are sized in the first step to ensure the generation is large enough to meet the load.

The concept of "Loss of Power Supply Probability" (LPSP), which describes the probability that the load cannot be met, was chosen as a reliable measurement for wind turbine and battery sizing study. The LPSP is the ratio of total energy deficit over the total load demand (see Eq. 4.5) and the LPSP approach has already been used in many works [108-110]. According to Eq. 4.5, the LPSP value ranged from 0 to 1: the value 0 means the load is satisfied all the times and 1 means that the load will never be satisfied. Setting the LPSP as 0.5 can be used to configure a system with a 50% penetration of wind generation, with the rest being met by other resources. In this study, the target LPSP is set as 0, which suggested that the load demand will be always met by the wind power and battery. Based on the LPSP method, the battery is sized at 244 Ah in the case study. The detailed description of this study is given in Appendix.

$$LPSP = \frac{\sum Energy\ deficit}{\sum Load\ demand} \tag{4.5}$$

B. SMES sizing

Previous studies [31, 44, 111] have presented a similar approach to size the SMES in an HESS based on the largest power requirement and the mean power demand. Fig.

4.10 illustrates this method. As shown in Fig. 4.10, the SMES should be able to handle the power difference between the maximum power (P_{max}) and average power (P_{mean}) during the cycle period. However, this may result in oversizing the SMES. The intermittent and unpredictable renewable source may cause extremely high or low power output, which produces an extremely high value of P_{max}. As a result, the big difference between maximum power and average power implies a large SMES is required. Currently, SMES technology is expensive and, in order to improve the utilisation of the SMES, a new sizing algorithm is shown in Fig. 4.11.

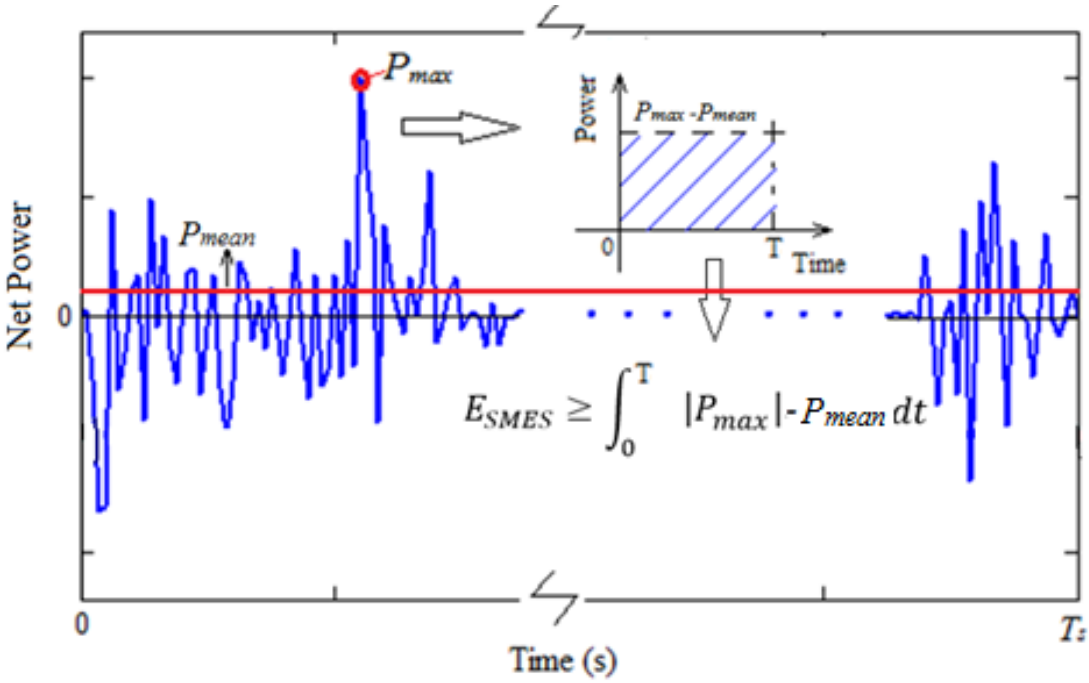

Fig. 4.10 Previous SMES sizing method

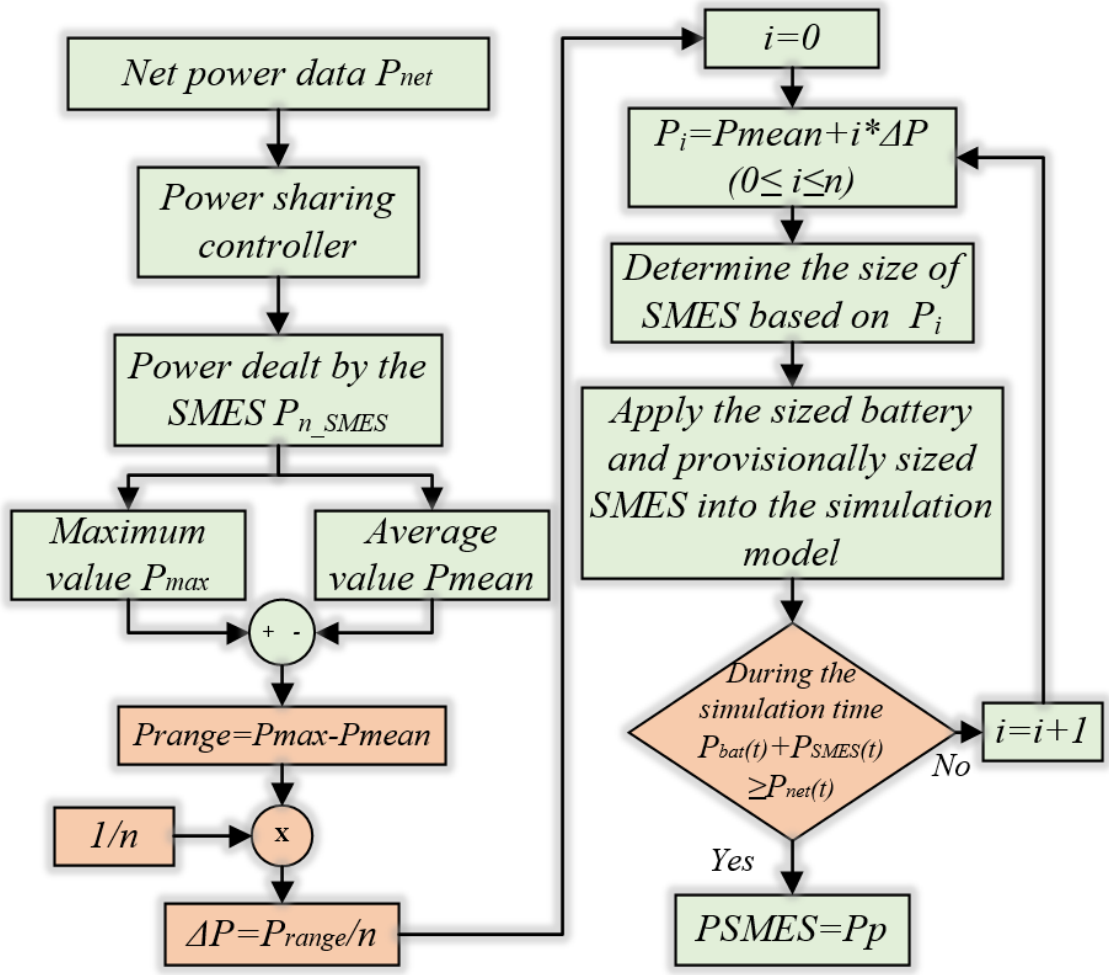

Fig. 4.11 The new SMES sizing method

Fig. 4.11 shows the iteration process of the new SMES sizing method. The power difference data (P_{net}) between the generated power and load demand is the main input. The power (P_{n_SMES}) processed by the SMES can be estimated from the proposed HESS controller. Then, the maximum value P_{max} and the average value P_{mean} of P_{n_SMES} during the simulation time may be determined. A power increment ΔP may be obtained by introducing a factor n to divide the difference between P_{max} and P_{mean}. The provisional SMES power is defined as $P_i = P_{mean} + i \cdot \Delta P$ $(0 \leq i \leq n)$. Then, based on the provisional SMES power, the size of SMES can be determined. The sized battery

and provisionally sized SMES are applied into the simulation model and, then, the power data of the SMES P_{SMES} and the battery P_{bat} can be obtained.

During the full simulation time, if $P_{SMES}(t) + P_{bat}(t) \geq P_{net}(t)$, the SMES capacity may meet the requirements of the system. Otherwise, the increment needs to be added to the provisional SMES power and the SMES resized.

As shown in Fig. 4.12, the value of n has a large effect on the final size of the SMES. It is obvious that the bigger n is, the more cost effective size of SMES can be obtained. When n = 1, the SMES is sized by the maximum power requirement, as in the previous SMES sizing method, and returns an oversized value, 1.82kJ. An asymptotic line can be drawn with Y =0.72, which means the optimal size of SMES in the proposed system is 0.72 kJ.

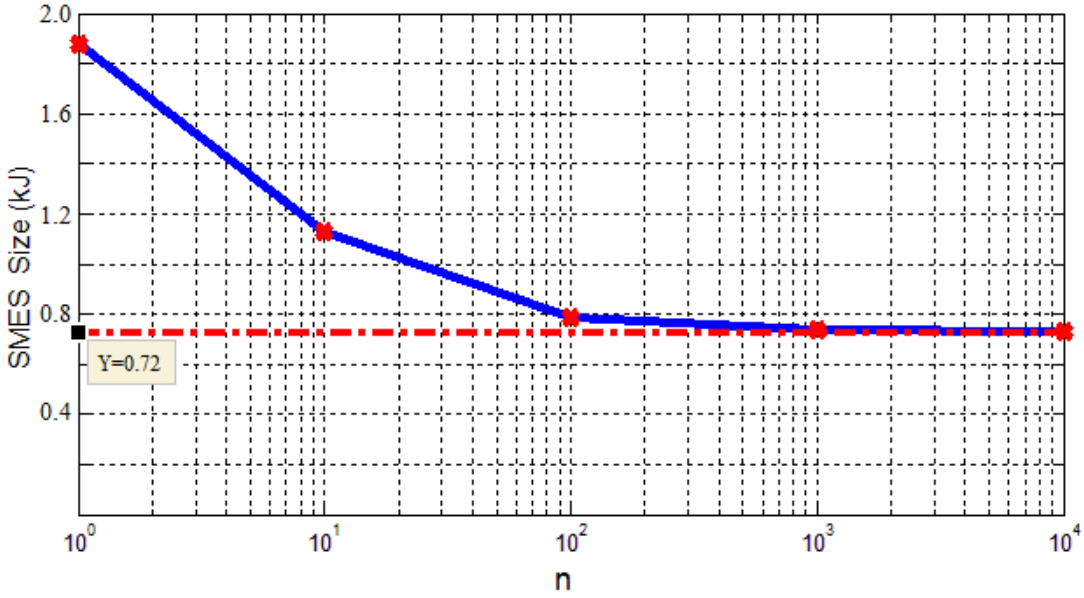

Fig. 4.12 The relationship between n value and the size of the SMES

Once the capacity of the SMES is determined, the optimal design configuration should be considered in order to reduce the cost of expensive superconducting materials. The double pancake SMES coils configuration was chosen as suggested in [67].

4.3 The control method of the hybrid energy storage system

Power balancing is the major challenge for the efficient use of the energy storage devices in different power applications and the achievement of the system power balancing function mainly depends on the control method. The control algorithm for a HESS is more complicated because of the requirement to effectively combine the harmonious operation of two storage technologies such that they complement each other.

Many power control algorithms for HESS are reported in the literature. Fuzzy control, which can realise power management in nonlinear systems without precise system modelling has been proven suitable for coordination of multiple energy sources. Ise. et al. [16] propose a fuzzy control based method in railway power systems, achieving effective power sharing between the battery and the SMES. Similarly, fuzzy control has been used for power management of the HESS in electric vehicles [39, 112, 113] and wind applications [70] with the benefits of protecting the battery and improving system efficiency. However, some specific constraints and fuzzy regions used in this control are selected empirically, which sometimes may lead to sub-optimal design choices. Li. et al. [22] and Song. et al. [47] proposed the conceptually simple power grading control that classifies the power requirements manually and distributes the power demands to the different energy storage systems based on their classification. Obviously, the accuracy of this controller is highly dependent on the specific implementation. The filter

based power control method which uses the inherent filtration characteristic of the SMES and supercapacitors to allocate low-frequency charge cycling to the battery has been applied in micro-grid applications [43], EVs [114] and renewable generation[14]. The main problem with this technique is that the optimal cut-off frequency of the filter is very difficult to determine. Model predictive control has been shown to effectively reduce battery peak currents in a HESS [71], but at the cost of poor efficiency of the short-term energy storage system. Allègre. et al. [115] introduce a real-time data-driven control of the supercapacitor/battery HESS achieving a high utilisation factor of the supercapacitor by delaying battery activation until after the supercapacitor reaches its voltage limitation. The drawback of this approach is that the battery may be damaged when the supercapacitor is fully discharged.

Droop control, which is able to take advantage of various kinds of power sources to match different load demands, has been proven to have a high efficacy in a decentralised DC grid [116], renewable sources [6], EVs [117] and AC grid [118]. It achieves optimal allocation of multiple energy sources to various demands by setting appropriate droop coefficients for different converters [6, 116-118].

This chapter introduces the novel use of a droop control method for controlling the power sharing between the SMES and battery. Less complex than previous approaches, the proposed control method is able to maintain power system stability by compensating both the high-frequency and low-frequency power fluctuations. Furthermore, compared with previous hybrid control methods, the new control has several advantages. Firstly, it is capable of prioritising the operation of the SMES over the battery for short-term power fluctuations. Secondly, the charge/discharge level and rate-of-change for the SMES and the battery can be controlled by the droop factor.

Thirdly, the proposed control is able to apply different energy storage system charge and discharge rates according to their distinct characteristics by setting different droop factors.

It should be noted that the droop control method presented in this Chapter mainly references my published works [82, 119] as shown in Appendix.

4.3.1 The principle of the droop control

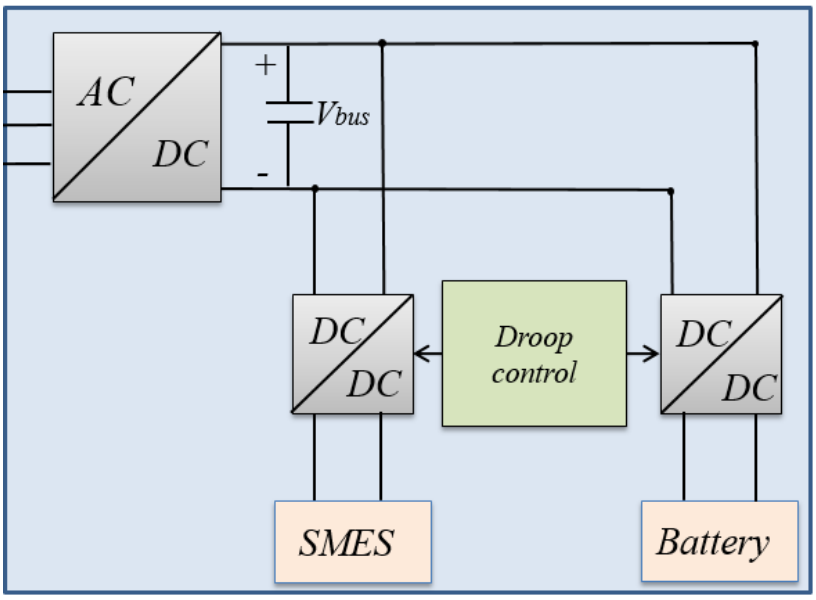

Fig. 4.13 Typical control topology for the SMES/battery hybrid scheme

The typical arrangement of power converters and energy storage components of a SMES/battery hybrid energy storage system is shown in Fig. 4.13. The initial objective of the hybrid energy storage system is to maintain the DC bus voltage within a target range. The battery and the SMES are both connected to the DC bus through the DC/DC converters. The purpose of the power sharing control is to generate different converter references to charge and discharge the different energy storage devices at different rates.

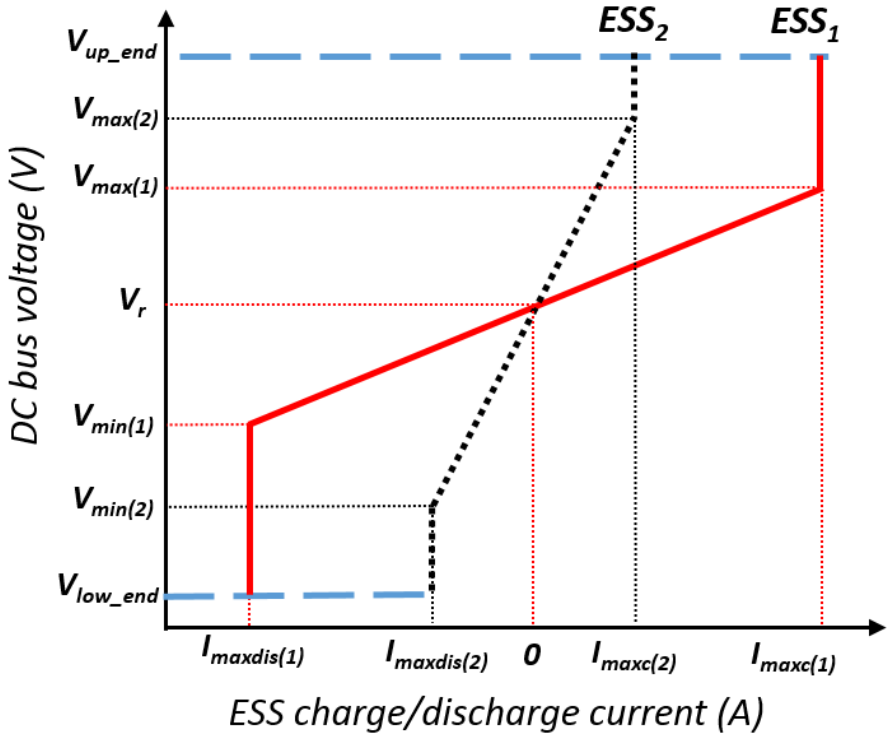

Fig. 4.14 Hybrid energy storage system voltage vs. current characteristic for active droop control

Decentralised control of the power contributions may be implemented using a droop controller as successfully demonstrated in a multi-terminal DC system [6, 116, 120]. This study proposes the novel use of active current droop control in power sharing between the SMES and the battery by adjusting the droop factors for different ESSs. The working principles of the voltage versus current active droop control for HESS are illustrated by Fig. 4.14. Based on the DC bus voltage measurement, the energy storage systems ESS_x (where x refers to the one of a number of ESS) charge or discharge at a level controlled by the following four conditions:

- When the DC bus voltage $V_{bus} \geq V_{max(x)}$ (where $V_{max(x)}$ is the upper voltage limit of the ESS_x), the ESS is charged at a maximum charge current $I_{maxc(x)}$.
- When $V_{bus} \leq V_{min(x)}$ (where $V_{min(x)}$ is the lower voltage limit of the ESS_x), the

energy storage system discharges at a maximum discharge current $I_{maxdis(x)}$.

- In between $V_{max(x)}$ and $V_{min(x)}$, the current is controlled based on the current vs. DC bus voltage relationship:

$$I_x = (V_{bus} - V_r) \cdot k_x \quad 4.6$$

In Eq. 4.6, for a particular ESS$_x$, I_x is the charge or discharge current, k_x is the droop coefficient and V_r is DC bus reference voltage.

- When $V_{bus} = V_r$, the energy storage device is in stand-by, and there is no charge or discharge current.

The upper and lower voltage limit can be pre-defined based on manufacturer's data for energy storage devices. The DC bus voltage V_{bus} is derived from measurement. The different energy storage devices have different charge/discharge rates for different droop coefficients (k_x). To control the power ratio between different ESS, the droop coefficients for the battery and the SMES are set based on their different energy storage characteristics and operating constraints. Additionally, the battery and the SMES are protected from over charge/discharge by setting the voltage upper and lower boundaries, V_{up_end} and V_{low_end}.

4.3.2 DC/DC Controller for the energy storage systems

A. DC/DC controller for the battery

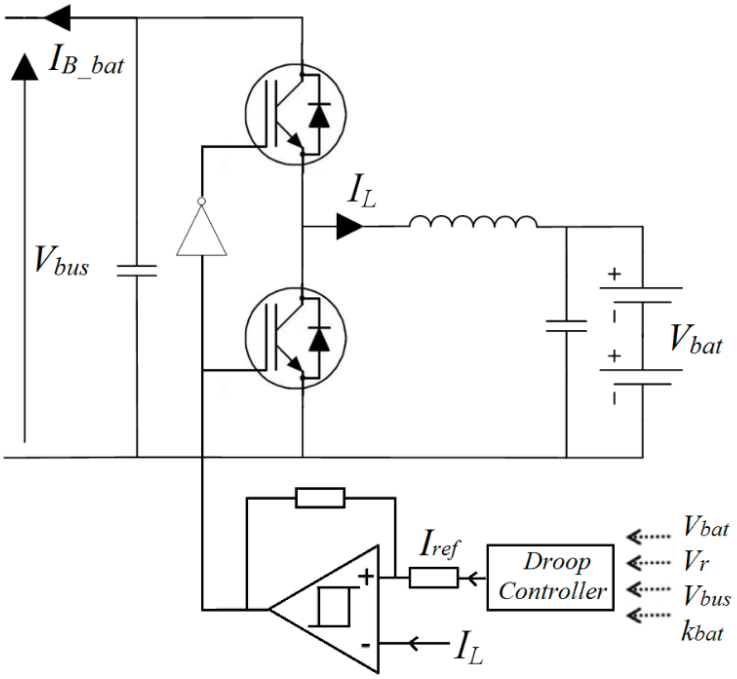

Fig. 4.15 Battery DC/DC converter with hysteresis current control

The battery DC/DC converter with hysteresis current control is shown in the Fig. 4.15. The hysteresis control has been shown to have good tracking capability and good robust performance [121, 122]. The inductor current I_L in Fig. 4.15, is regulated to track the reference current I_{ref} using the sliding mode control as described in [123, 124].

Based on the droop control method in Eq. 4.7, the droop control for the battery can be written:

$$I_{B\_bat} = (V_{bus} - V_r) \cdot k_{bat} \quad 4.7$$

The output current of the battery DC/DC converter I_{B_bat} can also be written as Eq. 4.8

$$I_{B\_bat} = I_{ref} \cdot \frac{V_{bat}}{V_{bus}} \quad 4.8$$

Based on the Eq. 4.7 and Eq. 4.8, the reference current I_{ref} should be set as:

$$I_{ref} = k_{bat} \cdot (V_{bus} - V_r) \cdot \frac{V_{bat}}{V_{bus}} \quad 4.9$$

B. DC/DC controller for the SMES

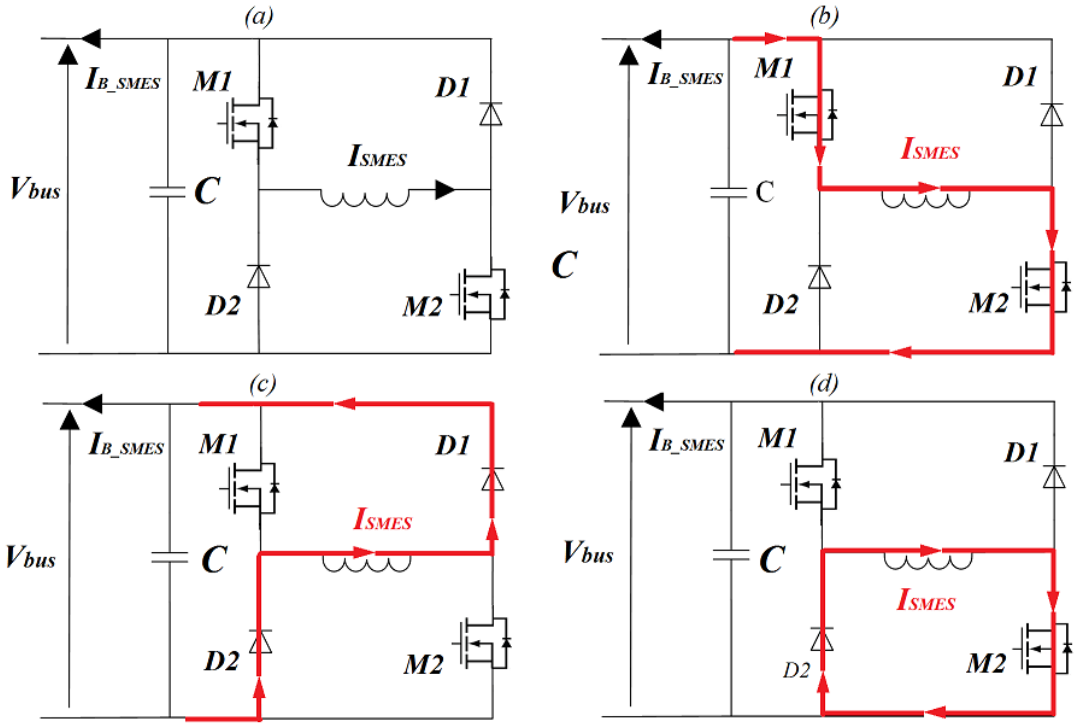

Fig. 4.16 SMES DC/DC converter showing current paths in different modes: (a) circuit topology; (b) charge mode; (c) discharge mode; (d) standby mode

The asymmetric full bridge DC/DC converter of the SMES in Fig. 4.16 (a) comprises diodes (D1, D2), MOSFETs (M1, M2) and an output capacitor (C). Three operating modes are used: charge mode by switching between conduction paths in Fig. 4.16 (b)

and (d); discharge mode by switching between conduction paths in Fig. 4.16 (c) and (d); and stand-by mode with I_{SMES} circulated as in Fig. 4.16 (d). The relative values of the bus and SMES voltages determine the operating mode at any time as illustrated below.

1. Charge mode ($V_{bus} > V_r$):

Applying Kirchhoff's current law at the capacitor positive node and state space averaging the switching interval gives Eq. 4.10.

$$C\frac{dV_{bus}}{dt} = -I_{B\_SMES} - I_{SMES} \cdot d_1 \tag{4.10}$$

I_{SMES} is the current flowing through the superconducting coil, $-I_{B\_SMES}$ is the output current from SMES DC/DC converter and d_1 is conduction duty ratio of M1 while M2 is constantly on. SMES charge current can be regulated by controlling d_1.

2. Discharge mode ($V_{bus} < V_r$)

Applying Kirchhoff's current law at the positive capacitor node gives Eq. 4.11

$$C\frac{dV_{bus}}{dt} = -I_{B\_SMES} + I_{SMES} \cdot (1 - d_2) \tag{4.11}$$

d_2 is the conduction duty ratio of M2 while M1 is constantly off. The discharge current can be regulated by controlling d_2.

3. Stand-by mode ($V_{bus} = V_r$)

During this condition, the bus voltage is equal to the SMES nominal voltage, and hence no output current is required from the SMES DC/DC converter.

If the DC/DC converter capacitor is chosen to be sufficiently large, its voltage may be assumed approximately constant during a switching interval. Equations 4.10 and 4.11 may then be approximated by Eqs. 4.12 and 4.13 for the charging and discharging conditions, respectively.

$$-I_{B\_SMES} = I_{SMES} \cdot d_1 \tag{4.12}$$

$$-I_{B\_SMES} = -I_{SMES} \cdot (1 - d_2) \tag{4.13}$$

By applying the general droop control equation Eq. 4.6 to the SMES gives Eq. 4.14. Using Eqs. 4.12 to 4.14 in this give Eqs. 4.15 and 4.16.

$$-I_{B\_SMES} = (V_{bus} - V_r) \cdot k_{SMES} \tag{4.14}$$

$$d_1 = \frac{(V_{bus} - V_r) \cdot k_{SMES}}{I_{SMES}} \tag{4.15}$$

$$d_2 = 1 + \frac{(V_{bus} - V_r) \cdot k_{SMES}}{I_{SMES}} \tag{4.16}$$

I_{SMES} and V_{bus} values are both determined by measurement. V_r is the pre-defined value. Therefore, the conduction duty ratio d_1 of M1 during the charge condition and duty ratio d_2 of M2 during discharge condition may be readily calculated. As a result, the charge/discharge current of the SMES may be easily regulated using a DC/DC

converter and droop control. In addition, during the stand-by condition where the V_{bus} is equal to predefined reference value V_r, $d_1 = 0$ and $d_2 = 1$, which simply requires that M1 is held constantly off and M2 constantly on.

4.3.3 Droop coefficient study

As introduced at the very beginning, the droop control is capable of combining multiple ESSs according to their own features by selecting different droop coefficients. However, to the author's best knowledge, there is no previous work describe how to determine the different droop coefficients for different ESSs. In addition, the capacities of the battery and the SMES may limit the performance of the hybrid control. Therefore, the control strategy needs to be designed with the consideration of both the sizes of the battery and the SMES. In this section, a new method which takes the sizes and various constraints of the ESSs into account is proposed to give the reasonable ranges of the droop factors for both the battery and the SMES.

A. The droop coefficient for the battery

Reduction of peak battery current is one of the advantages of HESS. The battery manufacturers often give an optimal range of battery discharge current beyond which the voltage of the battery will drop more substantially. Therefore, the battery maximal current $I_{\max\_bat}$ should not be higher than the maximum current limit I_m:

$$I_{\max\_bat} \leq I_m \tag{4.17}$$

The largest energy deficiency can be estimated by integrating the power in the largest net power fluctuation cycle with the fluctuation duration t:

$$E_{max} = \int_0^t P_m(t)dt \tag{4.18}$$

The battery provides long-term energy storage in the HESS, which offers energy support for the system. The battery charge/discharge currents are determined by the droop controller. The battery should be able to buffer the largest energy deficiency E_{max}. Hence, the battery maximal current in the duration t should meet the condition as Eq. 4.19

$$I_{\max\_bat} \cdot V_{bat} \cdot t \geq E_{max} \tag{4.19}$$

Based on Eq 4.6, the battery maximal current is given by:

$$I_{\max\_bat} = (V_{\max\_bat} - V_r) \cdot k_{bat} \tag{4.20}$$

Hence, using Eq. 4.17 to Eq.4.18, a range for k_{bat} can be obtained:

$$\frac{E_{max}}{V_{bat}(V_{\max\_bat} - V_r) \cdot t} \leq k_{bat} \leq \frac{I_m}{V_{\max\_bat} - V_r} \tag{4.21}$$

B. The droop coefficient for the SMES

The SMES has low energy density but high power capacity and is controlled to charge or discharge quickly to deal with most of the immediate power surplus or deficiency. Hence the maximal SMES current should be high enough to meet the maximum net power requirement, as given in Eq. 4.22:

$$I_{\max\_SMES} \geq \frac{P_{net\_max}}{V_{SMES}} \tag{4.22}$$

Based on the Eq 4.6, the battery maximal current can be obtained as:

$$I_{\max\_SMES} = (V_{\max\_SMES} - V_r) \cdot k_{SMES} \tag{4.23}$$

Hence:

$$k_{SMES} \geq \frac{P_{net\_max}}{(V_{\max\_SMES} - V_r) \cdot V_{SMES}} \tag{4.24}$$

4.3.4 Methodology discussion

The power fluctuations on the AC side cause DC bus voltage oscillations. Based on the droop control method introduced in this chapter, the energy storage units are controlled to contribute to regulating the DC bus voltage, and hence attenuate the power fluctuations. Therefore, the presented control method is applicable more generally to

address power fluctuation mitigation. Moreover, in the droop coefficient study, the energy storage capacities are successfully coupled with the droop control, with makes the control method more effective and more convincing. It also should be figured out that, in this study, the SMES and the battery are controlled as a voltage source to maintain the DC bus voltage within the desired range. Topologically, the energy storage units (SMES and battery) can be replaced by other energy storage devices e.g. supercapacitors.

However, the disadvantages of the droop control cannot be neglected. First of all, it is a challenge to determine the optimal droop factors for different units. Many factors need to be considered, such as the system constraints, different power applications and different characteristics of the ESSs. Any changes of the system parameters may lead to a failure of the control. Secondly, in the case of adding new devices, the total droop method needs to be redesigned which means the droop method may be less flexible.

4.4 Conclusions

The methodologies for the SMES/battery HESS are introduced in this chapter.

Three kinds of the PMSs are summarised. The advantages and disadvantages of each method are discussed. In respect of the different features of the PMSs, their application occasions are investigated. Additionally, a case study is introduced to describe the detailed implementation of the power-dominate PMS in an electrical vehicle system.

A sizing algorithm which takes advantages of the different features of the ESSs in the HESS is developed. The different energy and power demands for the battery and the SMES are considered in the sizing method; hence, the energy and power

complementary function of the HESS is enabled. A case study is carried out to give an introduction to the implantation of the proposed method. The case study also highlights anther merit of the sizing algorithm in that it is able to solve the over-sizing issue of the SMES.

A novel use of a droop control method for controlling the power sharing between the SMES and battery is proposed. By selecting the optimal droop coefficients for the different ESSs, the charge and discharge priority of the SMES and the battery are differentiated according to the power situations. The implementation of the droop control in the DC/DC converters is introduced for both the SMES and the battery. The droop coefficient study which successfully couples with the system constraints is also presented.

Chapter 5 Experimental Verification

5.1 Introduction

The proposed SMES and battery hybrid scheme together with its control method is tested experimentally to be used in a CHP system. The background is introduced at the beginning of this chapter. Then the experimental platform setup and the Hardware-in-the-loop (HIL) circuit is described in detail. The capacities of the battery and the SMES in the HESS are estimated by the sizing method presented in Chapter 4. The performance of the HESS together with the PMS and the hybrid energy storage control are verified by the RTDS and the HIL platform.

This chapter is organised as follows. The background of the application case of the proposed HESS is discussed in Section 5.2. Section 5.3 gives an instruction of the RTDS. Section 5.4 introduces the HIL circuit and the hardware used in this experiment. Section 5.5 gives the system power management. The laboratory test system and the experimental results are given in Section 5.6. After that, the conclusions are presented in Section 5.7. T.

5.2 Background

Developing a more efficient energy system using existing energy conversion infrastructure is considered a vital transitionary pathway to a low carbon future by both policy makers and academic experts [125-127]. One of the most promising technologies in achieving this transition is micro-combined heat and power systems [127-130]. M-CHP systems which broadly range from 1 kW and 15 kW in capacity [127, 129-131], are able to take advantage of the waste heat from the heat engine for building heating and hot water requirements. By harnessing the wasted thermal energy, the overall efficiency of m-CHP can be raised to over 80%, up from approximately 20% for an equivalent rated generator [126, 128, 132, 133] thus dramatically increasing primary energy savings.

The buildings and housing sector account for a significant proportion of the primary energy demand: about 60% in the EU [134], over 50% in the UK [135] and averaging approximately 40% in most developed countries [136]. Many previous works have investigated the benefits of using m-CHP in a domestic setting. Maghanki, et al. conclude from an energy perspective that the m-CHP is able to meet most of the domestic thermal energy demand, achieving over 20% energy saving index[128]. The m-CHP system is predicted in [131] to meet about 25%-46% of annual energy demand of a typical British household, together with achieving over 40% reduction in the peak electrical load in the winter days.

However, energy balancing is one of the major challenges for the effective application of m-CHP in a residential context. Several factors combine together to exacerbate this problem, namely: (a). load demands are highly fluctuating, often with random seasonal

components, which may cause intermittent bi-directional flows of electricity [131, 137]; (b). tariff design impacts the operation of m-CHP, which makes the power balancing more complicated [125, 138], (c). the thermal energy and electric power demands often do not coincide with each other [137, 138]. To solve these problems, localised energy storage systems have therefore often been proposed as a complementary technology to m-CHP [125, 139, 140]. M-CHP systems with high heat to power ratio are more suitable for domestic applications where the power demand is continuously much lower than the heating demand [138]. In such systems, the CHP is dispatched to follow the heating load, which gives a stronger indication for electrical energy storage than thermal storage. This chapter therefore mainly focuses on the electric storage system in a residential m-CHP system.

Battery energy storage systems have high efficiency, large energy density, high levels of robustness and the inherent ability to load time-shift and are therefore widely used in many power applications. However, the battery has a very low power density resulting in a slower response speed to fluctuations in demand [97]. Moreover, the short life-span of the lead-acid battery discourages its usage [73]. The highly variable output and demand mismatch of a residential m-CHP lead to more discharge and charge cycles and also accelerates the battery's degradation process, resulting in shorter battery service life and increased battery replacement costs. To address these problems, the inclusion of another complementary storage, to form a hybridised energy storage system (HESS) has therefore been the focus of this study.

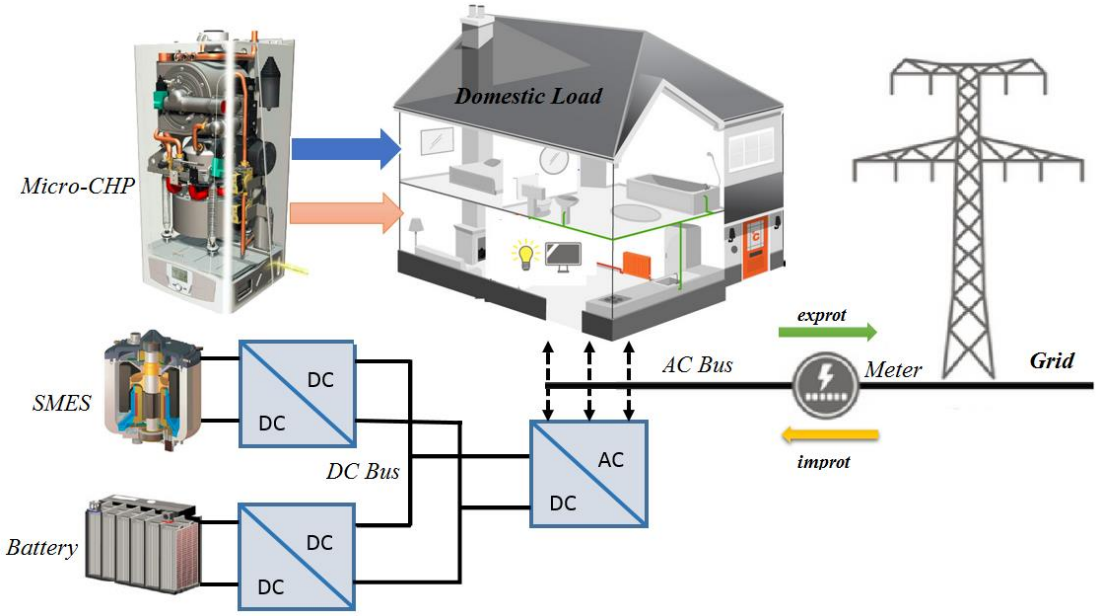

Fig. 5.1 The residential m-CHP system with the SMES/battery HESS

Fig. 5.1 shows the configuration of the proposed domestic power system including the m-CHP, the battery, the SMES, power converters, the grid and the load demand. The battery and the SMES are controlled using bidirectional DC/DC converters and then interfaced with the AC bus by a DC/AC converter. All the power converters are modelled using the small-time-step model in the RTDS [141], and the novel control algorithm is implemented in the external hardware. The SMES are modelled as an equivalent large inductance using the method described in [14, 111]. The dynamic battery model that described in [73] is able to represent the battery current and depth of discharge (DOD) variations is developed in the RTDS. The parameters of the battery and the SMES subsystem are given in detail in Section 5.3.2. In the UK, the m-CHP rated at up to 16 A per phase and therefore prime mover capacities of up to about 2.7kW are of interest [131]. As this study mainly focuses on electric energy part, the m-CHP is built using the method described in [142] and the heat generation from the CHP is not considered.

5.3 Real-time digital simulator

The simulation is a powerful tool for verification of the proposed power system with the HESS. However, the effectiveness of the simulation much depends on the accuracy of the power modules and the algorithm built in the software. To some extent, the real-time experiments are more convincing than the simulations. In this study, the proposed hybrid energy storage was designed to be used in the domestic power system. Even the rated power is not very high, it is very difficult to build a real domestic power system in the laboratory environment at the University of Bath. In additional, the proposed domestic system is grid connected; the security is also an important concern for testing the HESS design in the real system.

The RTDS uses parallel processing techniques on rack-mounted processors to maintain continuous real-time digital simulation of a power system [143]. The benefit of real-time operation means that the power system operates in its own closed loop and users are able to interact with the simulation in real time observing the effect of control actions. As a result, because of the real-time computing capability, the RTDS is regarded as the very effective tool for the experimental verification of power systems. The other significant advantage of the RTDS over the software simulation is that in the RTDS environment, all the signals and measurements are the real-time data, which make it is possible to interface the external hardware/devices to the RTDS. In this study, a very effective test platform is developed based on the RTDS and the hardware-in-loop circuit. The effectiveness of the experimental method is analysed as follows:

- Compared with the simulation works based on the software, the HIL and RTDS test platform is more convincing.

- The main contributions of this study are the design of the HESS concept and the power sharing control among the SMES and the battery. Therefore, it makes sense that establishing the power system in the RTDS and testing the control method in outside hardware controller (DSP). In this topology, the RTDS will generate real-time measurements which will be sent to the DSP in the external circuit. The DSP will generate the physical control signals (PWM signals) which used to control the devices in the RTDS. As it can be seen from this process, the system is tested in the real-time, and the control algorithm is verified at an experimental level.

- Because of the real-time computing capability, there is no need to build a real power system, which will save a lot of time and money.

- The proposed experiment is more flexible. For example, the control system can be verified under various conditions easily and inexpensively.

- The proposed experimental platform is safe and free from high currents and voltage.

- The experiment based on the RTDS and HIL can be used as an intermediary step before implementation in an actual real world system.

Therefore, it is very reasonable to establish the proposed RTDS and HIL platform to test the design of the HESS and its control.

5.4 Hardware in loop circuit

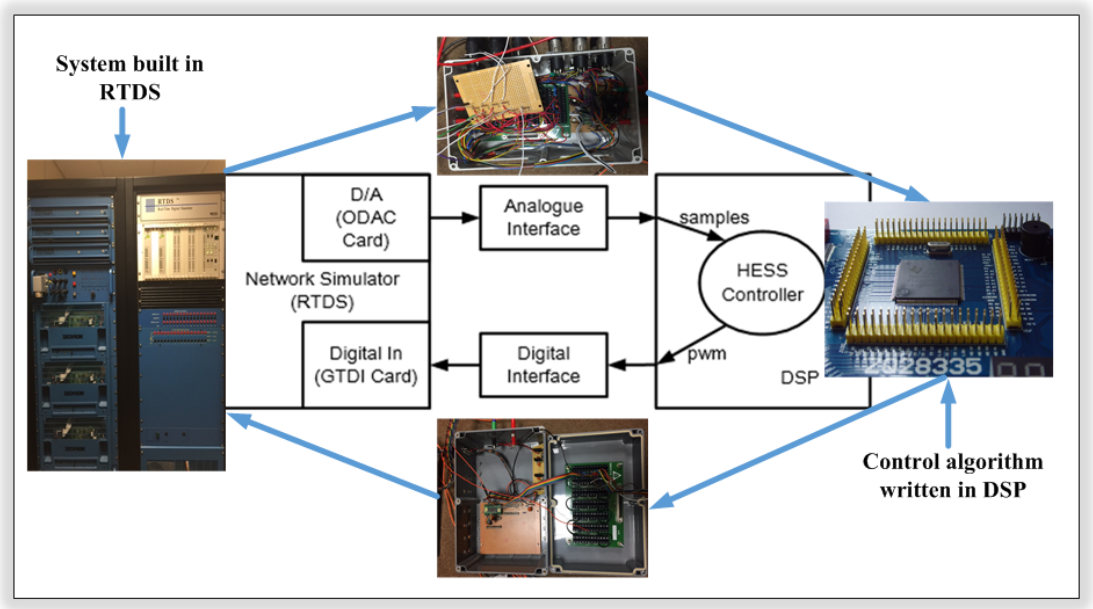

Fig. 5.2 Hardware-in-the-loop (HIL) testing system

In this section, the hardware in the real-time platform is introduced. Fig. 5.2 shows the HIL configuration which consists of the RTDS embed with the ODAC and GTDI cards, the analogue and the digital interfacing module and the DSP (TMS320F28335). The primary system is established and simulated in the RTDS. Analogue output is achieved through the onboard RTDS ODAC cards, which is responsible for converting the digital values from the RTDS to the analogue outputs. The analogue and the digital interfaces are used to connect the two hardware systems (the RTDS and the DSP). The function of the interfacing module is to process the output signals of the RTDS and the DSP and to make sure the input signals to each system are at the desired levels. The power management strategy and the HESS controller are implemented in the DSP. The DSP captures the analogue output signals from the ODAC card in RTDS and converts them to the digital signal by using the embedded ADC module. Then, based on the measurement data from

the RTDS, the DSP generates the control signals. The control algorithms are also debugged in the DSP board. The PWM pulses generated by the DSP are read by the RTDS through its GTDI card.

5.4.1 RTDS hardware

Fig. 5.3 RTDS in University of Bath

The RTDS consists of two types of processing units, and they are named by the RTDS Technologies Inc. as 3PC and GPC cards. The “3” in the 3PC card means three digital

signal processors (ADSP−21062 SHARC Processors) and the clock frequency for each processor is about 40 MHz The 3PC cards are usually arranged in parallel to increase the computing speed. The RTDS hardware in the University of Bath as shown in Fig. 5.3, has ten 3PC cards, five in each rack. Five 3PC cards are used in this study. There are also two Giga processor cards (GPC) in the RTDS in University of Bath, but they are not used in this study. The ODAC card and the GTDI card are embedded in the RTDS. The function of the ODAC card is to converter the digital values from the RTDS to the analogue outputs to the DSP. The GTDI card is responsible for reading the PWM signals from the DSP.

5.4.2 Interface modules

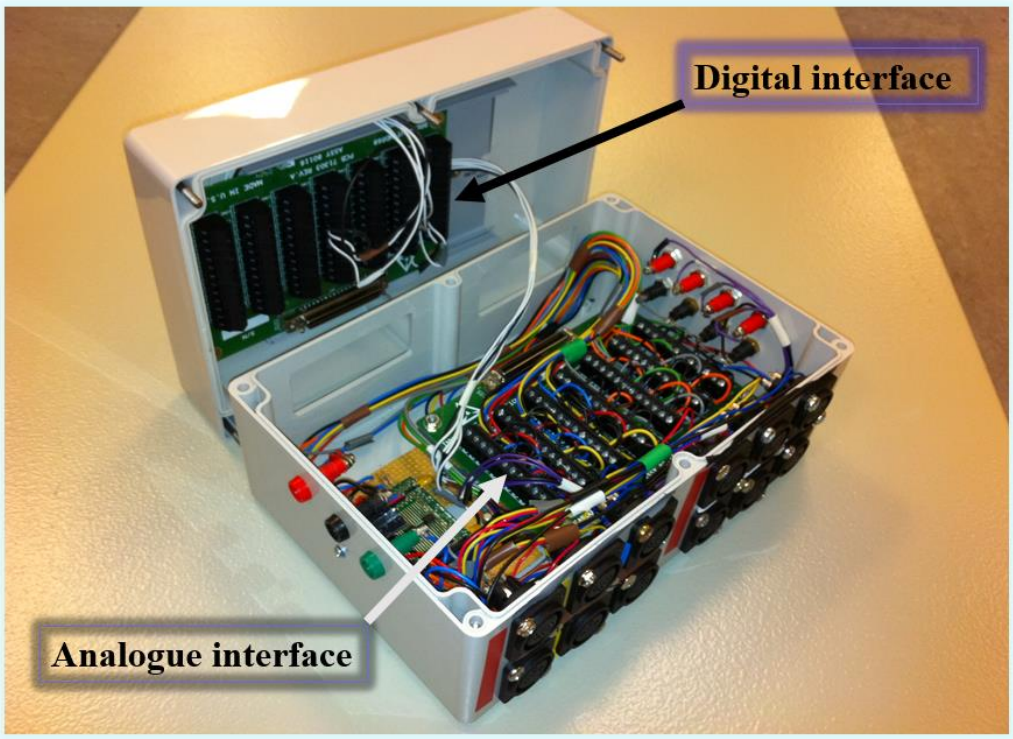

Fig. 5.4 The analogue and the digital interfaces used in the HIL circuit

The interface modules are necessary to convert output signals between the RTDS and the DSP to acceptable input levels. As it can be seen from Fig. 5.2, two interfacing

modules are needed in the HIL circuit, the analogue and the digital interfaces (as shown in Fig. 5.4). The analogue interface module physically connected the analogue signal from the ODAC cards to the DSP ADC module. The ODAC card generates the analogue signal at ±10V, whereas the input signal for the DSP 28335 peaks at 3.3V. Hence the interface circuit is needed to level the signals. The situation for the digital signal back circuit is similar to the analogue one that out signal from the DSP 28335 is driven by 3.3V logic, whereas digital input port of the GTDI card takes 5V logic. Therefore, in the signal back circuit, a digital interface is also needed.

5.4.3 The TMS320F28335 microcontroller

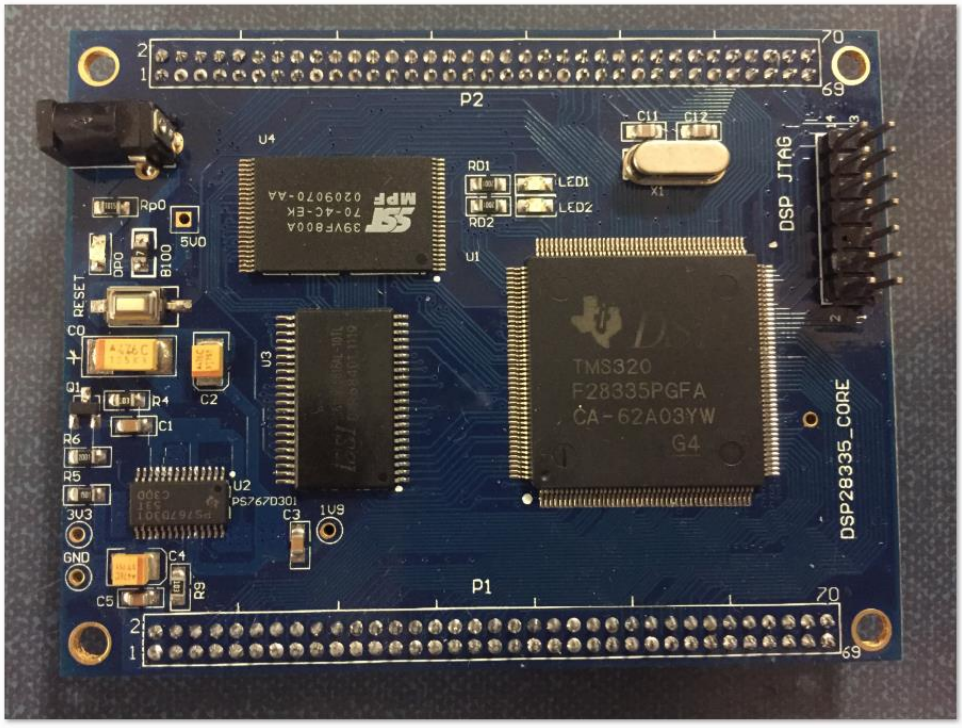

Fig. 5.5 DSP TMS320F28335

The microcontroller used to implement the control algorithm and generate physical PWM signals is the TMS320F28335 (as shown in Fig. 5.5) from Texas Instruments.

The software based on the C++ named Code Composer Studio (CCS) is used to develop the code for the control implementations. The detailed introductions of the TMS320F28335 are beyond the scope of this study. The very detailed description of DSP including the structures, the different registers and various functions can be found in reference [144].

5.5 Methodologies

5.5.1 Power management strategy

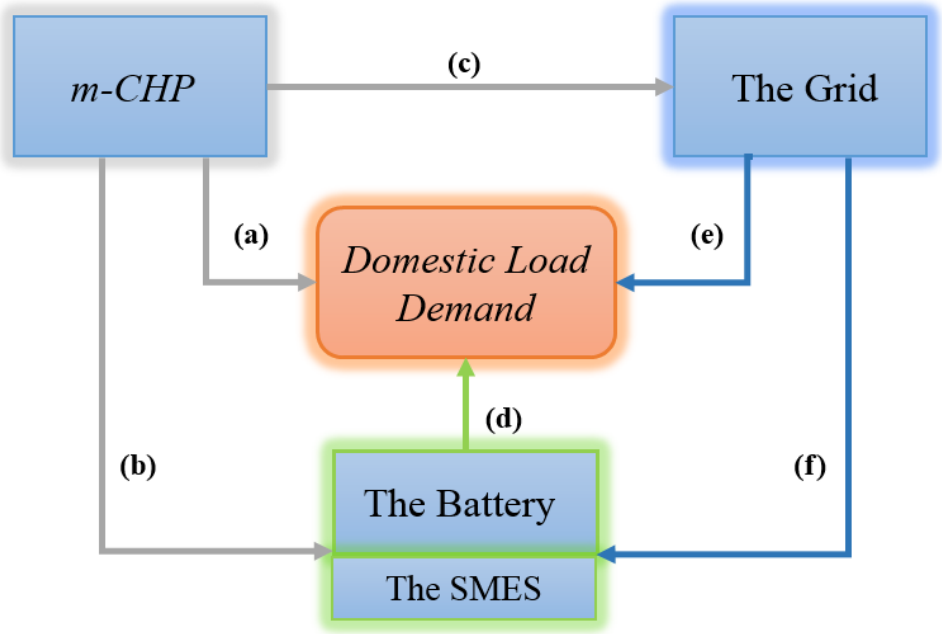

Fig. 5.6 The power management strategy

To achieve coordination control of different devices, a power-dominated power management strategy is proposed as shown in Fig. 5.6. This strategy can be illustrated by the following a-f cases:

a. In normal condition, the electrical power generated from the m-CHP (P_{CHP}) will support the load demand (P_{load}), preferentially.

b. The m-CHP will charge the HESS when $P_{CHP} > P_{load}$ and the battery state of charge $SOC < SOC_{max}$, the up-limit of battery SOC (97%). It should be figured out that, the SMES has low energy density which means it cannot store much energy and in this study, the battery is designed as an energy buffer to the SMES. Hence, the battery state of charge is used as charge/discharge criterion of the HESS.

c. The residential power system will export the electricity to the grid when $P_{CHP} > P_{load}$ and $SOC \geq SOC_{max}$.

d. The HESS system will discharge to meet the load demand when $P_{CHP} < P_{load}$ and $SOC \geq SOC_{min}$ (20%).

e. The residential power system will also buy electrical power in two conditions: 1. $P_{CHP} < P_{load}$ and $SOC \leq SOC_{min}$ or 2. $P_{CHP} < P_{load}$ and the time-of-use electric tariff is low.

f. The grid will also charge the battery when the tariff is low and battery $SOC \leq SOC_{max}$.

The main function of the overall power flow control, in this study, is to obtain the power export and import requirements of the HESS. The six power flow paths also illustrate other key points of the overall power management strategy:

- The electricity generated from the m-CHP is fully used in this system (shown by a, b and c).
- The m-CHP, the HESS and the grid are all able to support the load demand (shown by a, d and e), hence load demand can always be met.
- The HESS works as a kind of power transitional device shifting the power among the m-CHP, the load and the grid (shown by b, d and f), which means the energy storage system will undergo many reverse charge or discharge processes.

- The proposed domestic power system is able to either export or import the electric power according to the time-of-use electric tariffs (shown by c, e and f).
- The battery is kept within a safe operating region by setting the up and bottom limits.

5.5.2 System sizing and control parameters

Based on the sizing algorithm given in Chapter 4, the battery is selected as 240Ah and the SMES is sized at 5.27 kJ. The battery and the SMES parameters are shown in Table 5.1 and Table 5.2.

Table 5.1 Battery subsystem parameters

Battery type	60Ah lead acid
Maximal discharge current limit $\boldsymbol{I_m}$	29A
Longest discharge time t at $\boldsymbol{I_m}$	66s
Battery bank capacity	240 Ah
Largest energy deficiency	20.2kJ
Battery bank structure	Two in series and two cell banks in parallel
Battery bank terminal voltage	2×12 V
Maximal voltage of the battery converter	540V
DC bus voltage	500V

Table 5.2 SMES subsystem parameters

Inductance	0.47 H
Normal current	150 A
SMES voltage	120
Maximal voltage of the battery converter	520V
DC bus voltage	500V
Energy capacity	5.27 kJ

Based on Table 5.1, the range of k_{bat} is calculated as 0.32 to 0.72. The small k_{bat} value ($k_{bat} = 0.44$) is selected in order to decrease battery peak current as much as possible. Based on the parameters in Table 5.2, the required droop coefficient value of the SMES, k_{SMES}, is seen to be 0.87 or more. Unlike the battery, the SMES is able to charge/discharge quickly at high current and high frequency without degradation. Hence, the maximum current is not limited by the SMES itself but by other factors such as the rated current of the interfacing DC/DC converter and the storage capacity or size of the SMES. To reduce the size of the SMES, the droop coefficient of SMES should be constrained to be the lower value. Considering the observational error (0.3-0.5%) the $k_{SMES} = 0.87$ is selected to enhance system error tolerance.

5.6 Real-time verification

5.6.1 Laboratory test system configuration

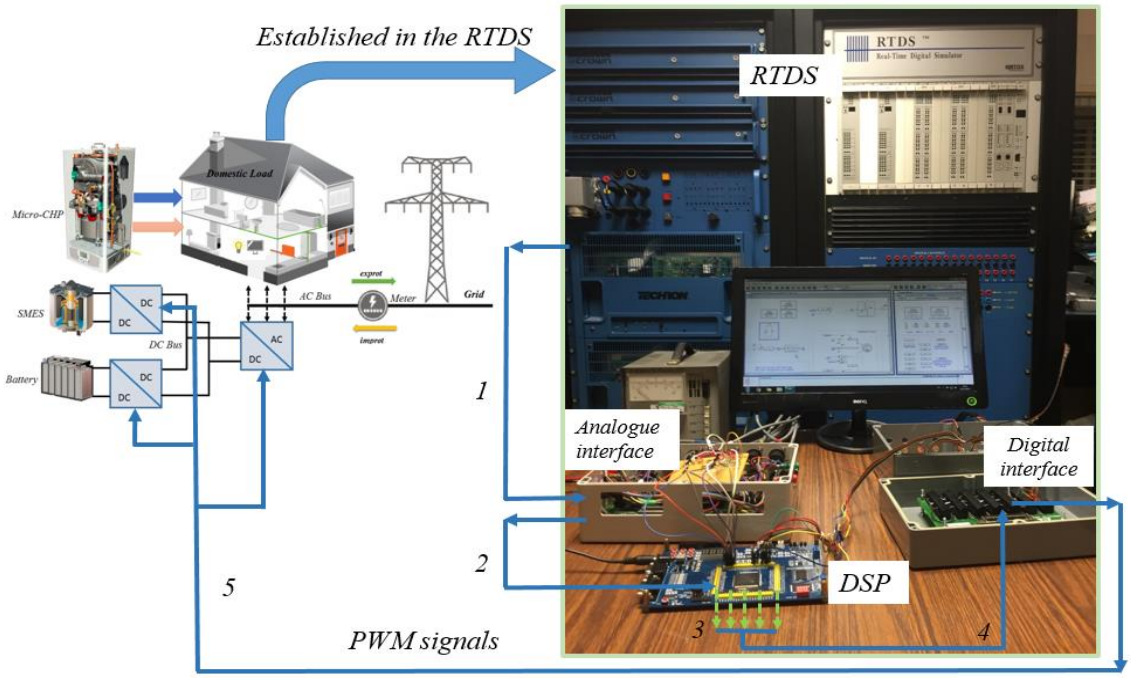

Fig. 5.7 The RTDS and HIL system configuration

A hardware in the loop test circuit is developed working together with the RTDS to verify the proposed control algorithm. As shown in the Fig. 5.7, the residential m-CHP system is built in the RTDS. To effectively verify the main contribution of this study, all the control algorithms are written in the external circuit using DSP.

As shown in the Fig. 5.7, the signalling process may be illustrated in 5 steps:

1. The parameters that used for the control are measured by the RTDS and sent to the interface as analogue data.
2. The analogue output signals are captured by the DSP from the analogue interface.
3. DSP generates the PWM control signals based on the measurement using the novel control algorithm
4. The digital control signals are sent to the digital interface.
5. The control PWM signals are read by the GTDI card in the RTDS and delivered to the converters.

As a result, the converters in the RTDS is controlled by the proposed control algorithm that implemented in the outside DSP circuit. The sampling rate of the digital to the analogue card is 50 μs. The switching frequency of the converters is selected as 2.5 kHz in order to increase the resolution of the PWM signals. The normal DC bus voltage regarded as reference voltage in this system is 500 V, the initial SMES current is 150 A.

5.6.2 The results from the RTDS and discussion

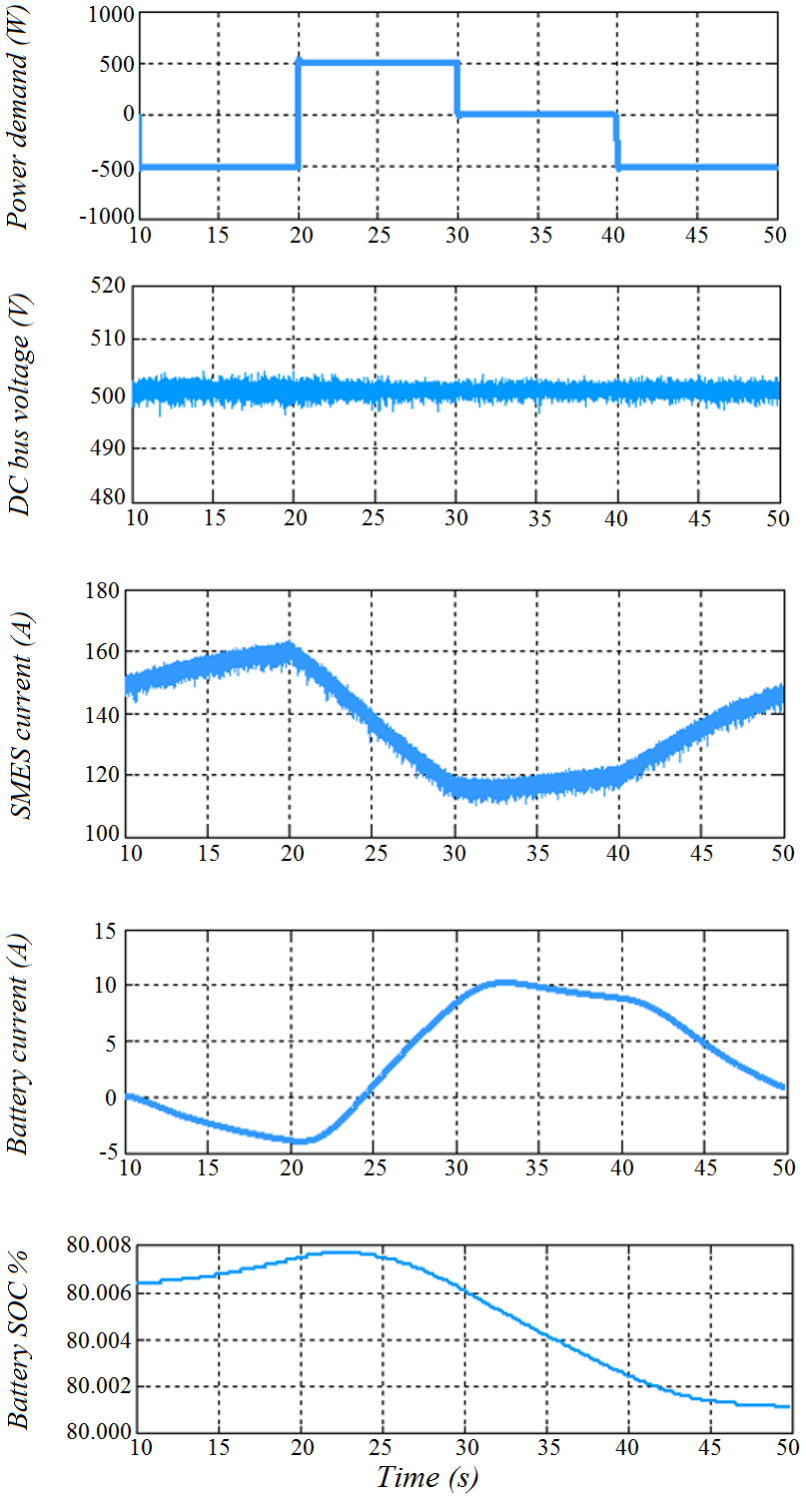

Fig. 5.8 Experimental results in the SMES/battery HESS

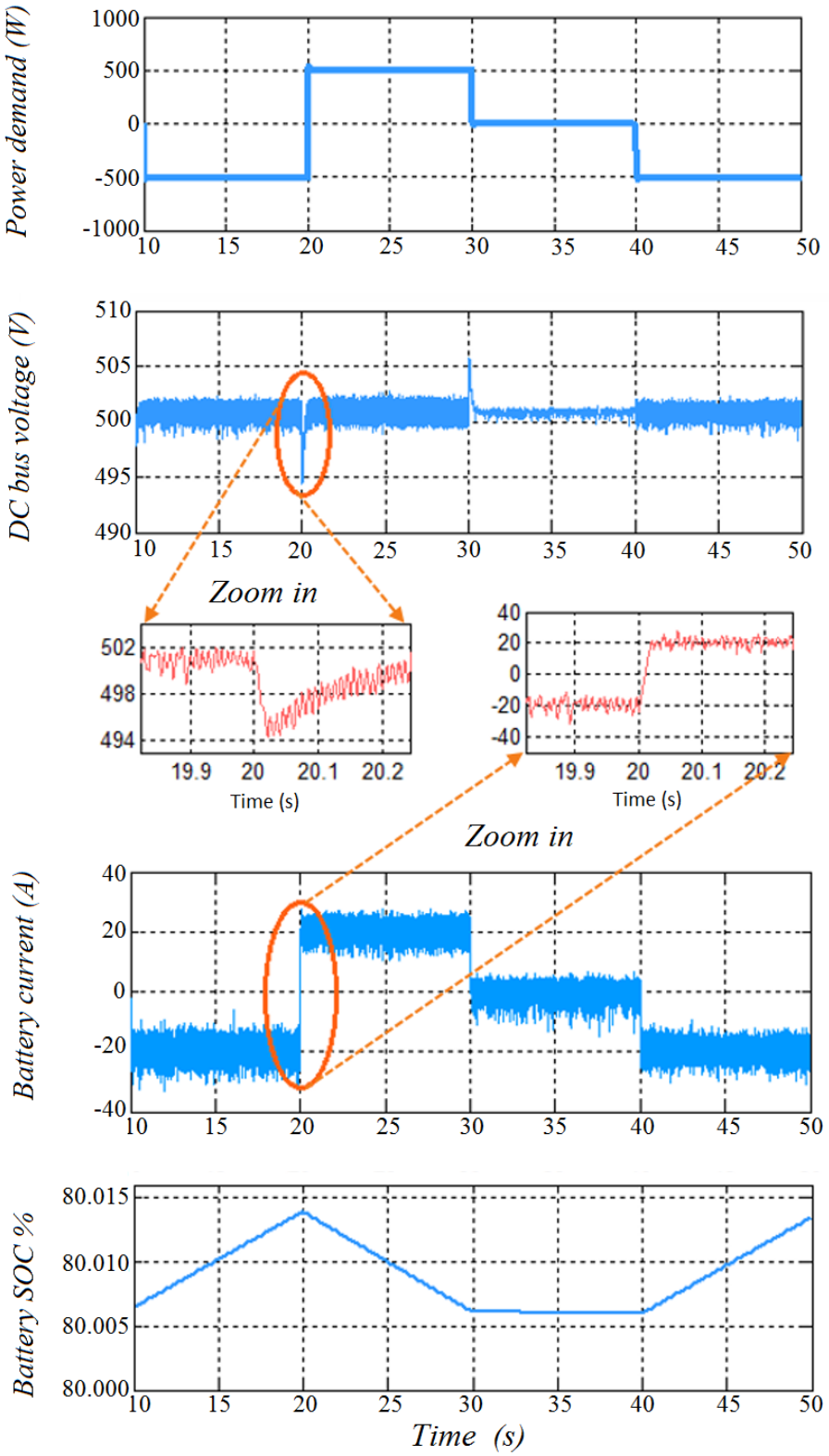

Fig. 5.9 Experimental results in the battery only system

Fig. 5.8 and Fig. 5.9 show the experimental results in two scenarios: the domestic power system with SMES/battery HESS and with battery only system. Using the PMS, the net power requirement for the energy storage can be obtained. Fig. 5.8 and Fig. 5.9 show the same power demand with the duration of 40 seconds (10s to 50s) in the two scenarios.

As shown in Fig. 5.8, in the first 10 second, the power demand is -500 W (Power demand= load - generation) and this amount of power surplus will raise the DC bus voltage. However, in order to maintain the DC bus voltage in the desired range, the SMES current rises to 162 A and the battery has a negative current, which means both the SMES and the battery come into action to absorb the excess energy.

Also, in Fig. 5.8, when the power demand becomes 500W in the following 10 seconds, the SMES current encounter with a dramatic decrease from 162 A to 114 A to discharge the stored energy. The battery current changes from negative to positive but compared with the SMES, the battery current climbing speed is much slower. This verifies the benefit of the HESS that the SMES is controlled to deal with the immediate power changes while the battery provides long-term energy support to compensate power fluctuations. In this way, the battery is protected from the abrupt high power changes.

In the third 10 seconds, there is no surplus or deficient power flowing in the system, but as it can be observed from Fig. 5.8, the SMES current increases, which means the SMES is charged. In addition, when there is no power demand, the battery current does not come to the zero but stay in a positive value to discharge its energy. The reason for this phenomenon is that the SMES current is lower than the initial current hence the battery delivers its energy to charge the SMES. This situation further proved the HESS control

that the battery works as an energy buffer to the SMES and at the same time, is kept from the immediate change of state.

In contrast to the SMES/battery HESS, Fig. 5.9 shows the system performance of the battery only case. As can be seen from Fig. 5.9, the battery current changes immediately with the power demand variations. These abrupt changes of the current will accelerate the battery degradation process hence reducing battery service life. In addition, the DC bus voltage is not as stable as that in the HESS and some cusps can be observed at the power change points. The zooming in figures of the DC bus voltage and the battery current at the power change point (20 s) may be used to explain the cause of the cusps. The lead-acid battery cannot response very quickly to the power demand, hence cause the delay of the charge/discharge current, resulting in the jut of the DC bus voltage.

5.7 Conclusions

This Chapter investigates the use of a SMES/battery hybrid energy storage system in a domestic power system with m-CHP. An overall system power management strategy is designed and the HESS droop control method is used in this study to prioritise the power demand sharing between the SMES and the battery. To verify the new control method, the hardware in the loop test circuit is established coupled with the real-time simulator. A representative domestic grid-connected power system with the m-CHP and the HESS is developed in the RTDS and the physical control signals are generated by the DSP in the external circuit. The experimental results show that the proposed methods are able to exploit the different characteristics of the SMES and the battery to meet the unbalance power in the residential system. The battery in the experiment is

protected from the continual short-term charge/discharge cycles and abrupt power changes and, as a result, the battery lifetime is improved.

A quantitative analysis of battery lifetime extension in the HESS is also needed in this study. To give an accurate prediction of the battery lifetime, a long sample of the battery performance is needed. However, the laboratory experiment is always designed as a test system to show the short-term performance of the proposed HESS. A short time duration performance is not generally enough to present normal charge/discharge processes of the battery as the battery is working as the long-term ESS in the HESS. Therefore, the simulation verification of the HESS is very necessary. The following Chapter introduces the simulation works for battery lifetime extension evaluation.

Chapter 6 Battery Lifetime Extension and Associated Cost-benefit Analysis

6.1 Introduction

Chapter 5 presents the RTDS and HIL experiment to test the SMES/battery HESS in a domestic power system. As can be seen from the experimental results in Chapter 5, the battery is protected by the SMES from the frequent charges/discharges and abrupt current. The battery service time, therefore, is extended. Nevertheless, we cannot know from the experiment by how much lifetime the battery is improved. In consideration of the battery lifetime extension evaluation, long-term simulation work is needed. The simulation model is established in the Matlab/Simulink based on the same case as introduced in Chapter 6. The contribution of this chapter mainly lies in the quantitative analysis of the battery lifetime. The methodology is firstly introduced in Section 6.2. After that, the simulation results and discussions are given in Section 6.3. The extension of the battery lifetime may also have an impact on the long-term cost of the HESS. Hence, by taking advantage of the battery lifetime study, the cost analysis of the SMES/battery HESS is also presented in this chapter.

6.2 Simulation model

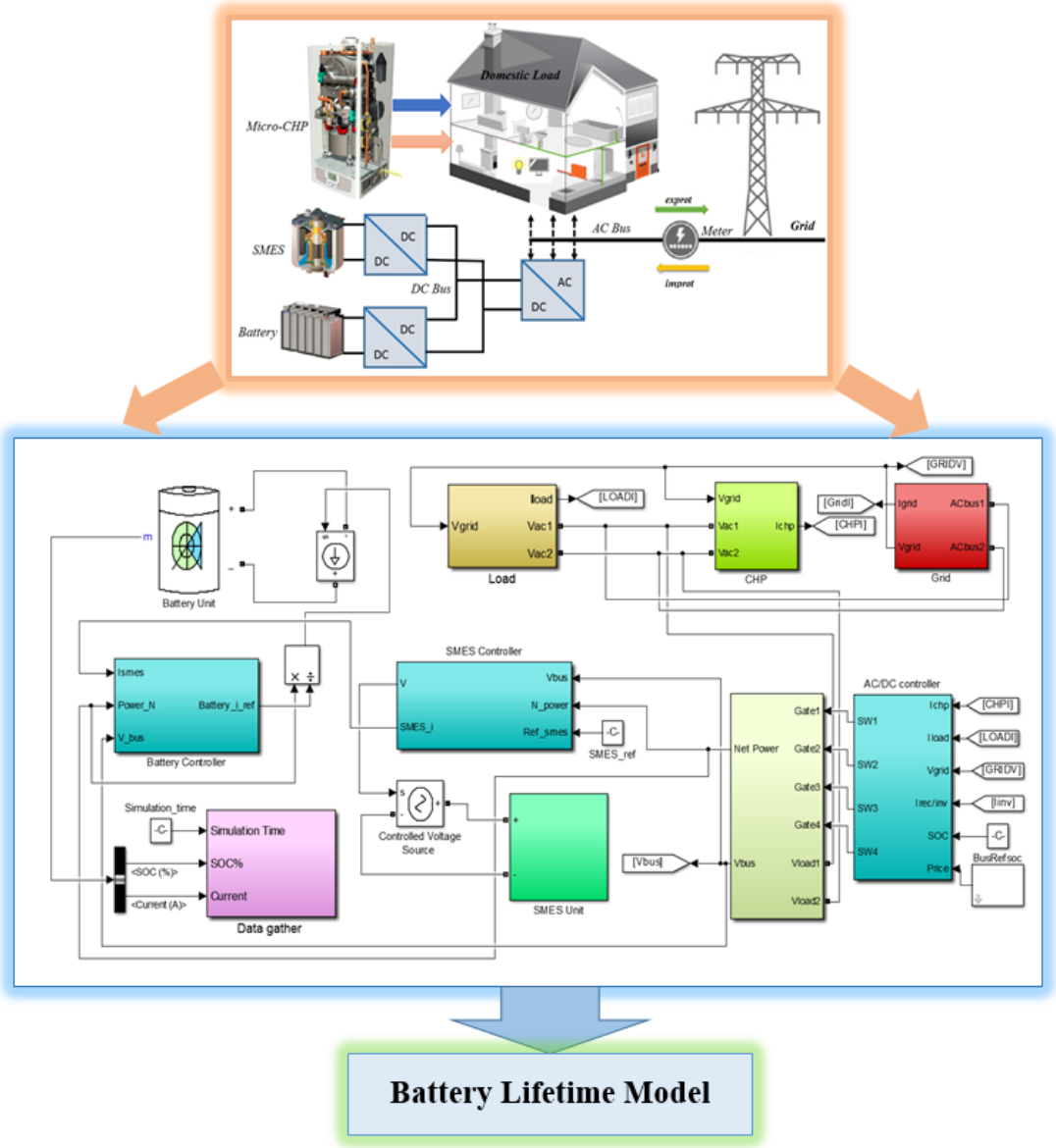

Fig. 6.1 The flow path of quantitative analysis of the battery lifetime

Fig. 6.1 gives the flow path to describe the quantitative analysis of the battery lifetime in this study. In the first step, the domestic power system is developed in the Matlab/Simulink. The battery and the SMES are controlled using two bidirectional DC/DC converters and then interfaced with the AC bus by a DC/AC converter. The battery and the SMES are established based on the work described in [14]. The

electrical performance of the grid-connected CHP system is modelled according to the method in [82]. The data of battery SOC and battery current during the simulation period can be obtained by running the simulation in Matlab. Then, the battery performance data are used as the key input to the battery lifetime prediction model.

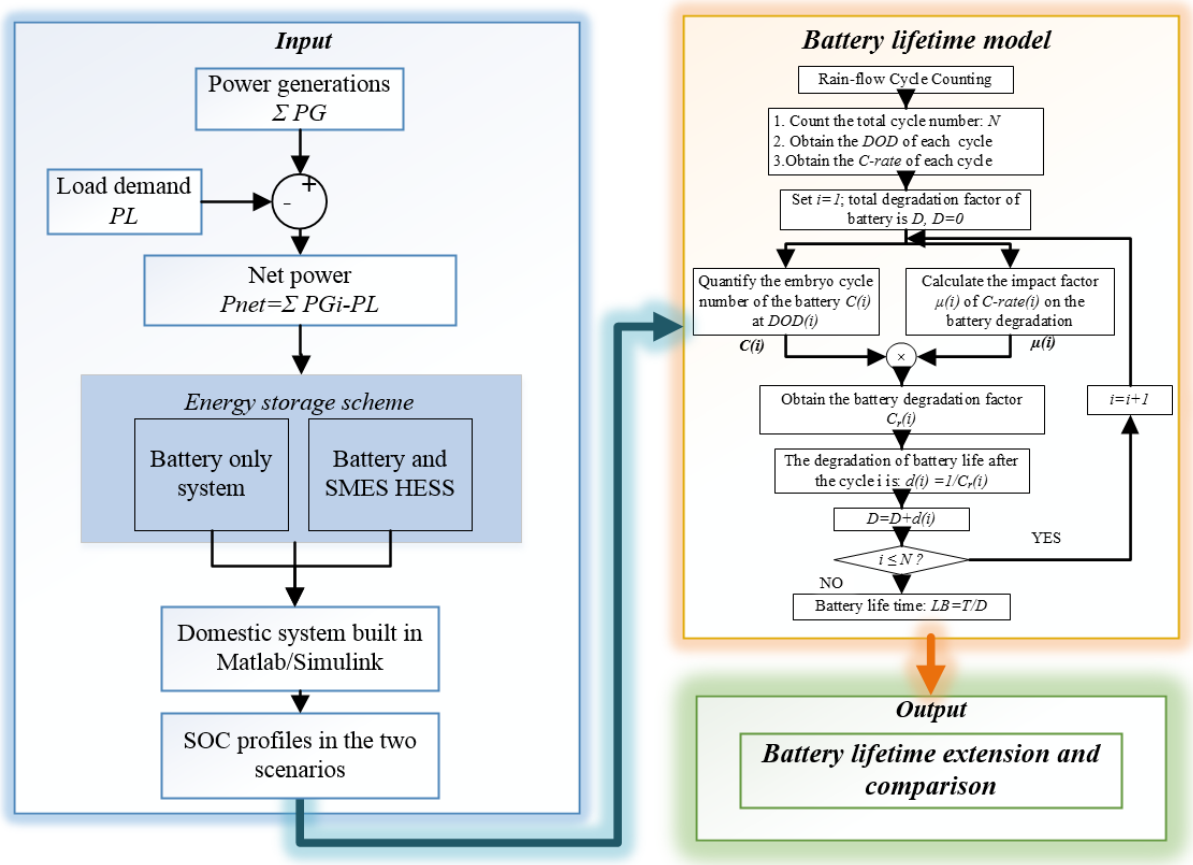

Fig. 6.2 Quantitative analysis of the battery lifetime extension

The quantitative analysis method of the battery lifetime extension is shown in Fig. 6.2. As shown in Fig. 6.2, the input data for the algorithm is the battery depth of discharge data during the simulation time *T*. By using the battery lifetime model introduced in Chapter 3, the irregular charge and discharge cycles are resolved into sub-cycles and then recomposed into an array of full cycles. Then, three factors, the total cycle number N, the DOD of each rearranged full cycle and the C-rate of each cycle, can be obtained.

Based on the "cycle-to-failure" curve [14, 145], the embryo cycle number *C(i)* of battery at the *DOD(i)* can be obtained. Also, the impact factor $\mu(i)$ of the *C-rate (i)* can be calculated based on the battery lifetime modelling. The cycle number *C(i)* multiplied by $\mu(i)$ will return the battery degradation factor *Cr(i)*.

Then, the effect on battery lifetime of cycle i is *d(i)*, where *d(i)=1/Cr(i)*. With the given simulation duration T, the predicted battery lifetime L can be obtained with Eq. 6.1:

$$L = \frac{T}{\sum_{i=1}^{i=N} d(i)} \tag{6.1}$$

Therefore, the battery lifetime extension $L_{ext}$is easy to calculate:

$$L_{ext} = L(HESS) - L(BOS) \tag{6.2}$$

Where the $L(HESS)$ is the battery lifetime prediction in the HESS, and $L(BOS)$ is the prediction in battery only system.

6.3 Results

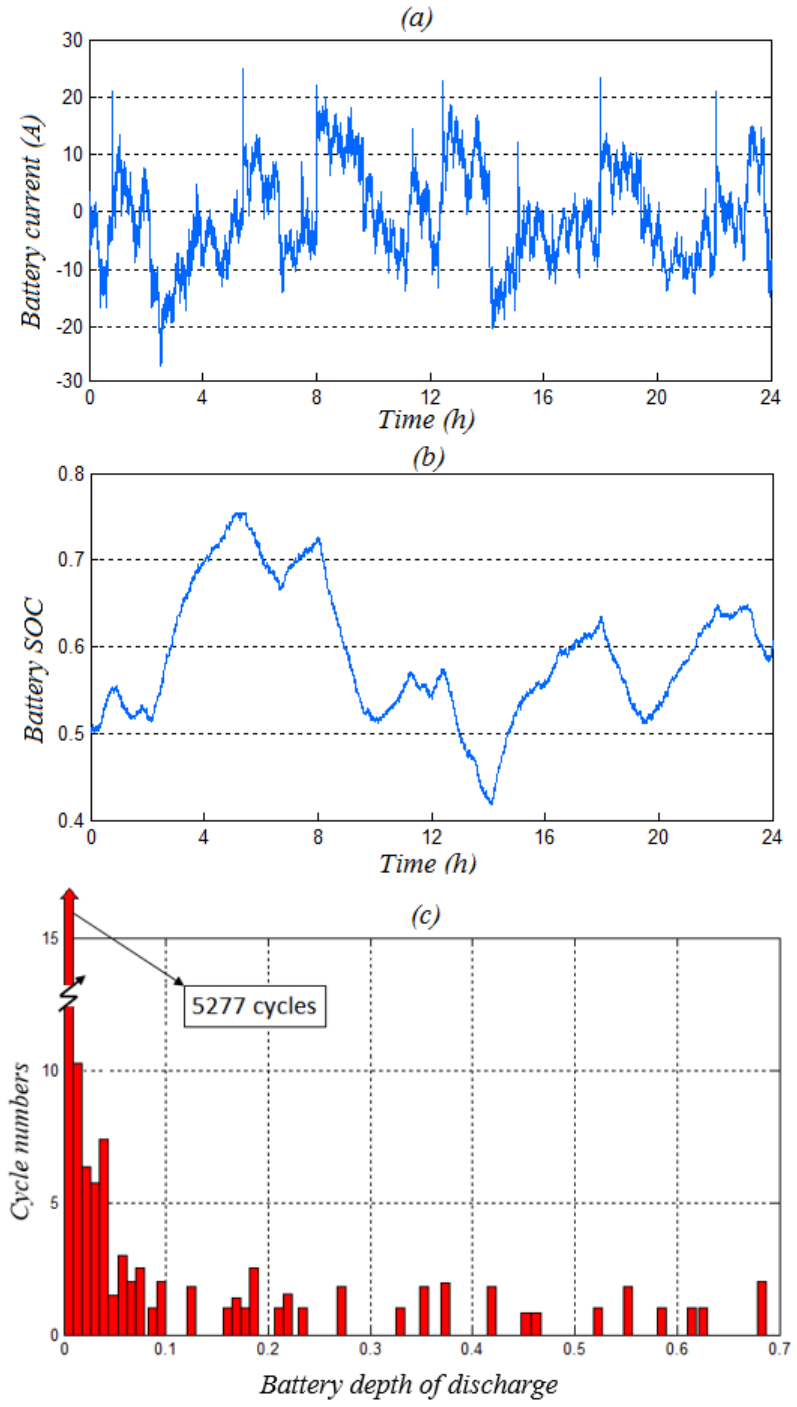

Fig. 6.3 Simulation result in SMES/battery system (a) battery current (b) battery SOC (c) histograms of cycle numbers at different DODs

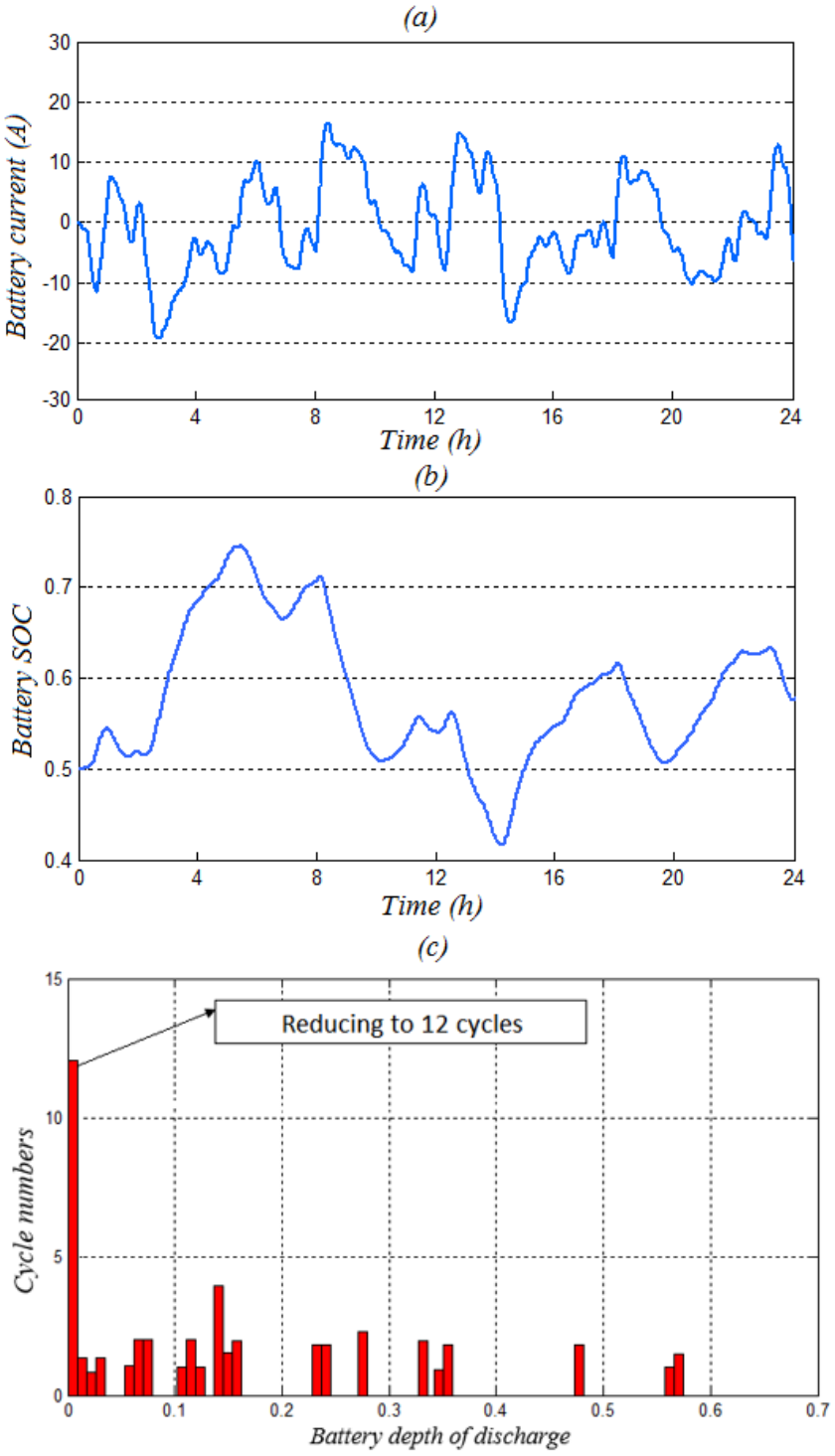

Fig. 6.4 Simulation result in battery only system (a) battery current (b) battery SOC (c) histograms of cycle numbers at different DODs

The long-term performances (24 hours) of the battery are compared between Fig. 6.3, the HESS, and Fig. 6.4, the battery only system. Comparison of Fig. 6.3 (a) and Fig. 6.4 (a) illustrates that the battery in the HESS experiences significantly fewer high-frequency fluctuations and polarity reversals. As a result, the state of charge (SOC) in the HESS (Fig. 6.3 (b)) undergoes fewer short-term charge and discharge cycles than that in the battery only system (Fig. 6.4(b)). Additionally, as can be seen from the two figures, the absolute value of the peak currents in the BOS is much higher than that in the HESS. Similarly with the current, the battery in the BOS has deeper DODs.

Fig. 6.3 and Fig. 6.4 also give histograms to describe the cycle numbers of batteries at different depth of discharge in the battery only system and the HESS. The inputs are the battery state of charge data, which returns the cycle numbers at different depth of discharge. As can be seen from the histograms, the batteries undergo extensively fewer small-scale cycles and also a relatively lighter depth of discharge in the HESSs.

Table 6.1 Comparison of battery lifetimes in the BOS and the HESS

Scenarios	**Quantified Battery Lifetime (years**	**Battery lifetime extension compared with BOS (%)**
BOS	6.2	0
HESS	8.7	40.32%

The battery service times are quantified, as shown in Table 6.1. In the case of the SMES/battery HESS, the predicted battery lifetime is 8.7 years, whereas that in the

battery only system is only 6.2 years. Hence, a 2.5 years (over 40%) extension of battery service lifetime is achieved.

6.4 Cost-benefit analysis

The superconducting energy storage system is costly because of the material cost and the high investment of the SMES is the main reason that discourages people from using it. However, in the hybrid energy storage scheme, with the integration of the battery, the size requirement for both the SMES and battery can be dramatically reduced. Also, compared with the battery only system (BOS), the hybrid design has the advantage of extending battery lifetime. As introduced in Section 6.3, the battery service life is quantitatively improved by 40% from 6.2 years to 8.7 years. Moreover, with the rapid development of superconductor manufacturing technology, there are more and more commercial companies around the world able to produce cheap superconducting tape, such as SuNam and Shanghai Superconductor [89, 90]. The price of superconductor has fallen from $60 per metre in 2012 to $22 per metre in 2016, which is a significant cost reduction in the last five years. Some published works also estimate that, in the future, it would be possible to reduce the price of superconductor to under $10 [91, 92]. Therefore, with the continuous development of superconductive material, it can be seen that the cost of SMES could be further reduced.

Table 6.2 The comparison of the battery only system and hybrid energy storage system

Cases	Battery			SMES			Total cost ($)
	Size	Replace-ment	Cost($)	Size	Replace-ment	Cost($)	
Battery only system	28×60 Ah	6 times	41160	N/A	N/A	N/A	41160
SMES/ battery HESS	4×60Ah	4 times	3920	5.27 kJ	0	44800	48720

Based on the sizing method, the SMES is selected as 5.27kJ and the battery is 240 Ah (60Ah each × 4 cells). If only the battery energy storage system is used in the same situation, based on the same sizing method, an extra 24 battery cells are needed to meet the instantaneous power demand. Based on the SMES design method [67, 146] and the current superconductor price [91], the total cost of the 5.27kJ SMES is $44.8k, including the cryocooler. The unit price for the 60Ah lead acid battery is quoted as $245. The total lifetime of the energy storage project is assumed as 35 years. There is almost no lifetime degradation for the SMES system and, therefore, the SMES in the hybrid design does not need to be replaced. According to the lifetime analysis in Section 8.3, the battery in the hybrid scheme needs to be replaced four times, whereas, in the battery only system, the number is six. Table 6.2 illustrates the investments in the proposed two cases.

As shown in Table 6.2, the total cost of the SMES/battery hybrid system is higher than that of the battery only system by 18.37%. The estimation of Table 6.2 is based on the price of $22/m for the superconductor tape.

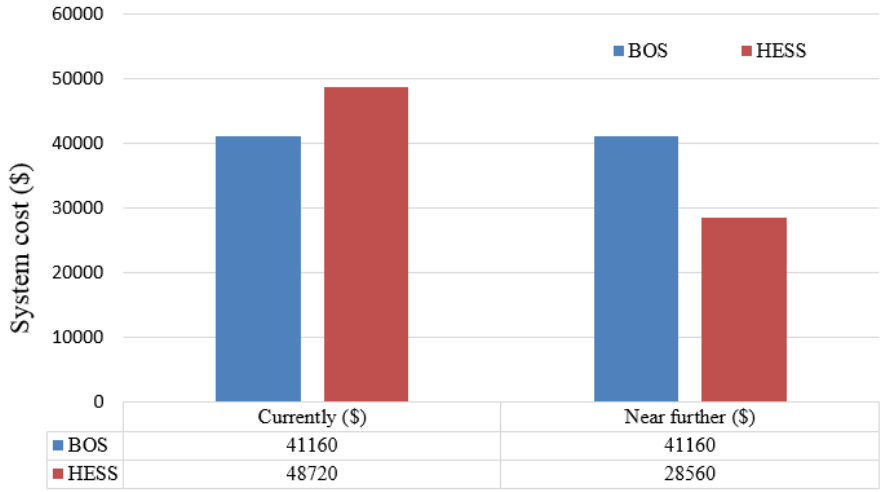

Fig. 6.5 Comparison of the system costs

However, as mentioned earlier, with the continuous development of superconductive material, the price of the superconductor has been falling and it is believed that the price will reduce down to at least $7.2/m in the near future [89, 91, 92]. Based on the same cost analysis method, the results indicate that the hybrid design will be more economical in the near future. As shown in Fig. 6.5, if the superconductor decreases to $7.2/m, the system cost of the hybrid energy storage will fall to $28,560, which is 30.6% cheaper than the battery only system. It should be noted that this cost-benefit analysis is made based on the simple situation and some factors such as the maintenance fee and the investment interest is not considered in this study.

6.5 Conclusions

The quantitative analysis of the battery lifetime is introduced in this chapter based on the long-term simulation. The simulation results show that, as the SMES filters the high-frequency power fluctuations, the battery DOD and current in the SMES/battery HESS undergo significantly fewer polarity reversals than in the battery only system. The reduction in both the charge/discharge frequency and the discharge rate results in the improvement of the battery lifetime in the HESS. The battery lifetime mode presented in Chapter 3 is used to quantify the battery lifetime extension. The estimated battery lifetime for BOS is 6.2 years, whereas, with the HESS, it is significantly higher at 8.7 years, resulting in a 2.5 years (over 40%) improvement. The cost analysis is also carried out in this chapter and the SMES/battery HESS is shown to have an economic benefit in a long-term project.

Chapter 7 Conclusions

7.1 Summary

This dissertation has investigated the SMES/battery hybrid energy storage scheme with respect to the system design, sizing, control and evaluation. Both the simulations and experiments are implemented to assess the proposed hybrid system. The accomplished results can be summarised as follows:

- As the extension of the battery lifetime is one of the key merits of the SMES/battery HESS. An original battery lifetime model based on a modified rain-flow cycle-counting algorithm has been developed in this thesis. The new method advances the previous ones by taking the C-rate into consideration and, hence, is able to return a more accurate prediction of battery lifetime.

- To achieve the effective combination of two kinds of ESSs, an overall power management method integrating the different characteristics of SMES and battery is needed. Three kinds of power management strategies have been introduced to be used in the HESS for the power sharing between the SMES and the battery. The application of each PMS is summarised with respect to their advantages and disadvantages. The frequency-dominant PMS is recommended to be applied to wind power systems because of its good high-frequency power handling capability. The SMES is highly efficient in the SMES fully active PMS, but the practical constraints challenge the sound operation of SMES. Hence, it

is better to use this PMS for a power system in small scale. Both the SMES and the battery in the power-dominant PMS have high efficiency, but the design of the strategy is very complicated. Therefore, the power-dominant PMS is the ideal choice in the case of complex power situations.

- The different energy and power demands for ESSs are considered in the sizing method to ensure the complementary function between the SMES and the battery. Working as the long-term storage in the HESS, the battery has large energy density and is very suitable for energy management functions. Whereas, the SMES is used as the short-term energy storage and, while it cannot store much energy, it can handle high-frequency power fluctuations. Therefore, it is reasonable to divide the sizing study into two steps. Firstly, in terms of energy dispatching requirement, size the battery to ensure that the load energy demand is always met. Secondly, regarding the high-frequency power fluctuation, determine the size of SMES. The relative sizing of the battery and the SMES capacities within a HESS is performed using the new method in a case study, which is also shown to benefit in addressing the SMES oversizing problem.

- A novel use of a droop control method for controlling the power sharing between the SMES and battery has been introduced in this thesis. The novel control method is able to prioritise the power sharing between the SMES and the battery and manage the charge/discharge rates of the different ESSs by adjusting the droop factor to exploit different characteristics of the ESSs. The detailed implementation of the droop control method is also described. To verify the new control method, the hardware in the loop test circuit is established, coupling with the real-time simulator. A representative domestic power system

with the CHP and the HESS has been developed in the RTDS. The physical control signals are generated by the DSP in the external circuit. Experimental results show that the proposed method is able to control charge/discharge prioritisation and, hence, protect the battery from high power demand and rapid transient cycling.

- The quantitative evaluation of the battery lifetime extension in the HESS has been presented in this thesis. The quantitative method has been introduced by the simulation work to enable the long-term operation and, hence, provide rich samples for the battery lifetime analysis. The simulation shows that the battery in the HESS undergoes significantly fewer small cycles than that in the battery only system. As a result, the battery lifetime can be extended by reducing the peak current and smoothing the sharp charge/discharge transient content. The battery lifetime model presented in Chapter 3 is able to quantify both the impacts of the charge/discharge cycles and current rates on the battery degradations and is exactly designed for these cases. The battery lifetime in the battery only system is estimated at 6.2 years, whereas, with the HESS, it is significantly higher at 8.7 years, resulting in a 2.5 years (over 40%) improvement, This is very meaningful for battery-based energy storage projects. The cost analysis is also carried out based on the simulation results and the SMES/battery HESS is shown to have an economic benefit in long-term operation.

7.2 Further work

The SMES in this study is modelled as a super-inductor. The SMES modelling method is according to published works [14, 147]. The detailed modelling, design and test of

the SMES at the device-level is another topic that is out of the scope of this study. However, when it comes to the implementation of the proposed methods in the real SMES system, additional constraints need to be considered. As the superconductivity can be maintained below the characteristic critical temperature, the temperature is undoubtedly a critical consideration for the SMES design. The critical current is defined as the maximum current the superconductive material can withstand while still maintaining its superconductivity. If the current in the SMES goes beyond the critical current (quench phenomenon), the SMES will lose the benefits and, worse still, the SMES coil may be totally destroyed. The critical current of the SMES greatly depends on the cooling system and SMES design. The temperature, the critical current and the SMES configuration are closely related to the real operation of the SMES; hence, this may impact the SMES control method. A new kind of control method may be proposed to be particularly designed for the SMES with consideration of its specific operation constraints.

Although the critical current of the SMES has been considered in the coefficient factor study, the simple model of the SMES does not greatly reflect the relationship between the control method and the critical current in the simulation results. A more detailed modelling of the SMES coupling with the control method, involving superconducting factors (e.g. the temperature and the critical current), may be a novel proposal.

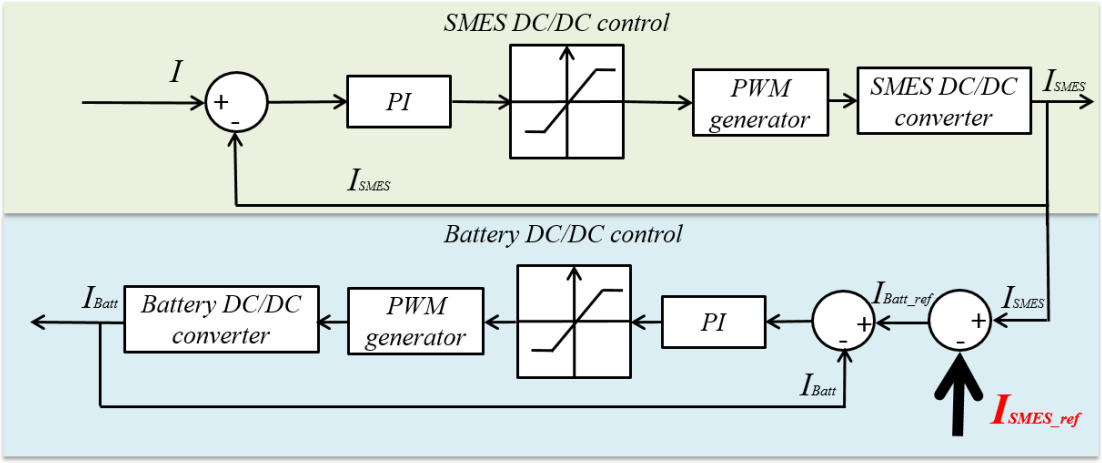

Fig. 7.1 Example of the multi-functional control strategy

Moreover, as regards security concerns, the quench protection is necessary for the real operation of the SMES. The interaction between the quench protection algorithm and the SMES control method may generate innovative ideas about a multi-functional control strategy. For example, to maintain the SMES current in an optimal range, a new control topology, as shown in Fig. 7.1, may be efficient. In this control scheme, the battery works as an energy buffer to constantly maintain the SMES current at the desired value. Hence, the quench-protection function is enabled. Furthermore, due to the inductive characteristic of the SMES coil, the battery is protected from sudden currents. It should also be noted that Fig. 7.1 shows a type of conceptual control that is not implemented in this study and the I_{SMES_ref} also needs to be explored according to the SMES quenching characteristics.

A novel battery lifetime model has been presented to give a quantitative evaluation of battery lifetime extension in the HESS. With this method, the rate of the battery current is added as a new factor that causes battery degradation. The impact of the current rate is, therefore, quantified in the new model. The new algorithm is shown to give a more

accurate prediction of the battery service time. Nevertheless, there are still many other factors that are not included in the battery lifetime prediction method. For example, the environment temperature influences the electrochemical process of the battery and, hence, has an impact on battery lifespan, whereas the temperature is assumed as 20 degrees Celsius (the indoor temperature) in this study. The battery lifetime model may be further improved by adding more ageing factors, such as the temperature and the current mean-values into the qualification. However, the main challenge in terms of further improvement may lie in the lack of accurate and abundant test data of the battery. A starting point would be to provide battery life curve data which reflect the effects of different stress factors on the battery ageing process.

References

[1] X. Luo, J. Wang, M. Dooner, and J. Clarke, "Overview of current development in electrical energy storage technologies and the application potential in power system operation," *Applied Energy*, vol. 137, pp. 511-536, 1/1/ 2015.

[2] H. Chen, T. N. Cong, W. Yang, C. Tan, Y. Li, and Y. Ding, "Progress in electrical energy storage system: A critical review," *Progress in Natural Science*, vol. 19, pp. 291-312, 2009.

[3] H. Lund and G. Salgi, "The role of compressed air energy storage (CAES) in future sustainable energy systems," *Energy Conversion and Management*, vol. 50, pp. 1172-1179, 2009.

[4] Q. Yang, C. Gu, S. Le Blond, and J. Li, "Control scheme for energy storage in domestic households," in *Power Engineering Conference (UPEC), 2014 49th International Universities*, 2014, pp. 1-6.

[5] M. Farhadi Kangarlu and M. R. Alizadeh Pahlavani, "Cascaded multilevel converter based superconducting magnetic energy storage system for frequency control," *Energy*, vol. 70, pp. 504-513, 6/1/ 2014.

[6] M. N. Kabir, Y. Mishra, G. Ledwich, Z. Xu, and R. C. Bansal, "Improving voltage profile of residential distribution systems using rooftop PVs and Battery Energy Storage systems," *Applied Energy*, vol. 134, pp. 290-300, 12/1/ 2014.

[7] J. Zhu, M. Qiu, B. Wei, H. Zhang, X. Lai, and W. Yuan, "Design, dynamic simulation and construction of a hybrid HTS SMES (high-temperature superconducting magnetic energy storage systems) for Chinese power grid," *Energy*, vol. 51, pp. 184-192, 3/1/ 2013.

[8] G. Panayiotou, S. Kalogirou, and S. Tassou, "Design and simulation of a PV and a PV–Wind standalone energy system to power a household application," *Renewable Energy*, vol. 37, pp. 355-363, 1// 2012.

[9] M. Mohamed Thameem Ansari and S. Velusami, "DMLHFLC (Dual mode linguistic hedge fuzzy logic controller) for an isolated wind–diesel hybrid power system with BES (battery energy storage) unit," *Energy*, vol. 35, pp. 3827-3837, 9// 2010.

[10] H. Zhao, Q. Wu, S. Hu, H. Xu, and C. N. Rasmussen, "Review of energy storage system for wind power integration support," *Applied Energy*, vol. 137, pp. 545-553, 1/1/ 2015.

[11] P. Zhao, Y. Dai, and J. Wang, "Design and thermodynamic analysis of a hybrid energy storage system based on A-CAES (adiabatic compressed air energy storage) and FESS (flywheel energy storage system) for wind power application," *Energy*, vol. 70, pp. 674-684, 6/1/ 2014.

[12] Y. Gao, S. Shao, H. Zou, M. Tang, H. Xu, and C. Tian, "A fully floating system for a wave energy converter with direct-driven linear generator," *Energy*, vol. 95, pp. 99-109, 1/15/ 2016.

[13] H. L. Ferreira, R. Garde, G. Fulli, W. Kling, and J. P. Lopes, "Characterisation of electrical energy storage technologies," *Energy*, vol. 53, pp. 288-298, 5/1/ 2013.

[14] J. Li, A. M. Gee, M. Zhang, and W. Yuan, "Analysis of battery lifetime extension in a SMES-battery hybrid energy storage system using a novel battery lifetime model," *Energy*, vol. 86, pp. 175-185, 6/15/ 2015.

[15] F. Díaz-González, A. Sumper, O. Gomis-Bellmunt, and R. Villafáfila-Robles, "A review of energy storage technologies for wind power applications," *Renewable and Sustainable Energy Reviews*, vol. 16, pp. 2154-2171, 2012.

[16] T. Ise, M. Kita, and A. Taguchi, "A hybrid energy storage with a SMES and secondary battery," *IEEE Transactions on Applied Superconductivity*, vol. 15, pp. 1915-1918, 2005.

[17] T. M. I. Mahlia, T. J. Saktisahdan, A. Jannifar, M. H. Hasan, and H. S. C. Matseelar, "A review of available methods and development on energy storage; technology update," *Renewable and Sustainable Energy Reviews*, vol. 33, pp. 532-545, 5// 2014.

[18] A. P. Mohammad Reza, M. Hossine Ali, and S. Abbas, "Voltage stabilization of VSI SMES capacitors and voltage sag compensation by SMES using novel switching strategies," *Energy*, vol. 35, pp. 3131-3142, 8// 2010.

[19] Y. Yamada and T. Hattori, "Development of cost-effective HTS superconductor.: Simple heat treatment and low-cost substrate Ni/NiO," *Physica C: Superconductivity*, vol. 335, pp. 78-82, 2000.

[20] A. Malozemoff, S. Fleshler, M. Rupich, C. Thieme, X. Li, W. Zhang, *et al.*, "Progress in high temperature superconductor coated conductors and their applications," *Superconductor Science and Technology*, vol. 21, p. 034005, 2008.

[21] W. Yuan, *Second-generation high-temperature superconducting coils and their applications for energy storage*: Springer, 2011.

[22] J. Li, M. Zhang, Q. Yang, Z. Zhang, and W. Yuan, "SMES/Battery Hybrid Energy Storage System for Electric Buses," *IEEE Transactions on Applied Superconductivity*, vol. 26, pp. 1-5, 2016.

[23] W. Li, G. Joós, and J. Bélanger, "Real-time simulation of a wind turbine generator coupled with a battery supercapacitor energy storage system," *IEEE Transactions on Industrial Electronics*, vol. 57, pp. 1137-1145, 2010.

[24] O. Briat, J. M. Vinassa, W. Lajnef, S. Azzopardi, and E. Woirgard, "Principle, design and experimental validation of a flywheel-battery hybrid source for heavy-duty electric vehicles," *Electric Power Applications, IET*, vol. 1, pp. 665-674, 2007.

[25] J. Cao and A. Emadi, "A new battery/ultracapacitor hybrid energy storage system for electric, hybrid, and plug-in hybrid electric vehicles," *Power Electronics, IEEE Transactions on*, vol. 27, pp. 122-132, 2012.

[26] M.-E. Choi, S.-W. Kim, and S.-W. Seo, "Energy management optimization in a battery/supercapacitor hybrid energy storage system," *Smart Grid, IEEE Transactions on,* vol. 3, pp. 463-472, 2012.

[27] D. Toke, "The UK offshore wind power programme: A sea-change in UK energy policy," *Energy Policy,* vol. 39, pp. 526-534, 2011.

[28] D. C. Beddows and R. M. Harrison, "Comparison of average particle number emission factors for heavy and light duty vehicles derived from rolling chassis dynamometer and field studies," *Atmospheric Environment,* vol. 42, pp. 7954-7966, 2008.

[29] T. R. Hawkins, O. M. Gausen, and A. H. Strømman, "Environmental impacts of hybrid and electric vehicles—a review," *The International Journal of Life Cycle Assessment,* vol. 17, pp. 997-1014, 2012.

[30] L. Lu, X. Han, J. Li, J. Hua, and M. Ouyang, "A review on the key issues for lithium-ion battery management in electric vehicles," *Journal of power sources,* vol. 226, pp. 272-288, 2013.

[31] J. Li, A. M. Gee, M. Zhang, and W. Yuan, "Analysis of battery lifetime extension in a SMES-battery hybrid energy storage system using a novel battery lifetime model," *Energy,* 2015.

[32] R. Carter, A. Cruden, and P. J. Hall, "Optimizing for efficiency or battery life in a battery/supercapacitor electric vehicle," *Vehicular Technology, IEEE Transactions on,* vol. 61, pp. 1526-1533, 2012.

[33] K. C. Divya and J. Østergaard, "Battery energy storage technology for power systems—An overview," *Electric Power Systems Research,* vol. 79, pp. 511-520, 4// 2009.

[34] H. Bindner, T. Cronin, P. Lundsager, J. F. Manwell, U. Abdulwahid, and I. Baring-Gould, "Lifetime modelling of lead acid batteries," Risø Nat.Lab. Roskilde, Denmark 8755034411, 2005.

[35] W. Gu, Z. Sun, X. Wei, and H. Dai, "A New Method of Accelerated Life Testing Based on the Grey System Theory for a Model-Based Lithium-Ion Battery Life Evaluation System," *Journal of Power Sources,* 2014.

[36] R. Dufo-López, J. L. Bernal-Agustín, and J. A. Domínguez-Navarro, "Generation management using batteries in wind farms: Economical and technical analysis for Spain," *Energy policy,* vol. 37, pp. 126-139, 2009.

[37] N. Vichare, P. Rodgers, V. Eveloy, and M. G. Pecht, "In situ temperature measurement of a notebook computer-A case study in health and usage monitoring of electronics," *IEEE Transactions on Device and Materials Reliability,* vol. 4, pp. 658-663, 2004.

[38] L. Benini, A. Bogliolo, and G. De Micheli, "A survey of design techniques for system-level dynamic power management," *IEEE transactions on very large scale integration (VLSI) systems,* vol. 8, pp. 299-316, 2000.

[39] Z. Song, H. Hofmann, J. Li, J. Hou, X. Han, and M. Ouyang, "Energy management strategies comparison for electric vehicles with hybrid energy storage system," *Applied Energy,* vol. 134, pp. 321-331, 2014.

[40] S. Zhang, R. Xiong, and J. Cao, "Battery durability and longevity based power management for plug-in hybrid electric vehicle with hybrid energy storage system," *Applied Energy,* vol. 179, pp. 316-328, 10/1/ 2016.

[41] N. Mendis, K. Muttaqi, and S. Perera, "Active power management of a super capacitor-battery hybrid energy storage system for standalone operation of DFIG based wind turbines," in *Industry Applications Society Annual Meeting (IAS), 2012 IEEE*, 2012, pp. 1-8.

[42] M. E. Glavin and W. G. Hurley, "Optimisation of a photovoltaic battery ultracapacitor hybrid energy storage system," *Solar Energy,* vol. 86, pp. 3009-3020, 10// 2012.

[43] H. Zhou, T. Bhattacharya, D. Tran, T. S. T. Siew, and A. M. Khambadkone, "Composite energy storage system involving battery and ultracapacitor with dynamic energy management in microgrid applications," *IEEE Transactions on Power Electronics,* vol. 26, pp. 923-930, 2011.

[44] Z. X. Nie, X. Xiao, Q. Kang, R. Aggarwal, H. M. Zhang, and W. J. Yuan, "SMES-Battery Energy Storage System for Conditioning Outputs From Direct Drive Linear Wave Energy Converters," *IEEE Transactions on Applied Superconductivity,* vol. 23, pp. 5000705-5000705, Jun 2013.

[45] A. Etxeberria, I. Vechiu, H. Camblong, and J.-M. Vinassa, "Comparison of three topologies and controls of a hybrid energy storage system for microgrids," *Energy Conversion and Management,* vol. 54, pp. 113-121, 2012.

[46] H. Jia, Y. Mu, and Y. Qi, "A statistical model to determine the capacity of battery–supercapacitor hybrid energy storage system in autonomous microgrid," *International Journal of Electrical Power & Energy Systems,* vol. 54, pp. 516-524, 1// 2014.

[47] Z. Song, H. Hofmann, J. Li, X. Han, and M. Ouyang, "Optimization for a hybrid energy storage system in electric vehicles using dynamic programing approach," *Applied Energy,* vol. 139, pp. 151-162, 2/1/ 2015.

[48] C. Wang, R. Xiong, H. He, X. Ding, and W. Shen, "Efficiency analysis of a bidirectional DC/DC converter in a hybrid energy storage system for plug-in hybrid electric vehicles," *Applied Energy,* vol. 183, pp. 612-622, 2016.

[49] A. Castaings, W. Lhomme, R. Trigui, and A. Bouscayrol, "Comparison of energy management strategies of a battery/supercapacitors system for electric vehicle under real-time constraints," *Applied Energy,* vol. 163, pp. 190-200, 2/1/ 2016.

[50] H. Ibrahim, A. Ilinca, and J. Perron, "Energy storage systems—Characteristics and comparisons," *Renewable and Sustainable Energy Reviews,* vol. 12, pp. 1221-1250, 6// 2008.

[51] I. Hadjipaschalis, A. Poullikkas, and V. Efthimiou, "Overview of current and future energy storage technologies for electric power applications," *Renewable and Sustainable Energy Reviews,* vol. 13, pp. 1513-1522, 2009.

[52] J. Kaldellis and D. Zafirakis, "Optimum energy storage techniques for the improvement of renewable energy sources-based electricity generation economic efficiency," *Energy,* vol. 32, pp. 2295-2305, 2007.

[53] J. McDowall, "Integrating energy storage with wind power in weak electricity grids," *Journal of Power sources,* vol. 162, pp. 959-964, 2006.

[54] C. J. Rydh, "Environmental assessment of vanadium redox and lead-acid batteries for stationary energy storage," *Journal of power sources,* vol. 80, pp. 21-29, 1999.

[55] K. Divya and J. Østergaard, "Battery energy storage technology for power systems—An overview," *Electric Power Systems Research,* vol. 79, pp. 511-520, 2009.

[56] R. M. Dell and D. A. Rand, "Energy storage—a key technology for global energy sustainability," *Journal of Power Sources,* vol. 100, pp. 2-17, 2001.

[57] F. Beck and P. Rüetschi, "Rechargeable batteries with aqueous electrolytes," *Electrochimica Acta,* vol. 45, pp. 2467-2482, 2000.

[58] A. Du Pasquier, I. Plitz, S. Menocal, and G. Amatucci, "A comparative study of Li-ion battery, supercapacitor and nonaqueous asymmetric hybrid devices for automotive applications," *Journal of Power Sources,* vol. 115, pp. 171-178, 2003.

[59] W. F. Pickard, A. Q. Shen, and N. J. Hansing, "Parking the power: Strategies and physical limitations for bulk energy storage in supply–demand matching on a grid whose input power is provided by intermittent sources," *Renewable and Sustainable Energy Reviews,* vol. 13, pp. 1934-1945, 2009.

[60] N. Clark and D. Doughty, "Development and testing of 100kW/1min Li-ion battery systems for energy storage applications," *Journal of power sources,* vol. 146, pp. 798-803, 2005.

[61] E. Barbour, I. G. Wilson, J. Radcliffe, Y. Ding, and Y. Li, "A review of pumped hydro energy storage development in significant international electricity markets," *Renewable and Sustainable Energy Reviews,* vol. 61, pp. 421-432, 2016.

[62] M. Beaudin, H. Zareipour, A. Schellenberglabe, and W. Rosehart, "Energy storage for mitigating the variability of renewable electricity sources: An updated review," *Energy for Sustainable Development,* vol. 14, pp. 302-314, 2010.

[63] W. Li and G. Joos, "A power electronic interface for a battery supercapacitor hybrid energy storage system for wind applications," in *Power Electronics Specialists Conference, 2008. PESC 2008. IEEE,* 2008, pp. 1762-1768.

[64] I. Ngamroo and S. Vachirasricirikul, "Design of Optimal SMES Controller Considering SOC and Robustness for Microgrid Stabilization," *IEEE Transactions on Applied Superconductivity,* vol. 26, pp. 1-5, 2016.

[65] T.-T. Nguyen, H.-J. Yoo, and H.-M. Kim, "Applying Model Predictive Control to SMES System in Microgrids for Eddy Current Losses Reduction," *IEEE Transactions on Applied Superconductivity,* vol. 26, pp. 1-5, 2016.

[66] J. X. Jin, X. Y. Chen, L. Wen, S. C. Wang, and Y. Xin, "Cryogenic Power Conversion for SMES Application in a Liquid Hydrogen Powered Fuel Cell Electric Vehicle," *Applied Superconductivity, IEEE Transactions on,* vol. 25, pp. 1-11, 2015.

[67] W. Yuan, W. Xian, M. Ainslie, Z. Hong, Y. Yan, R. Pei, *et al.*, "Design and test of a superconducting magnetic energy storage (SMES) coil," *IEEE Transactions on Applied Superconductivity,*, vol. 20, pp. 1379-1382, 2010.

[68] R. Hemmati and H. Saboori, "Emergence of hybrid energy storage systems in renewable energy and transport applications – A review," *Renewable and Sustainable Energy Reviews,* vol. 65, pp. 11-23, 11// 2016.

[69] Y. Y. Chia, L. H. Lee, N. Shafiabady, and D. Isa, "A load predictive energy management system for supercapacitor-battery hybrid energy storage system in solar application using the Support Vector Machine," *Applied Energy,* vol. 137, pp. 588-602, 1/1/ 2015.

[70] R. Sarrias-Mena, L. M. Fernández-Ramírez, C. A. García-Vázquez, and F. Jurado, "Fuzzy logic based power management strategy of a multi-MW doubly-fed induction generator wind turbine with battery and ultracapacitor," *Energy,* vol. 70, pp. 561-576, 6/1/ 2014.

[71] B. Hredzak, V. G. Agelidis, and M. Jang, "A model predictive control system for a hybrid battery-ultracapacitor power source," *Power Electronics, IEEE Transactions on,* vol. 29, pp. 1469-1479, 2014.

[72] F. Zhang, T. Zhang, X. Yang, L. Zhang, K. Leng, Y. Huang, *et al.*, "A high-performance supercapacitor-battery hybrid energy storage device based on graphene-enhanced electrode materials with ultrahigh energy density," *Energy & Environmental Science,* vol. 6, pp. 1623-1632, 2013.

[73] A. M. Gee, F. V. P. Robinson, and R. W. Dunn, "Analysis of Battery Lifetime Extension in a Small-Scale Wind-Energy System Using Supercapacitors," *IEEE Transactions on Energy Conversion,* vol. 28, pp. 24-33, Mar 2013.

[74] A. Kuperman and I. Aharon, "Battery–ultracapacitor hybrids for pulsed current loads: A review," *Renewable and Sustainable Energy Reviews,* vol. 15, pp. 981-992, 2// 2011.

[75] M. Ortúzar, J. Moreno, and J. Dixon, "Ultracapacitor-based auxiliary energy system for an electric vehicle: Implementation and evaluation," *Industrial Electronics, IEEE Transactions on,* vol. 54, pp. 2147-2156, 2007.

[76] G. Genta, *Kinetic energy storage: theory and practice of advanced flywheel systems*: Butterworth-Heinemann, 2014.

[77] H. Lee, B. Y. Shin, S. Han, S. Jung, B. Park, and G. Jang, "Compensation for the power fluctuation of the large scale wind farm using hybrid energy storage applications," *IEEE Transactions on Applied Superconductivity,* vol. 22, pp. 5701904-5701904, 2012.

[78] J. Zhu, W. Yuan, M. Qiu, B. Wei, H. Zhang, P. Chen, *et al.*, "Experimental demonstration and application planning of high temperature superconducting energy storage system for renewable power grids," *Applied Energy,* 2014.

[79] J. W. Shim, Y. Cho, S.-J. Kim, S. W. Min, and K. Hur, "Synergistic control of SMES and battery energy storage for enabling dispatchability of renewable energy sources," *IEEE transactions on applied superconductivity,* vol. 23, 2013.

[80] S. Wang, Y. Tang, J. Shi, K. Gong, Y. Liu, L. Ren, *et al.*, "Design and advanced control strategies of a hybrid energy storage system for the grid integration of wind power generations," *IET Renewable Power Generation,* vol. 9, pp. 89-98, 2014.

[81] J. Li, R. Xiong, Q. Yang, F. Liang, M. Zhang, and W. Yuan, "Design/test of a hybrid energy storage system for primary frequency control using a dynamic droop method in an isolated microgrid power system," *Applied Energy,* 2016.

[82] J. Li, X. Wang, Z. Zhang, S. Le Blond, Q. Yang, M. Zhang, *et al.*, "Analysis of a new design of the hybrid energy storage system used in the residential m-CHP systems," *Applied Energy,* vol. 187, pp. 169-179, 2017.

[83] R. T. Doucette and M. D. McCulloch, "A comparison of high-speed flywheels, batteries, and ultracapacitors on the bases of cost and fuel economy as the energy storage system in a fuel cell based hybrid electric vehicle," *Journal of Power Sources,* vol. 196, pp. 1163-1170, 2/1/ 2011.

[84] S. C. Smith, P. Sen, and B. Kroposki, "Advancement of energy storage devices and applications in electrical power system," in *Power and Energy Society General Meeting-Conversion and Delivery of Electrical Energy in the 21st Century, 2008 IEEE*, 2008, pp. 1-8.

[85] M. Ali, B. Wu, and R. A. Dougal, "An overview of SMES applications in power and energy systems," *IEEE Transactions onSustainable Energy,* vol. 1, pp. 38-47, 2010.

[86] B. Alamri and A. Alamri, "Technical review of energy storage technologies when integrated with intermittent renewable energy," in *Sustainable Power Generation and Supply, 2009. SUPERGEN'09. International Conference on*, 2009, pp. 1-5.

[87] T. Sannomiya, H. Hayashi, T. Ishii, and R. Ikeda, "Test results of compensation for load fluctuation under a fuzzy control by a 1 kWh/1 MW SMES," *IEEE Transactions on Applied Superconductivity,* vol. 11, pp. 1908-1911, 2001.

[88] W. Buckles and W. V. Hassenzahl, "Superconducting magnetic energy storage," *Power Engineering Review, IEEE,* vol. 20, pp. 16-20, 2000.

[89] S. H. Moon, "HTS development and industrialization at SuNAM," in *1st Workshop on Accelerator Magnets in HTS (Hamburg, Germany)*, 2014.

[90] T. Le, J. Kim, D. Kim, C. Boo, and H. Kim, "Status of the technology development of large scale HTS generators for wind turbine," *Progress in Superconductivity and Cryogenics,* vol. 17, pp. 18-24, 2015.

[91] A. Morandi, "HTS dc transmission and distribution: concepts, applications and benefits," *Superconductor Science and Technology,* vol. 28, p. 123001, 2015.

[92] F. Grilli and A. Kario, "How filaments can reduce AC losses in HTS coated conductors: a review," *Superconductor Science and Technology,* vol. 29, p. 083002, 2016.

[93] S. Nomura, N. Watanabe, C. Suzuki, H. Ajikawa, M. Uyama, S. Kajita, *et al.*, "Advanced configuration of superconducting magnetic energy storage," *Energy,* vol. 30, pp. 2115-2127, 8// 2005.

[94] S. Suzuki, J. Baba, K. Shutoh, and E. Masada, "Effective application of superconducting magnetic energy storage (SMES) to load leveling for high speed transportation system," *IEEE Transactions on Applied Superconductivity*, vol. 14, pp. 713-716, 2004.

[95] A. Khaligh and Z. Li, "Battery, ultracapacitor, fuel cell, and hybrid energy storage systems for electric, hybrid electric, fuel cell, and plug-in hybrid electric vehicles: State of the art," *IEEE Transactions on Vehicular Technology*, vol. 59, pp. 2806-2814, 2010.

[96] J. Moreno, M. E. Ortúzar, and L. Dixon, "Energy-management system for a hybrid electric vehicle, using ultracapacitors and neural networks," *IEEE Transactions on Industrial Electronics*, vol. 53, pp. 614-623, 2006.

[97] E. M. Krieger, J. Cannarella, and C. B. Arnold, "A comparison of lead-acid and lithium-based battery behavior and capacity fade in off-grid renewable charging applications," *Energy*, vol. 60, pp. 492-500, 10/1/ 2013.

[98] J. F. Manwell, J. G. McGowan, U. Abdulwahid, and K. Wu, "Improvements to the Hybrid2 battery model," in *American Wind Energ Association Windpower 2005 Conference*, American,Colorado 2005.

[99] B. Garcia, S. Lavallée, G. Perron, C. Michot, and M. Armand, "Room temperature molten salts as lithium battery electrolyte," *Electrochimica Acta*, vol. 49, pp. 4583-4588, 2004.

[100] G. Ning, B. Haran, and B. N. Popov, "Capacity fade study of lithium-ion batteries cycled at high discharge rates," *Journal of Power Sources*, vol. 117, pp. 160-169, 2003.

[101] D. Jeong and J. Lee, "Electrode design optimization of lithium secondary batteries to enhance adhesion and deformation capabilities," *Energy*, vol. 75, pp. 525-533, 10/1/ 2014.

[102] N. Omar, P. V. d. Bossche, T. Coosemans, and J. V. Mierlo, "Peukert Revisited—Critical Appraisal and Need for Modification for Lithium-Ion Batteries," *Energies*, vol. 6, pp. 5625-5641, 2013.

[103] D. Wang, H. Li, S. Shi, X. Huang, and L. Chen, "Improving the rate performance of LiFePO4 by Fe-site doping," *Electrochimica Acta*, vol. 50, pp. 2955-2958, 2005.

[104] Q. Zhang and R. E. White, "Capacity fade analysis of a lithium ion cell," *Journal of Power Sources*, vol. 179, pp. 793-798, 5/1/ 2008.

[105] T. Guan, P. Zuo, S. Sun, C. Du, L. Zhang, Y. Cui, *et al.*, "Degradation mechanism of LiCoO2/mesocarbon microbeads battery based on accelerated aging tests," *Journal of Power Sources*, vol. 268, pp. 816-823, 12/5/ 2014.

[106] R. Agrawal, A. Arning, R. Seiffert, and R. Srikant, "Self-adaptive method and system for providing a user-preferred ranking order of object sets," ed: Google Patents, 2002.

[107] B. Dunn, H. Kamath, and J.-M. Tarascon, "Electrical energy storage for the grid: a battery of choices," *Science*, vol. 334, pp. 928-935, 2011.

[108] Y. Bakelli, A. Hadj Arab, and B. Azoui, "Optimal sizing of photovoltaic pumping system with water tank storage using LPSP concept," *Solar Energy*, vol. 85, pp. 288-294, 2011.

[109] B. Ould Bilal, V. Sambou, P. Ndiaye, C. Kébé, and M. Ndongo, "Optimal design of a hybrid solar–wind-battery system using the minimization of the annualized cost system and the minimization of the loss of power supply probability (LPSP)," *Renewable Energy*, vol. 35, pp. 2388-2390, 2010.

[110] W. Zhou, C. Lou, Z. Li, L. Lu, and H. Yang, "Current status of research on optimum sizing of stand-alone hybrid solar–wind power generation systems," *Applied Energy*, vol. 87, pp. 380-389, 2010.

[111] J. Li, M. Zhang, J. Zhu, Q. Yang, Z. Zhang, and W. Yuan, "Analysis of Superconducting Magnetic Energy Storage Used in a Submarine HVAC Cable Based Offshore Wind System," *Energy Procedia*, vol. 75, pp. 691-696, 2015.

[112] A. Ferreira, J. A. Pomilio, G. Spiazzi, and L. de Araujo Silva, "Energy management fuzzy logic supervisory for electric vehicle power supplies system," *Power Electronics, IEEE Transactions on*, vol. 23, pp. 107-115, 2008.

[113] O. Erdinc, B. Vural, and M. Uzunoglu, "A wavelet-fuzzy logic based energy management strategy for a fuel cell/battery/ultra-capacitor hybrid vehicular power system," *Journal of Power Sources*, vol. 194, pp. 369-380, 10/20/ 2009.

[114] E. Schaltz, A. Khaligh, and P. O. Rasmussen, "Influence of battery/ultracapacitor energy-storage sizing on battery lifetime in a fuel cell hybrid electric vehicle," *Vehicular Technology, IEEE Transactions on*, vol. 58, pp. 3882-3891, 2009.

[115] A.-L. Allègre, A. Bouscayrol, and R. Trigui, "Flexible real-time control of a hybrid energy storage system for electric vehicles," *IET Electrical Systems in Transportation*, vol. 3, pp. 79-85, 2013.

[116] C. Gavriluta, J. I. Candela, C. Citro, J. Rocabert, A. Luna, and P. Rodriguez, "Decentralized primary control of MTDC networks with energy storage and distributed generation," *Industry Applications, IEEE Transactions on*, vol. 50, pp. 4122-4131, 2014.

[117] J. Meng, Y. Mu, H. Jia, J. Wu, X. Yu, and B. Qu, "Dynamic frequency response from electric vehicles considering travelling behavior in the Great Britain power system," *Applied Energy*, vol. 162, pp. 966-979, 1/15/ 2016.

[118] J. M. Guerrero, J. C. Vasquez, J. Matas, D. Vicuna, L. García, and M. Castilla, "Hierarchical control of droop-controlled AC and DC microgrids—A general approach toward standardization," *Industrial Electronics, IEEE Transactions on*, vol. 58, pp. 158-172, 2011.

[119] J. Li, Q. Yang, F. Robinson, F. Liang, M. Zhang, and W. Yuan, "Design and test of a new droop control algorithm for a SMES/battery hybrid energy storage system," *Energy*.

[120] R. Asad and A. Kazemi, "A novel distributed optimal power sharing method for radial dc microgrids with different distributed energy sources," *Energy*, vol. 72, pp. 291-299, 8/1/ 2014.

[121] S. Naderi, E. Pouresmaeil, and W. D. Gao, "The frequency-independent control method for distributed generation systems," *Applied Energy,* vol. 96, pp. 272-280, 8// 2012.

[122] M. Castilla, J. Guerrero, J. Matas, J. Miret, and J. Sosa, "Comparative study of hysteretic controllers for single-phase voltage regulators," *IET Power Electronics,* vol. 1, pp. 132-143, 2008.

[123] I.-S. Kim, "Sliding mode controller for the single-phase grid-connected photovoltaic system," *Applied Energy,* vol. 83, pp. 1101-1115, 10// 2006.

[124] S.-C. Tan, Y. Lai, and C. K. Tse, "A unified approach to the design of PWM-based sliding-mode voltage controllers for basic DC-DC converters in continuous conduction mode," *Circuits and Systems I: Regular Papers, IEEE Transactions on,* vol. 53, pp. 1816-1827, 2006.

[125] P. Balcombe, D. Rigby, and A. Azapagic, "Energy self-sufficiency, grid demand variability and consumer costs: Integrating solar PV, Stirling engine CHP and battery storage," *Applied Energy,* vol. 155, pp. 393-408, 2015.

[126] M. Lantz, "The economic performance of combined heat and power from biogas produced from manure in Sweden–A comparison of different CHP technologies," *Applied Energy,* vol. 98, pp. 502-511, 2012.

[127] H. Ren and W. Gao, "Economic and environmental evaluation of micro CHP systems with different operating modes for residential buildings in Japan," *Energy and Buildings,* vol. 42, pp. 853-861, 6// 2010.

[128] M. M. Maghanki, B. Ghobadian, G. Najafi, and R. J. Galogah, "Micro combined heat and power (MCHP) technologies and applications," *Renewable and Sustainable Energy Reviews,* vol. 28, pp. 510-524, 2013.

[129] M. Bianchi, A. De Pascale, and P. R. Spina, "Guidelines for residential micro-CHP systems design," *Applied Energy,* vol. 97, pp. 673-685, 9// 2012.

[130] L. Dong, H. Liu, and S. Riffat, "Development of small-scale and micro-scale biomass-fuelled CHP systems – A literature review," *Applied Thermal Engineering,* vol. 29, pp. 2119-2126, 8// 2009.

[131] A. Peacock and M. Newborough, "Impact of micro-combined heat-and-power systems on energy flows in the UK electricity supply industry," *Energy,* vol. 31, pp. 1804-1818, 2006.

[132] K. Darcovich, B. Kenney, D. MacNeil, and M. Armstrong, "Control strategies and cycling demands for Li-ion storage batteries in residential micro-cogeneration systems," *Applied Energy,* vol. 141, pp. 32-41, 2015.

[133] C. Bang-Møller, M. Rokni, B. Elmegaard, J. Ahrenfeldt, and U. B. Henriksen, "Decentralized combined heat and power production by two-stage biomass gasification and solid oxide fuel cells," *Energy,* vol. 58, pp. 527-537, 2013.

[134] S. Riffat and X. Zhao, "A novel hybrid heat pipe solar collector/CHP system—Part 1: System design and construction," *Renewable energy,* vol. 29, pp. 2217-2233, 2004.

[135] W. Yagoub, P. Doherty, and S. Riffat, "Solar energy-gas driven micro-CHP system for an office building," *Applied thermal engineering,* vol. 26, pp. 1604-1610, 2006.

[136] K. Alanne, J. Paatero, and I. Beausoleil‐Morrison, "Performance assessment of a Stirling engine plant for local micro‐cogeneration," *International Journal of Energy Research,* vol. 36, pp. 218-230, 2012.

[137] S. Karmacharya, G. Putrus, C. Underwood, K. Mahkamov, S. McDonald, and A. Alexakis, "Simulation of energy use in buildings with multiple micro generators," *Applied Thermal Engineering,* vol. 62, pp. 581-592, 2014.

[138] K. Tapia-Ahumada, I. Pérez-Arriaga, and E. J. Moniz, "A methodology for understanding the impacts of large-scale penetration of micro-combined heat and power," *Energy Policy,* vol. 61, pp. 496-512, 2013.

[139] D. Jenkins, J. Fletcher, and D. Kane, "Model for evaluating impact of battery storage on microgeneration systems in dwellings," *Energy Conversion and Management,* vol. 49, pp. 2413-2424, 2008.

[140] J. Aghaei and M.-I. Alizadeh, "Multi-objective self-scheduling of CHP (combined heat and power)-based microgrids considering demand response programs and ESSs (energy storage systems)," *Energy,* vol. 55, pp. 1044-1054, 2013.

[141] P. Mitra and G. K. Venayagamoorthy, "An adaptive control strategy for DSTATCOM applications in an electric ship power system," *Power Electronics, IEEE Transactions on,* vol. 25, pp. 95-104, 2010.

[142] T. C. Fubara, F. Cecelja, and A. Yang, "Modelling and selection of micro-CHP systems for domestic energy supply: The dimension of network-wide primary energy consumption," *Applied Energy,* vol. 114, pp. 327-334, 2// 2014.

[143] S. P. Le Blond and R. K. Aggarwal, "Design of Adaptive Autoreclosure Schemes for 132 kV Network With High Penetration of Wind—Part I: Real-Time Modeling," *IEEE Transactions on Power Delivery,* vol. 27, pp. 1055-1062, 2012.

[144] T. Instruments. (2007). *TMS320F28335 - Texas Instruments*. Available: http://www.ti.com/lit/ds/symlink/tms320f28335.pdf

[145] R. Dufo-López, J. L. Bernal-Agustín, J. M. Yusta-Loyo, J. A. Domínguez-Navarro, I. J. Ramírez-Rosado, J. Lujano, *et al.*, "Multi-objective optimization minimizing cost and life cycle emissions of stand-alone PV–wind–diesel systems with batteries storage," *Applied Energy,* vol. 88, pp. 4033-4041, 2011.

[146] G. Wojtasiewicz, T. Janowski, S. Kozak, B. Kondratowicz-Kucewicz, J. Kozak, P. Surdacki, *et al.*, "HTS magnet for 7.3 kJ SMES system," in *Journal of Physics: Conference Series*, 2006, p. 821.

[147] M. G. Molina and P. E. Mercado, "Power flow stabilization and control of microgrid with wind generation by superconducting magnetic energy storage," *IEEE Transactions on Power Electronics,* vol. 26, pp. 910-922, 2011.

Appendixs

Publications

FIVE PUBLICATIONS HAVE BEEN REMOVED FROM THIS PUBLIC VERSION OF THE THESIS BECAUSE OF COPYRIGHT RESTRICTIONS